INVESTIGATION OF ELECTROSURGICAL TISSUE JOINING

by

Matthew Wayne Chastagner

A dissertation submitted in partial fulfillment
of the requirements for the degree of
Doctor of Philosophy
(Mechanical Engineering)
in The University of Michigan
2010

Doctoral Committee:

Professor Albert J. Shih, Chair
Professor Elijah Kannatey-Asibu, Jr.
Associate Professor Joseph L. Bull
Assistant Professor Kevin P. Pipe

ACKNOWLEDGMENTS

I would like to thank my advisor, Professor Albert Shih, for his help guiding me as I conducted the research for this thesis. As we both entered a new research area, I do not think either of us knew what to expect along the way.

I would also like to also thank my committee members, Professor Elijah Kannatey-Asibu, Joseph Bull and Kevin Pipe for their help with both guiding and critiquing the research as it progressed. I appreciate their support and advice throughout this entire process. I would also like to thank Dr. James Geiger for his help with answering my medical related questions and with obtaining the surgical devices used in this research.

This thesis would not have been possible without the help of many people from all over the University. First, I would like to thank Toby Donajkowski for his help with building almost every piece of equipment used in this thesis and for providing me with the encouragement to always do my best. Toby always seemed to have the solution to my problem, no matter how large or small. I would also like to thank Gail Rising and Sandy Holmes for their help with obtaining the some of the tissues used in this thesis. I am also appreciative to Drs. William Roberts and Kim Ives for their help with obtaining the other tissues. I would also like to thank Pablo LaValle, for his willingness to loan me a portion of the temperature measurement equipment used in this thesis.

I am also grateful to the friends I have met at the Wu Lab, especially Rob Dodde. Whether it was bouncing ideas off one another, or exploring the topic of "electrosurgery,"

he and I never knew what we would find around the next corner. I would also like to thank Roland Chen, Scott Miller and Jacob Gee for their help with conducting the experiments within this thesis.

Finally, I owe a big thank you to my family, for their encouragement and advice throughout this whole process. Mom, Dad and Kevin, I love you very much. Last but not least, the person who gave up the most for this thesis to happen, my wife Dawn. Thank you from the bottom of my heart for your encouragement and love; I love you.

TABLE OF CONTENTS

LIST OF FIGURES

LIST OF TABLES

LIST OF APPENDICES

CHAPTER 1

INTRODUCTION

1.1 Research Motivation

The first modern electrosurgical device was developed in 1926 by Drs. Bovie and Cushing [O'Conner and Bloom, 1996]. This device allowed surgeons to cut, coagulate and desiccate the tissue by sending electrical energy through the tissue. By delivering a high frequency electrical current through a surgical handpiece, the surgeon is able to resistively heat the tissue and alter its physiological properties [Massarweh et al., 2006]. The power density being delivered from the device and the amount of the resistive heating within the tissue will dictate whether the tissue is cut or coagulated.

During surgery, the two most commonly used modalities are: monopolar and bipolar. The key difference between the two modalities is the way in which the energy is delivered to the tissue. In the monopolar modality, as shown in Fig. 1.1(a), a high current density is created at the tissue-electrode interface and is used to cut the tissue. In the bipolar modality (Fig. 1.1(b)), both the active and passive electrodes are contained within the device and the electrical current is passed through the tissue contained between the electrodes. This electrical current, combined with compression is used to join the two tissues together [Wall and Gertner, 2001].

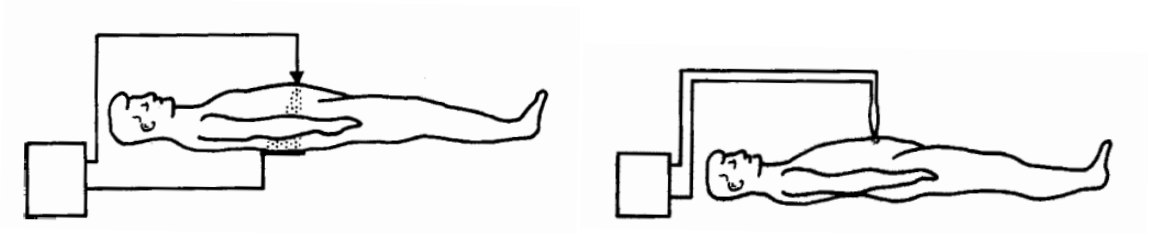

(a) **(b)**

Figure 1.1 The two most common electrosurgical modalities: (a) monopolar, showing current passing through patient, and (b) bipolar, with the current only passing between the electrodes. [Lee and Lambert, 2001]

For electrosurgery, the device is attached to an electrical generator which applies the desired waveform, depending on the desired effect. Since human nerve and muscle stimulation cease at frequencies over 100 kHz, high frequency electrical energy is able to pass through the tissue safely. One application of bipolar electrosurgery, which uses high current (4 A) and low voltage (<200 V), is for vessel sealing, [Carbonell et al., 2003]. The high current promotes the melting of the collagen and elastin within the tissue. As these proteins are melted, a flexible seal is created within the tissue [Matthews et al., 2001].

Today, bipolar electrosurgical devices are commonly used as a method of vessel ligation during laparoscopic procedures. Traditionally, vessel ligation was done by tying off the vessel with a suture. However, with the advent of bipolar electrosurgical devices, the speed and ease at which the ligation can be accomplished has improved. This has led to electrosurgical devices replacing traditional suture based ligation techniques.

One of the major problems with the current bipolar devices is the thermal spread from the device to the nearby tissues. Depending on the size of the vessel being sealed, the length of sealing time and amount of energy applied to the vessel will vary. As the size of the vessel increases, the sealing time will increase in order to compensate for the larger

sealing area [Newcomb et al., 2009]. However, this additional application time causes the amount of energy being delivered to the tissue to increase, causing the temperature to increase at both the sealing site and the nearby tissue. This elevated temperature in the surrounding tissue can cause damage to not only the tissue, but can also effect nearby nerves [Carlander et al., 2005]. If the nerves are damaged, critical bodily functions may not perform correctly after surgery. Therefore, accurate quantification of the temperature profile in the vessel and minimization of the thermal spread is needed. This is coupled with the need to better understand the quality of the vessel seal during surgery.

The clamping force is an important factor during electrosurgery because it directly influences the quality of the vessel seal. The quality of the vessel seal, measured by burst pressure, is dependent on a variety of different conditions including: the length of energy application time, vessel size, compressive force from the electrodes, and tissue temperature. One of the issues related to the compressive force is discerning the amount of force being applied to the vessel during the sealing process. Currently, the surgeon does not have any feedback in relation to the level of compressive force being applied to the tissue. Improving the awareness of the force being applied to the seal is crucial for the development of a high quality seal.

Further studies are needed to improve the quality of vessel sealing. First, the thermal spread from bipolar electrosurgical devices needs to be controlled in order to prevent damage to the surrounding tissues. Second, the use of clamping force measurements during sealing is needed to improve the reproducibility of the seal quality.

1.2 Research Objectives

The objectives of this research are to develop a better understanding of the physiological changes that occur in the tissue during bipolar electrosurgical vessel sealing and how these changes affect the quality of the vessel seal. The affects of the electrosurgical process on the thermal properties of tissue is not well known. This is especially true for the thermal conductivity, as the electrosurgical process subjects the tissue to both compression and drying. Understanding how the sealing process affects the thermal conductivity is important for developing new methods for minimizing the thermal spread within the tissue and for developing accurate predictive models for the vessel sealing process. The specific objectives of this research are as follow:

1. Develop a process to accurately measure the thermal conductivity of tissue subjected to compression and drying.
2. To measure and predict the tissue thermal profile during porcine vessel sealing, while identifying the key parameters that affect the sealing process.
3. Establish the effects of force, energy input, and vessel size on the burst pressure of vessels sealed using a bipolar electrosurgical device.

1.3 Organization of the Dissertation

This thesis presents observations, results, and future research goals related to vessel sealing. The layout of this thesis is described in the following paragraphs:

Chapter 2 examines the effect of compression and tissue water content on the thermal conductivity of tissue. The thermal diffusion probe technique is used to measure

the thermal conductivity of tissue. The tissue is altered by varying the water content level, compressing the tissue or a combination of the two effects. This serves as a means of replicating the effects that would occur on the tissue during electrosurgery. A Maxwell-Eucken model is also used to describe the response of the tissue thermal conductivity to these effects.

Chapter 3 examines the temperature profile of a femoral artery and the mesenteric artery vasculature during vessel sealing. Using the voltage and current data from the electrical energy being delivered to the tissue, the electrical impedance is calculated. A relationship between the change in local tissue temperature, temperature increase per electrical pulse and tissue impedance is identified and related to the tissue water content.

Chapter 4 develops a finite element model to simulate the temperature profile during experimental vessel sealing of a porcine artery. The model takes into account thermal damage by altering the electrical conductivity of the tissue. A comparison of the modeling and experimental results is also presented and discussed. The differences between the model and the experimental results are attributed to mass diffusion and water loss within the tissue during the sealing process.

Chapter 5 examines the effect of clamping force on the vessel seal quality during bipolar vessel sealing. A bipolar electrosurgical device is used to apply a range of compressive forces to the vessel tissue during sealing. The burst pressure, an indicator of the vessel seal quality, is used as a measure for determining the ideal compressive force for sealing. This preliminary work indentifies the need for the development of a surgical device that is able to display in real-time the current force that is being applied to the vessel during sealing.

Chapter 6 presents the final conclusions and summarizes the work. Possible future research topics are also proposed and discussed.

References

Carbonell, A.M., Joels, C.S., Kercher, K.W., Matthers, B.D., Sing, R.F., and Heniford, B.T., (2003), "A comparison of laparoscopic bipolar vessel sealing devices in the hemostasis of small-, medium-, and large-sized arteries," *Journal of Laparoendoscopic and Advanced Surgical Techniques*, Vol. 13, pp. 377-380.

Carlander, J., Johansson, K., Lindstrom, S., Velin, A.K., Jiang, C.H., and Nordborg, C., (2005), "Comparison of experimental nerve injury caused by ultrasonically activated scalpel and electrosurgery," *British Journal of Surgery*, Vol. 92, pp. 772-777.

Lee, M., and Lambert, S., (2001), "Thermal modification of connective tissue," *Current Orthopedics*, Vol. 15, pp. 364-375.

Massarweh, N.N., Cosgriff, N., and Slakey, D.P., (2006), "Electrosurgery: History, principles, and current and future uses," *Journal of the American College of Surgeons*, Vol. 202, pp. 520-530.

Matthews B.D., Pratt B.L., Backus C.L., Kercher K.W., Mostafa G., Lentzner A., Lipford E.H., Sing R.F., and Heniford, B.T., (2001), "Effectiveness of the ultrasonic coagulating shears, LigaSure vessel sealer, and surgical clip application in biliary surgery: A comparative analysis," *The American Surgeon*, Vol. 67, pp. 901-906.

Newcomb, W.L., Hope, W.W., Schmelzer, T.M. , Heath, J.J, Norton, H.J., Lincourt, A.E., Heniford, B.T., and Iannitti, D.A., 2009, "Comparison of blood vessel sealing among new electrosurgical and ultrasonic devices," *Surgical Endoscopy*, Vol. 23, pp. 90-96.

O'Connor, J.L., and Bloom, D.A., (1996), "William T. Bovie and electrosurgery," *Surgery*, Vol. 119, pp. 390-396.

Wall, J. and Gertner, M.E., (2008), "Energy transfer in the practice of surgery," In: Norton, J.A., Barie, P.S., Bollinger, R.R., Chang, A.E., Lowry, S., Mulvihill, S.J., Pass, H.I., Thompson, R.W. (Eds.), *Surgery: Basic Science and Clinical Evidence*. Springer, New York, 2nd ed., Chapter 113.

CHAPTER 2

EFFECT OF COMPRESSION AND WATER CONTENT ON THE THERMAL CONDUCTIVITY OF TISSUE

ABSTRACT

The effects of water content and compression level on the thermal conductivity of canine tissue are studied. As the tissue is often subjected to both compression and thermal heating, it is important to understand the effects of these parameters in electrosurgery. By using a desiccation technique, the water content of the canine spleen, heart and liver tissue was found to be between 69% and 76%. When the spleen tissue was ablated using a bipolar electrosurgical device, the tissue water content level was reduced to roughly 60%. A thermal diffusion probe technique was then used to measure the thermal conductivity of the tissue as the water content level decreased. The measured thermal conductivity decreased as the percentage of water within the tissue decreased. A three-phase Maxwell-Eucken model was applied to the experimental data to predict the thermal conductivity of the tissue. The model used air, tissue fiber and water to predict the thermal conductivity and was within 10% of the experimental data. Another set of experiments was conducted, where compression was applied to canine spleen, resulting in a 9% reduction in the thermal conductivity of the tissue. A final set of experiments was run with a combined drying and compression effect. For tissue that had been desiccated to a water content level of 64%, the thermal conductivity decreased by about 12% as the tissue was compressed by 70%. The three-phase Maxwell-Eucken model was applied to the compressed tissue, and for 64% water content tissue, predicted a reduction of 7% in thermal conductivity. For tissue with an even lower water content level, the difference between the model and the experimental results became more significant due to poor contact at the thermistor-tissue interface and excess air in the measurement volume.

2.1 Introduction

During surgery, tissue is often subjected to mechanical compression and thermal procedures that alter its physiological state. Examples of temperature gradient applications include increasing the temperature during electrosurgery to coagulate and dissect the tissue [Matthews et al., 2001] and using radio frequency ablation to elevate the tissue temperature for the treatment of cancerous liver tissues [Chang, 2003]. Tissue compression can occur any time a surgeon needs to manipulate a tissue during an operation. The application of these processes on the tissue can lead to major changes in the tissue thermal conductivity and the resulting surgical outcome.

At elevated temperatures, major physiological changes occur in the tissue. The increased temperature can permanently alter the biological properties and functions of the tissue. As the tissue is heated, the collagen and elastin within the tissue is melted as the tertiary hydrogen bonds between the collagen and the matrix denature and realign [Thomsen et al., 1989]. Once the heat is removed, the collagen cools and realigns, thus permanently altering the state of the collagen [Matthews et al., 2001].

The size of this altered collagen region is dependent on the tissue thermal conductivity, as it will determine how quickly the thermal energy spreads to the nearby tissue. Tissue subjected to high temperatures for extended periods of time can lead to permanent heat induced damage at the surgical site [Harold et al., 2003]. If a nerve is within the surgical site, the elevated temperature can also lead to collateral damage of the nervous functions [Ong et al., 2004; Dodde et al., 2008]. An accurate determination of the tissue thermal conductivity can help to predict the thermal spread in surgery when using energy-based devices.

Previous research on tissue thermal conductivity has focused on the effects of varying the temperature and has not considered the effect of either tissue drying or compression on the thermal conductivity. When using energy-based devices during surgery, the tissue is heated to an elevated temperature, which causes the water from the tissue to vaporize [Yang et al., 2007]. This change in water content alters the tissue thermal conductivity, since the tissue is predominantly fluid based. Cooper and Trezek [1971] reported on the thermal conductivity for tissues with water content levels above 66%, and showed that

the lower water content tissues had a lower thermal conductivity. Olsrud et al. [1998] reported that tissue coagulation caused the tissue to become drier, thus causing the thermal conductivity to decrease. Sweat [1986] showed that the thermal conductivity for a variety of meats decreased as the water content was reduced. Since the water content is reduced during electrosurgery, particularly during vessel sealing, a more complete understanding of the effects of water content on tissue thermal conductivity is needed. This leads to the first goal of this study, which is to develop a better understanding of the effect of water content on the tissue thermal conductivity.

During many surgical applications, before the energy can be delivered to the tissue, the tissue must first be compressed. This tissue compression causes physical changes to occur within the tissue as interstitial fluids are driven out of the tissue. Anderson et al. [1992] has hypothesized that the compression from a small (less than 2.5 mm diameter) thermistor on the tissue can cause a change in tissue's thermal conductivity. However, the effect of this tissue compression on the thermal conductivity has not been studied. Therefore, the second goal of this research is to examine the combined effect of drying and compression on the thermal conductivity.

Experimental testing of the tissue thermal conductivity has been reported for many soft and hard tissues. A comprehensive review of the experimental methods used to measure the thermal conductivity was presented by Bowman et al. [1975] with two distinct classes of methods: steady-state or transient. The steady-state methods place a temperature gradient across the tissue to allow for the direct calculation of the thermal conductivity via Fourier's law. However, due to the high water content of the tissue, the transient methods are superior since the sampling time is shorter, thus reducing the probability of changes in the water content during the experiment.

A variety of transient methods are available to measure tissue thermal conductivity [Bowman et al., 1975; Chato, 1968; Cooper and Trezek, 1972]. The self-heating thermistor technique has been developed to measure small tissue volumes. This method heats the thermistor by providing it with excess electrical power. The excess heat is then dissipated into the tissue, causing the tissue temperature to rise. At the same time, the tissue temperature is measured based on the resistance of the thermistor. Either a single

or multiple thermistor technique can be used. The single thermistor technique reduces the amount of tissue damage as it only has one insertion point.

Both a pulse decay and thermal diffusion probe method have been developed for the single thermistor technique [Baish, 2006]. The underlying principle is the same between the methods, but the process for determining the thermal conductivity is different. Chen et al. [1981] developed the pulse decay method using a single thermistor probe. The rate of the temperature decay after the addition of the self-heating power is used to determine the tissue thermal conductivity. This method requires knowledge of the density and specific heat of the tissue. For the thermal diffusion probe technique, the tissue temperature change during the application of the self-heating power is measured, instead of the thermal decay after the applied pulse. This technique, developed by Chato [1968], and further advanced by Balasubramaniam and Bowman [1977] and Valvano et al. [1985], does not require the knowledge of either the tissue density or specific heat. Instead, this technique requires two independent calibration coefficients to determine the thermal conductivity. This method is best suited for tissue that forms a close, tight contact with the thermistor, ensuring a low thermal contact resistance [Chato, 1968].

Since both methods utilize a small thermistor probe, with an active measurement volume close to that of a sphere, their overall measurement volume of tissue is very small. Most commonly, the diameter of the thermistor is less than 2.5 mm. Through experimental testing, Kravets [1988] concluded that the sample volume could be as small as 3.3 times the thermistor radius, while Valvano et al. [1985] has shown that this volume can be as large as 5 to 10 times the radius. Patel et al. [1987] has also shown that the measurement volume is dependent on the sampling time, since longer sampling times will dissipate more heat into the tissue.

The thermal diffusion probe technique is used to measure the thermal conductivity of the tissue in this study. The tissue is dried and compressed to various levels to simulate the conditions observed during electrosurgery. The thermal diffusion probe was used since it minimizes tissue trauma and allows for a relatively fast measurement of the thermal conductivity, while allowing for the tissue to be compressed.

In this paper, the effect of varying the water content on the thermal conductivity is first presented. Then, the combined effect of varying water content and compression is

studied. Finally, a Maxwell-Eucken model was fit to the experimental results, with a discussion of the differences between the experimental and modeling results.

2.2 Experimental Setup and Procedure

The circuit and formula for single thermistor thermal diffusion probe method is summarized in Appendix A. The experimental setup and procedure are discussed in the following two sections.

2.2.1 Experimental Setup

2.2.1.1 Varying Tissue Water Content

The effect of water content on the thermal conductivity of the tissue was measured using *ex vivo* canine spleen. Canine spleen was used due to its large area, relatively uniform thickness, and overall homogeneity. To simulate the drying of the tissue during surgical procedures, the water content within the tissue was altered by drying the tissue in an oven. This allowed for the tissue water content to be determined under a controlled setting. Spleen, liver and heart (ventricle) tissue were excised from a single mongrel canine weighing approximately 25 kg and were placed into saline for transportation to the lab. The desired tissue was cut into small 25 mm square pieces with heights ranging from 10-15 mm and placed onto metal measuring trays. These trays were weighed using a precision balance (Ohaus Adventurer Pro AV212). The tissue was then placed into an oven (National Appliance Model #5831), set at 60°C for the entire drying process.

2.2.1.2 Tissue Compression

Three additional mongrel canine models weighing between 25-55 kg were used for the *ex vivo* tissue compression measurements. An experimental apparatus, shown in Fig. 2.1(a), was constructed to measure the thermal conductivity of the tissue under compression. The instrument contained two 12.7 mm diameter plastic plates to compress

the tissue, with the upper plastic plate containing a partially exposed thermistor (GE Sensing P60DA102M). The thermistor was set into the plastic plate with half of the thermistor exposed. A load cell (Honeywell 13BN) was used to measure the applied load, while the height of the tissue was measured using a linear potentiometer (Omega LP804-2).

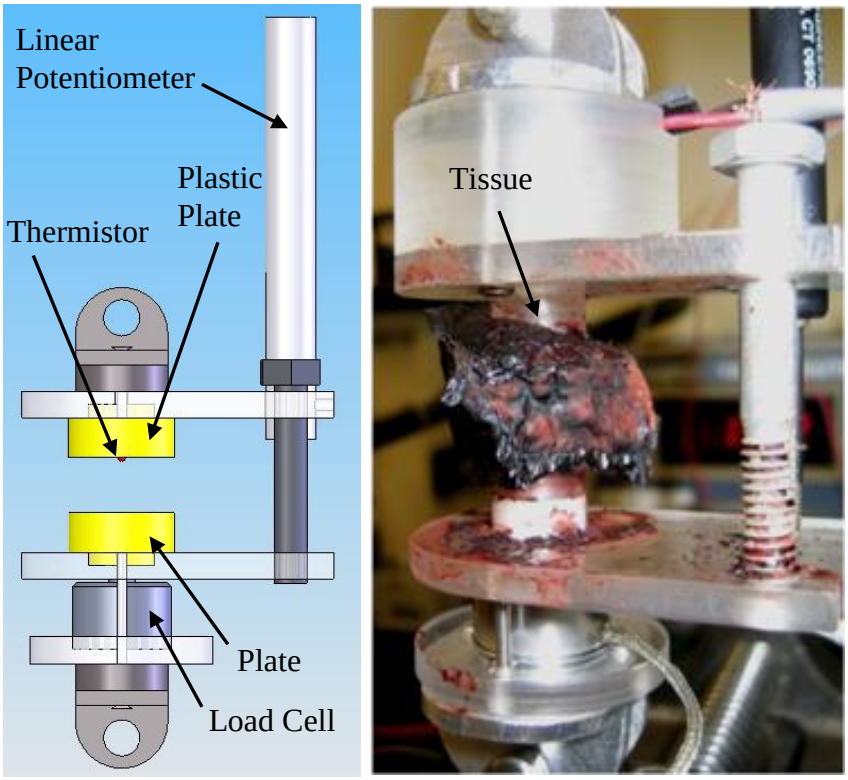

Figure 2.1 The device used to determine the thermal conductivity of the tissue under compression (a) schematic showing the key components of the device and (b) the device in use during tissue compression.

2.2.1.3 Thermal Conductivity Measurement with Water Content Effect

To measure the thermal conductivity of the tissue, a single thermistor (GE Sensing P60DA102M) with a diameter of 1.52 mm was inserted into the tissue. This thermistor was attached to the circuit, shown in Fig. 2.2, containing a relay that switches between a constant current source (Texas Instruments REF200) set at 0.1 mA and a constant voltage source set at 5 V DC (National Instruments [NI] PXI-4110 DC). The voltage drop across

both the resistor and the thermistor was measured using a 16-bit data acquisition board (NI PXI-6221). The circuit was attached to the PXI-6221 through a feedthrough module (NI SCC-FT01) contained within a signal conditioning box (NI SC-2345). The data was collected at a rate of 500 Hz with a program written in LabVIEW 8.6 (NI).

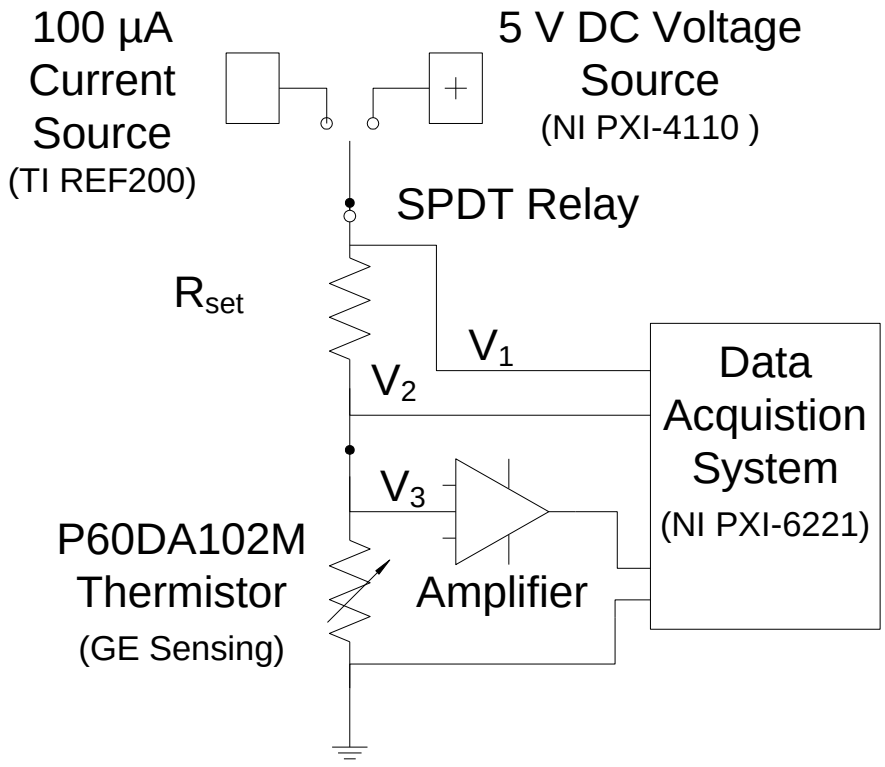

Figure 2.2 The electrical circuit used to apply power to the thermistor during the self-heating experiments.

During the temperature sensing portion of the experiment, the first 5 s, the relay sent the current through the thermistor to determine the initial temperature of the tissue. During the self-heating portion (the next 30 s of the experiment), the relay was closed to allow for 5 V to be applied to the thermistor. Based on the initial recorded temperature, the resistance of R_{set} was changed to provide the desired ΔT during the self-heating portion of the test. For the thermal diffusion probe technique, this ΔT needs to be above 2.5°C [Kravets, 1988]. The R_{set} value used for the drying tests was 932 ohm.

2.2.1.4 Thermal Conductivity Measurement with Compression Effect

For measuring the thermal conductivity of the tissue under compression, the thermistor portion of the compression device was attached to the same circuit as in Sec. 2.2.1.3. The leads of the load cell and linear potentiometer were attached to a strain gage module (NI SCC-SG24), contained within the same signal conditioning box that the circuit was attached to. However, due to the addition of the load cell and potentiometer, a second LabVIEW 8.6 (NI) program was developed to sample the voltage data from the circuit (R_{set} = 832 ohms), along with the load and displacement data at 500 Hz.

2.2.2 Experimental Procedure

Three sets of experiments were conducted to measure the water content of the tissue, the thermal conductivity of tissue under compression, and the thermal conductivity of tissue subjected to both variable water content and compression levels.

2.2.2.1 Desiccation Procedure for Tissue Water Content

In this study, two different methods were used to remove water from the tissue. The first method was a desiccation method, where the tissue was heated in an oven at an elevated temperature to remove the water by evaporation. The second method used electrosurgical forceps to resistively heat the tissue, causing the water within the tissue to vaporize.

In the desiccation method, the water content in canine spleen, heart and liver tissue was measured. Assuming a density of 1 g/ml for the tissue, the water content (V_w) can be calculated from the weight difference between the wet (W_{wet}) and dry (W_{dry}) tissue [Reinoso, 1997]:

$$V_w = \frac{W_{wet} - W_{dry}}{W_{wet}} \tag{2.1}$$

Measurements were conducted at regular intervals, with the sample being removed from the oven, weighed, the thermal conductivity tested, weighed again and then placed

back in the oven. The cumulative time in the oven was measured throughout the process. The water content was measured until the change in W_{dry} for subsequent measurements was less than 1%. Once W_{dry} reached steady state, the corresponding water content value, V_w, from the start of the experiment was determined. Three separate samples of each type of tissue (spleen, heart, and liver tissue) were used. The thermal conductivity of the tissue was determined at regular intervals along with the weight of the tissue. The weight of the tissue determined the water content of the tissue, while the thermistor circuit was used to determine the corresponding thermal conductivity.

The second process for removing water occurs during electrosurgery, as physical changes occur within the tissue as it reaches an elevated temperature and water is given off in the form of steam. The effect of this electrosurgical process on the water content level was studied by cutting out a section of spleen tissue and ablating it using a 5 mm bipolar cutting forceps (Gyrus ACMI #3005PK) attached to an electrosurgical generator (Gyrus ACMI SuperPulse Generator #744000). To ablate the tissue, electrical current was passed through the spleen tissue until the generator indicated that the electrosurgical process was complete. This process was repeated at multiple locations to make sure that the spleen tissue was fully ablated. Once this process was completed, the ablated tissue was subjected to the desiccation process.

2.2.2.2 Tissue Thermal Conductivity with Compression Effect

A section of tissue was cut directly from the spleen tissue and placed into the compression device, as shown in Fig. 2.2(b), for thermal conductivity measurement. The device was clamped down on the tissue until the load cell registered a slight load increase, indicating that contact was made. Adequate contact between the thermistor and tissue is important for minimizing contact resistance errors. The procedure outlined in Sec. 2.2.1.4 was used to measure the thermal conductivity. The baseline thermal conductivity of the spleen tissue was determined at this slightly loaded level. The tissue was then compressed further and subsequent thermal conductivity readings were taken. The experiment continued until the device reached its maximum compression level. Tissue

compression was limited by the exposed thermistor. If the tissue would have been compressed further, the thermistor would have been damaged.

2.2.2.3 Tissue Thermal Conductivity Due to Compression and Varying Water Content

To examine the combined effect of varying the water content and compression on the thermal conductivity of the spleen tissue, the spleen tissue was first desiccated and then subjected to the compression process outlined previously. Since the section of tissue cut from the spleen was larger than the area of tissue subjected to compression, a mathematical representation of the water loss occurring in the tissue under compression is needed. This water loss is then used to determine the final water content, V_{wf}, of the tissue after compression. Figure 2.3(a) shows a schematic of the tissue sample before compression, while Fig. 2.3(b) shows the tissue after compression. Figure 2.3(c) shows a flow chart for the calculation of the final tissue water content level after compression.

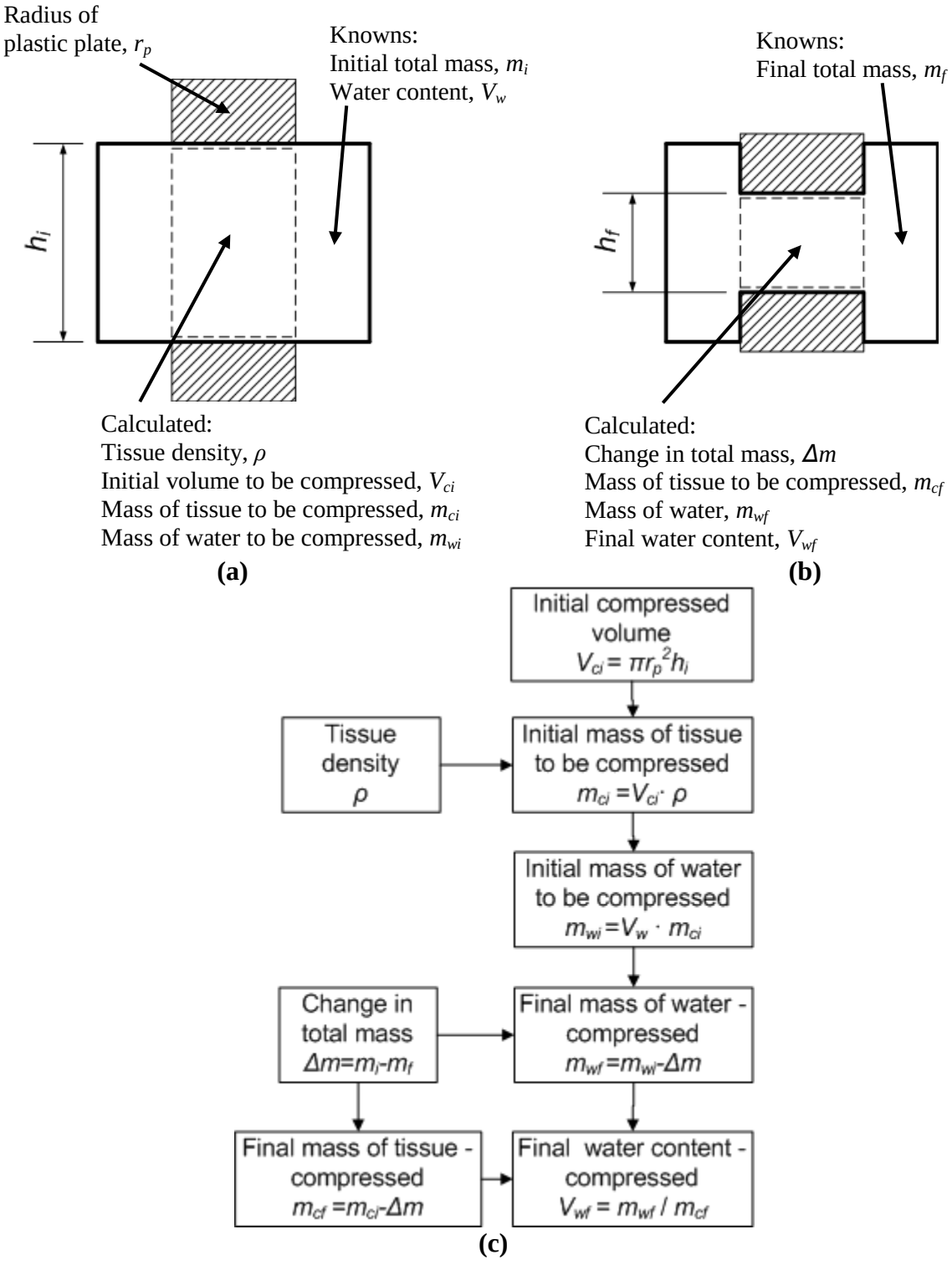

Figure 2.3 Schematic used to calculate the water content of the tissue (a) initial state before compression and (b) after compression and (c) flow chart for calculating final water content. (Shaded blocks represent the cylindrical plastic plates for tissue compression, while the dotted lines represent the volume of tissue to be compressed)

The first step in determining the water loss is to determine the initial volume of tissue that will be under compression, $V_{ci} = \pi r_p^2 h_i$, where r_p is the radius of the plastic plate. The mass of the tissue under compression, m_{ci}, is calculated by multiplying the volume, V_{ci}, by the apparent density of the tissue, ρ. The apparent density of the tissue is calculated by [Perez and Calvelo, 1984]:

$$\rho = \frac{\rho_o(1-V_{wo})}{(1-V_w)\left[1-\frac{\rho_o V_{wo}}{\rho_w}+\frac{\rho_o V_w(1-V_{wo})}{\rho_w(1-V_w)}+m(V_{wo}-V_w)^n\right]} \tag{2.2}$$

where V_{wo} is the original water content of the tissue, V_w is the water content of the tissue at the measurement, ρ_w is the density of water, ρ_o is the original density of the tissue (1053 kg/m^3), and m=0.186 and n=1.74 [Perez and Calvelo, 1984]. The mass of the water within the tissue to be compressed is calculated by multiplying V_w by m_{ci}.

Then by assuming that all of the total mass change ($\Delta m = m_i - m_f$) during the compression process occurs due to water being expelled from the compressed tissue and that there is no change in the density of the tissue, the mass of water within the tissue being compressed can be calculated from $m_{wf} = m_{wi} - \Delta m$. The final mass of the tissue, m_{cf}, is calculated by subtracting Δm from m_{ci}. The final water content of the compressed tissue, V_{wf}, is found by dividing m_{wf} by m_{cf}.

2.3 Thermal Conductivity Model

The Maxwell-Eucken model is further developed to predict the tissue thermal conductivity at different water content and compression levels. This model has been applied to a variety of foods, such as meats [Perez and Calvelo, 1984], vegetables [Maroulis et al., 1990], and multi-phase porous breads [Hamdami et al., 2003]. However, none of these models were applied to foods under compression or the combination of varying water content and compression. In this study, the thermal conductivity of a three-phase material (tissue, water and air) is represented by the Maxwell-Eucken model

[Eucken, 1940]. The model is applied to predict the tissue thermal conductivity subjected to varying water contents and compression levels.

The original Maxwell-Eucken model was developed for a two-phase system. By adding a second step to the model, a three-phase system can be considered [Perez and Calvelo, 1984; Hamdami et al., 2003]. In the first step, a continuous phase of dry fiber is modeled with a discontinuous phase of water. The resulting thermal conductivity is then used as the continuous phase, within a discontinuous phase of air in the second step to find the overall the thermal conductivity of the three-phase system. The effective thermal conductivity of the tissue, k, is [Perez and Calvelo, 1984]:

$$k = k_c \frac{1-(1-\alpha k_a / k_c)\beta}{1+(\alpha-1)\beta} \tag{2.3}$$

where $\alpha = 3k_c/(2k_c+k_w)$ and $\beta = 1(\rho/\rho')$, k_a is the thermal conductivity of the air, k_w is the thermal conductivity of water (0.61 W/m·K) [Nieto de Castro, 1986], ρ_w is the density of water, ρ' is the bulk density, and k_c the thermal conductivity of the continuous matrix is defined by [Perez and Calvelo, 1984]:

$$k_c = k'_c \frac{1-(1-\alpha' k_w / k'_c)\beta'}{1+(\alpha'-1)\beta'} \tag{2.4}$$

where k'_c is the thermal conductivity of the dry fiber, $\alpha' = 3k'_c/(2k'_c+k_w)$, and $\beta' = V_w(\rho'/\rho_w)$. When air is not considered ($m = 0$ in Eq. (2.2)) in the material, the apparent density is equivalent to the bulk density ($\rho = \rho'$), which gives [Perez and Calvelo, 1984]:

$$\rho' = \frac{1}{\frac{V_w}{\rho_w} + \frac{(1-V_w)}{(1-V_{wo})}\left(\frac{1}{\rho_o} + \frac{V_{wo}}{\rho_w}\right)} \tag{2.5}$$

The Maxwell-Eucken model can then be used to predict the thermal conductivity of the dry tissue fibers, k'_c, based on the thermal conductivity results obtained during the desiccation process. First, using the original water content of the tissue (V_{wo}), and the

water content of the tissue (V_w) at each measurement point, the instantaneous apparent and bulk density can be calculated. Since k is known from the experimental data, k_c' can be calculated by fitting Eq. (2.3) to the experimental data. This is done by using a least squares fit to minimize the residual between the k from the experimental data and the k calculated by the model. By iteratively fitting the model to the experimental data, the k_c' value can be calculated.

Once the thermal conductivity of the dry fiber is known, the thermal conductivity of the tissue subjected to compression can be predicted. Eqs. (2.3) and (2.4) are again used to predict the thermal conductivity of the tissue at both the beginning of the experiment (0% compression) and then at the final compression point. First, at the beginning of the experiment, the thermal conductivity is predicted by using the determined k_c' value, the initial water content of the tissue, V_{wo}, the measured water content of tissue, V_w, and Eqs. (2.2), (2.3) and (2.4). As the tissue is compressed, the water is expelled, and the process for predicting the thermal conductivity at the final compression point changes.

At the final compression point, the final water content of the tissue, V_{wf}, is determined by using the method presented in Sec. 2.2.2.3. Then by replacing the water content before compression, V_w, with the final water content value, V_{wf}, and making the assumption that all of the air within the tissue is lost due to the compressive effect, Eqs. (2.3), (2.4) and (2.5) are re-solved. The resulting values are then used to predict the thermal conductivity of the tissue at the final compression level.

2.4 Tissue Water Content Results

2.4.1 Water Content of Spleen Tissue

The average value and error bars for three test runs of tissue water fractional loss and water content, V_w, as a function of heating time for the spleen tissue, are shown in Fig. 2.4. The water fractional loss is defined as the change in the tissue weight during drying, divided by the tissue weight before drying. After drying the tissue for more than 78 h at 60°C, the water fraction loss of spleen tissue reaches a steady state of about 70% and V_w

approaches 0%. This result is similar to results found in the literature for other mammalian tissues [Cooper and Trezek, 1971; Tisavipat et al., 1974].

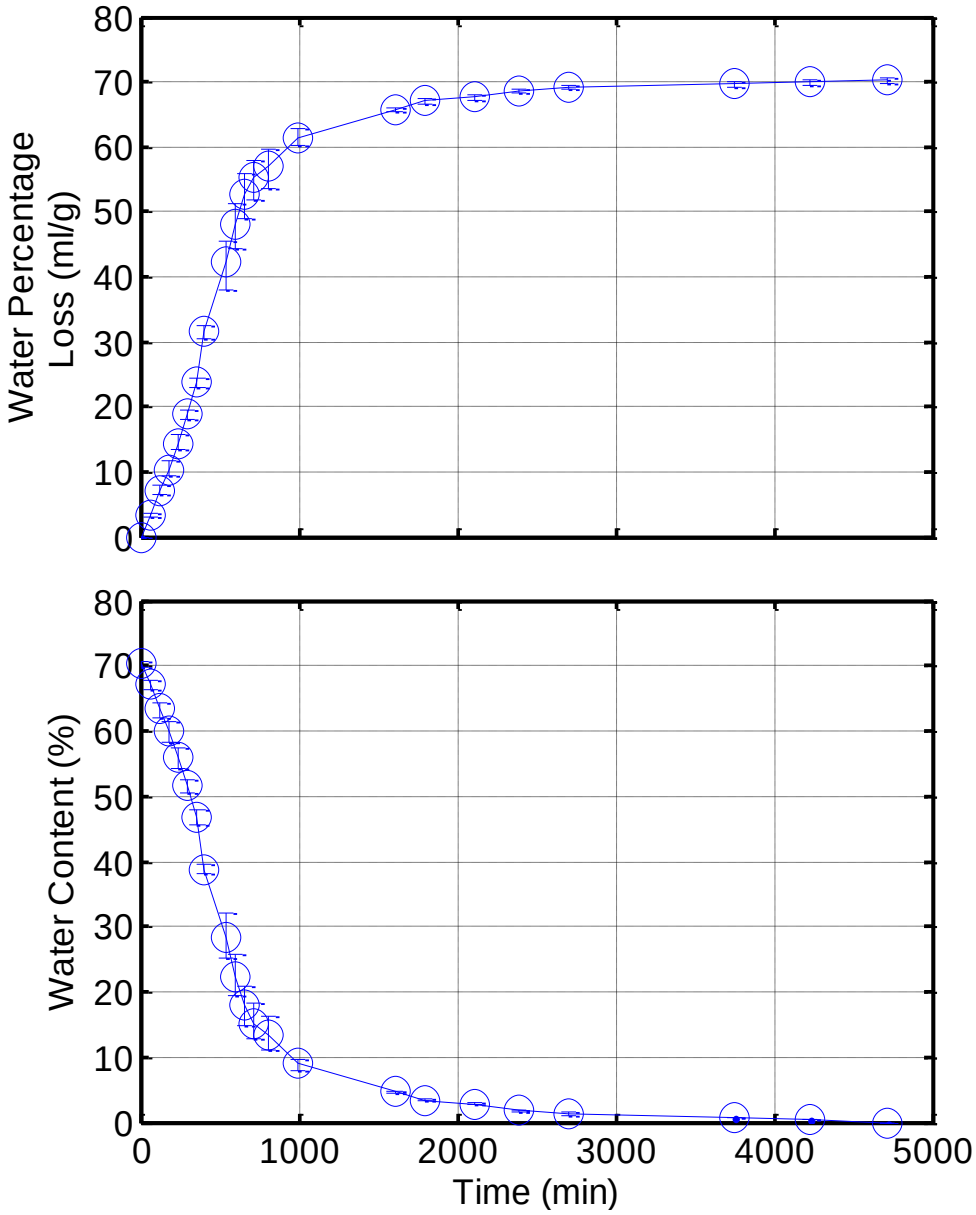

Figure 2.4 Tissue water percentage loss and the corresponding water content of spleen tissue.

2.4.2 Water Content of Ablated Spleen Tissue

After the electrosurgical ablation process, the water content, V_w, of the spleen tissue is about 59%, as shown in Table 2.1. The water content of the tissue is reduced by only 11%

after electrosurgical process. Based on this, the key water content range for the thermal conductivity measurements is roughly between 60% to 70%, since this is the water content range at which the electrosurgical process is affecting the tissue the most.

Table 2.1 Water contents for the four tests and the corresponding drying time needed.

Tissue Type	Water Content (%)	Drying Time (min)	k'_c (W/m·K)
Spleen	70	4710	0.31
Ablated Spleen	59	2070	-
Liver	69	4560	0.31
Heart	76	4560	0.32

2.4.3 Water Content of Heart and Liver Tissue

The water content for the heart and liver tissues is shown in Table 2.1. The water content was 69% for the liver tissue and 76% for the heart tissue. Compared to the spleen tissue, the heart tissue has a higher water content due to the higher volume fraction of blood. Reinoso et al. [1997] has shown the same trend for rat tissues, in which the highest water content was found in the heart; then the spleen, with the liver having the lowest water content.

2.5 Effect of Water Content on Thermal Conductivity

2.5.1 Experimental Results

Figure 2.5 shows the measured spleen thermal conductivity and the predicted Maxwell-Eucken thermal conductivity values. As the water content within the spleen tissue is reduced, the tissue thermal conductivity decreases. The initial thermal conductivity of the tissue was found to be 0.48 W/m·K at the 70% water content level. Previously, Yuan et al. [1993] had found the thermal conductivity of canine spleen to be 0.54 W/m·K immediately after euthanization. The thermal conductivity of the tissue had minimal changes until the water content level was below 50%. Once this water content level was reached, the thermal conductivity began to drop and at the 20% level, the thermal conductivity of the spleen had fallen by 43%. The 20% water content value was

the lowest water content level in which the thermal conductivity could be determined accurately. At lower water content levels, the contact between tissue and thermistor deteriorated, making readings susceptible to large amounts of error. Since the water in the tissue is the primary carrier medium for the thermal energy, as the percentage of water in the tissue is reduced, the thermal conductivity of the tissue will decrease. The modeling results, to be discussed later in Sec. 2.5.2, further confirm this observation.

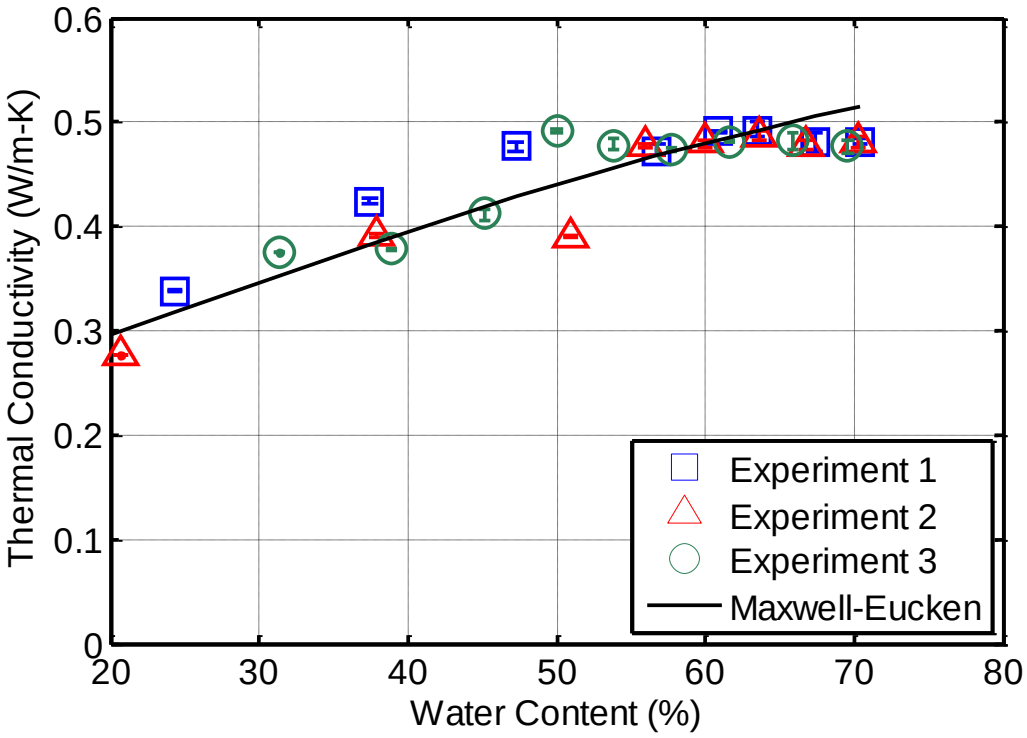

Figure 2.5 Tissue thermal conductivity of spleen tissue as the water content level of the tissue is reduced. The water content level of the tissue at the time of measurement is determined through the results of Fig. 2.4.

Figure 2.6 shows that the heart and liver tissue thermal conductivity results are also very dependent on the water content. Initially, the thermal conductivity of the heart tissue was 0.50 W/m·K at a water content level of 76%, while the liver tissue had a thermal conductivity of 0.49 W/m·K at a water content level of 69%. For the heart tissue, as the water content level was reduced to 33%, there was an overall reduction in the thermal conductivity of 17%, while the liver tissue thermal conductivity was reduced by 29% at a water content level of 31%.

The desiccation process subjected the tissue to temperature of 60°C for an extended period of time. However, the effect of this extended heating time was not accounting for in the thermal conductivity results. It is possible that protein denaturing is occurring during the desiccation process, which may alter the thermal conductivity of the tissue fiber. Thermal denaturization of collagen generally occurs around 60°C, however depending on the experimental conditions this can vary from 48-97°C [Thomsen, et al., 1989]. Bhattacharya and Mahajan [2003] have shown that heating cow liver up to 80°C and then cooling it, causes no hysteresis effect in the thermal conductivity results. Based on these results, it is expected that the effect of the desiccation process on thermal conductivity results should be minimal. However, the desiccation process subjected the tissue to an elevated temperature for a much longer time period and the effect of this on the thermal conductivity may need to be examined further.

The overall reduction in the tissue thermal conductivity agrees with the results observed by Cooper and Trezek [1971], Sweat [1986] and Perez and Calvelo [1984]. . However, Cooper and Trezek [1971] did not present water content results below 66%, while both Sweat [1986] and Perez and Calvelo [1984] showed that for meats, as the water content was reduced, the thermal conductivity of the tissue also was reduced.

When the water content of the spleen tissue was reduced from 70% to 60%, the range in which the tissue water content was affected by the electrosurgical ablation (Sec. 2.4.2), the thermal conductivity of the spleen tissue remained nearly constant, as shown in Fig. 2.5. For the liver tissue, Fig. 2.6(a) shows that this drop in water content, from 70% to 60%, only reduced the thermal conductivity by 5%, while Fig. 2.6(b) shows that the heart tissue thermal conductivity was reduced by 6% over this range. Independent of the tissue type, the overall reduction in thermal conductivity over this range is minimal. Therefore, there appears to be little impact on the thermal conductivity of the tissue during electrosurgery purely due to the drying effect.

2.5.2 Maxwell-Eucken Modeling Prediction

The Maxwell-Eucken model was applied to analyze the experimental data to predict the effect of water content on the thermal conductivity. Modeling results are shown as a

solid line in Fig. 2.5 for the spleen tissue, Fig. 2.6(a) for the liver tissue, and Fig. 2.6(b) for the heart tissue. For the spleen and liver tissues, the model fit the experimental data very well throughout the entire water content range. Most of the experimental data was within 10% of the predicted thermal conductivity. This validates the model and enables the prediction of tissue thermal conductivity for a given water content.

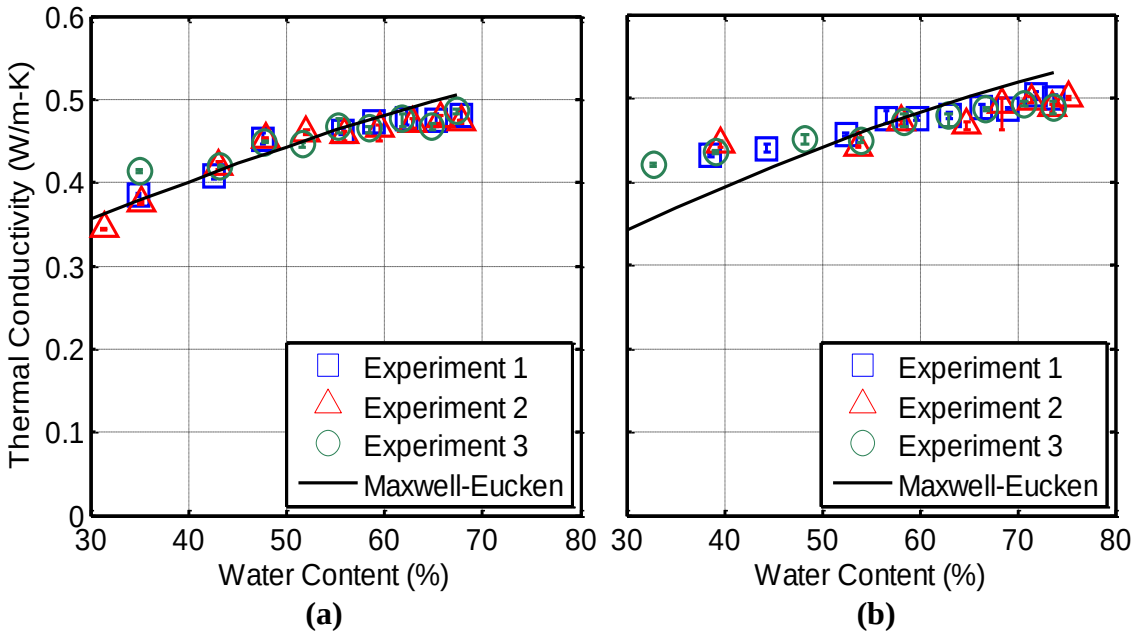

Figure 2.6 Tissue thermal conductivity of (a) liver and (b) heart tissue as the water content level of the tissue is reduced.

For the spleen tissue, the model tended to slightly over predict the thermal conductivity of the tissue above 65% water content. This over prediction of the experimental results was caused by the relatively constant thermal conductivity over the 50-65% range, coupled with the steep decline once the water content level fell below 50%. This phenomena caused the k'_c value to be 0.31 W/m·K. In general, the Maxwell-Eucken model fit the data very well throughout the entire range of values. For the liver tissue, the Maxwell-Eucken model also fit the data very well throughout the entire range of values, and the k'_c value was also 0.31 W/m·K. However, for the heart tissue, the k'_c value was higher than the other two tissues, 0.32 W/m·K. This higher heart tissue k'_c caused the predicted thermal conductivity values to not fit as well at the ends of the experimental data.

For the higher water content levels, the model tended to over predict the thermal conductivity, while at the lower water content levels the model under predicted the thermal conductivity. This difference between the model and the experiment occurred due to: (1) there are more data points at the higher water content levels and (2) the measured thermal conductivity of the heart tissue did not drop off at the lower water content levels as compared to the spleen and liver tissues. Since the fit minimizes the residual between the experimental and modeling results, the model is closer to the cluster of data points at the higher water content level and further away at the lower level water content levels.

2.6 Effect of Compression on Thermal Conductivity

Figure 2.7 shows the effect of compression on the spleen tissue thermal conductivity. The tissue was sectioned from the spleen and placed into the device. The water content level for this set of experiments was determined to be 71%. At 0% compression, the average thermal conductivity of the seven tests was 0.49 W/m·K. When compared to the thermal conductivity results obtained in Sec. 2.5.1, the results are within 4% of each other.

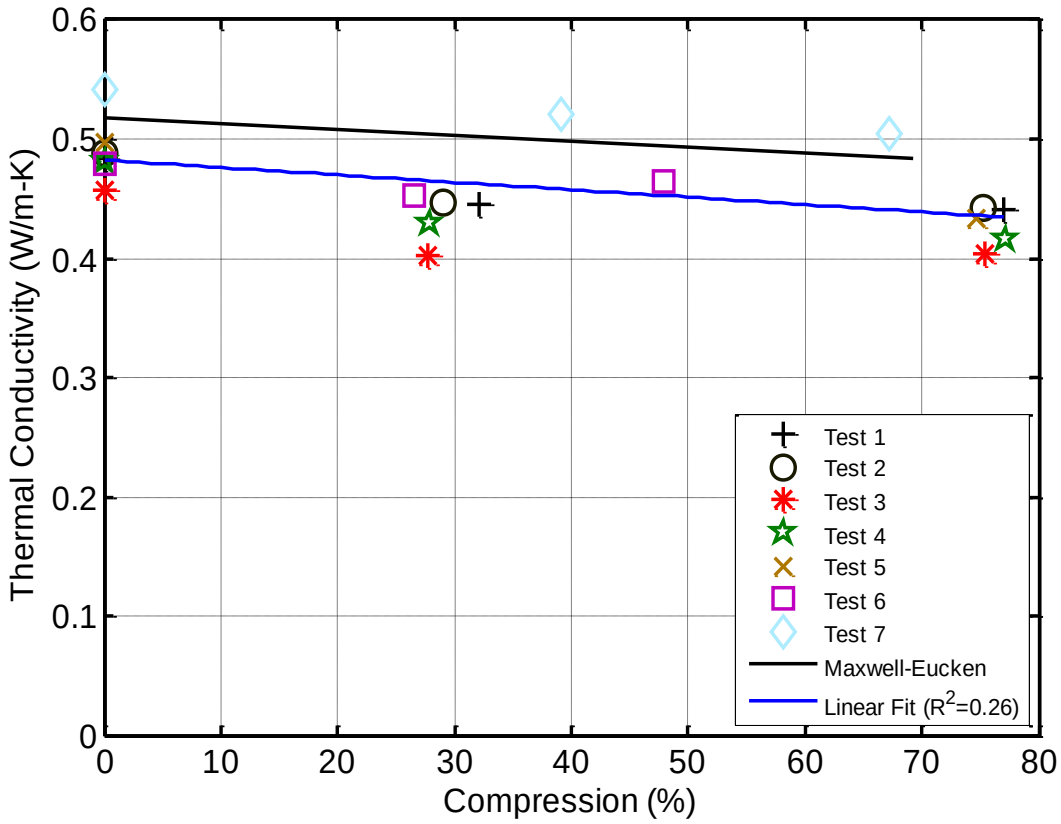

Figure 2.7 Spleen thermal conductivity as a function of compression level for the 71% tissue water content level. Maxwell-Eucken model is shown by the solid black line, while the linear regression is indicated by the blue line.

As the level of compression increased, the amount of water within the tissue was reduced. This reduction in tissue water content caused the thermal conductivity of the tissue to fall. The average final compression of the spleen tissue was 69%. A linear regression was applied to the thermal conductivity results and indicated an overall decrease in thermal conductivity to 0.44 W/m·K at the 69% compression level. The large variation in the experimental data occurred because the tissue used in the experiment was from multiple spleens and different regions within each spleen.

By measuring the change in height of the electrodes on the Gyrus ACMI 5 mm bipolar cutting forceps, an estimate of the level of tissue compression during surgery can be made. The open electrodes of the forceps had a height of 7 mm. When the electrodes were clamped down on the tissue, this height was reduced to 0.7 mm, leading to a compression level of 90%. This compression level exceeds the compression level

possible with the current setup, due to the exposed thermistor. This would indicate that during electrosurgery, the tissue thermal conductivity is likely to decrease even further.

The Maxwell-Eucken model was then applied to the experimental data, as shown by the solid line in Fig. 2.7. The model predicted a slightly higher initial thermal conductivity of 0.52 W/m·K at the 0% compression level. As the tissue was compressed to 69%, the thermal conductivity fell to 0.48 W/m·K. At the 0% compression level, the model was within 6% of the average experimental thermal conductivity result. As the compression level increased, the difference between the model and the experimental results increased slightly to 9%. From the mathematical model of Sec. 2.2.2.3, there was a 12% reduction in the tissue water content when it was subjected to the compressive effect.

It is important to note that the mathematical model is likely under predicting the amount of water lost from the compressed region since the model assumed that the change in water content was directly related to change in mass for the entire piece of tissue. This assumption does not account for water compressed out of the tissue and into the surrounding uncompressed tissue. Accounting for this water loss will reduce V_{wf} further and will result in a lower thermal conductivity prediction from the Maxwell-Eucken model. Therefore, developing a method to determine the water loss into the nearby tissue needs to be undertaken to improve the fit of the model to the experimental data.

2.7 Effect of Combined Water Content and Compression on Tissue Thermal Conductivity

Figure 2.8 shows the thermal conductivity of compressed spleen tissue with water content levels reduced to 64% and 54% (from the original 71%). At the 64% water content level, the thermal conductivity measured using the compression device (Fig. 2.1) with light initial contact averaged 0.5 W/m·K, which corresponded well to the experimental results shown Fig. 2.5. As the tissue was compressed similar to the results of Fig. 2.7, the thermal conductivity also was reduced. At an average compression level of 71%, the value of the linear regression was 0.42 W/m·K. The R^2 value for the linear

regression fit to the experimental thermal conductivity results was 0.46. The reduction in the thermal conductivity is caused by the loss of the water within the tissue as it is compressed. The Maxwell-Eucken model also predicted a similar reduction in thermal conductivity.

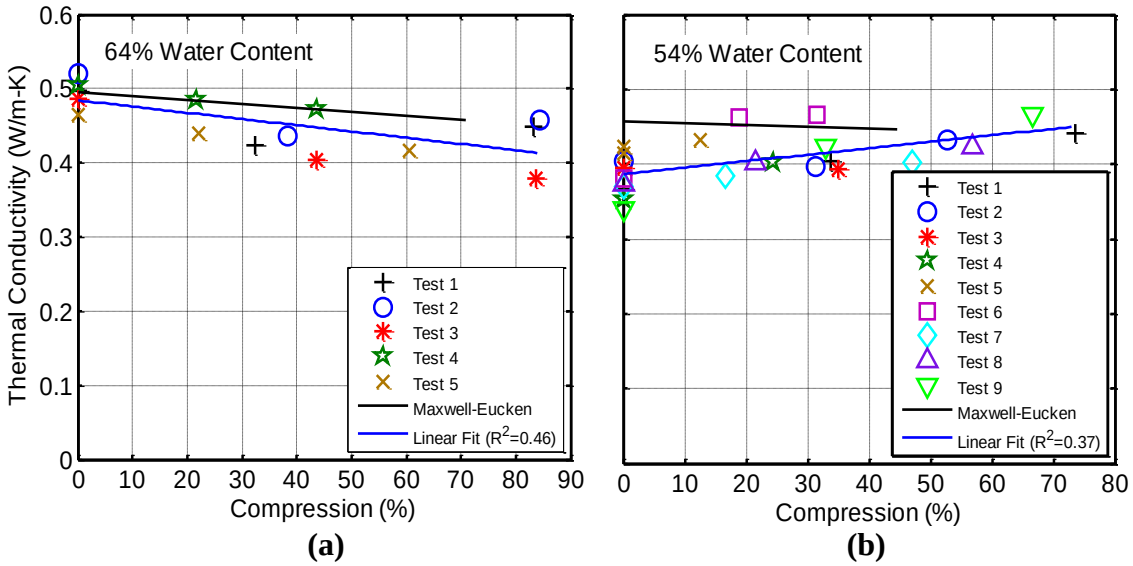

Figure 2.8 Spleen thermal conductivity as a function of compression level for (a) 64% and (b) 54% tissue water content level. The Maxwell-Eucken model is shown by the solid black line, while the linear regression is indicated by the blue line.

For the tissue further dried to 54% water content, Fig. 2.8(b) shows the thermal conductivity at 0% compression is 0.38 W/m·K; lower than the experimental results shown in Fig. 2.5. As the tissue was compressed, the thermal conductivity of the tissue increased, which is different from the results shown in Fig. 2.8(a). At a compression level of 45%, the linear regression fit indicated a thermal conductivity value of 0.43 W/m·K.

Applying the Maxwell-Eucken model to the data showed a couple of discrepancies. First, the model predicts a higher thermal conductivity value, 0.46 W/m·K at the 0% compression level. Comparing this to the experimental results of Fig. 2.8(b), the model over predicts the thermal conductivity by 19%. However, the model prediction matches well to the results of Sec. 2.5.1 for tissue with a similar water content value (54%). This indicates that the results for this experiment may be experiencing thermistor-tissue

contact issues. Experiments conducted in Sec. 2.5.1 used a fully exposed thermistor bead inserted into tissue, while this experiment uses a partially exposed thermistor bead. At the reduced water content levels, the tissue starts to become porous, while also developing a hard crust on its outer surfaces. Therefore, the tissue may not be making complete contact with the thermistor at the thermistor-tissue interface. This effect introduces air at the contact interface. The air, with a low thermal conductivity, causes the effective thermal conductivity result of the tissue to be lower than expected.

The Maxwell-Eucken results in Fig. 2.8(b) show that as the tissue is compressed, the model predicts a 2% change in the thermal conductivity. However, the experimental results showed a 13% increase in the thermal conductivity. This increase in the experimental results is caused by the air at the tissue-thermistor interface being expelled from the tissue as it is compressed. This effect is not captured by the model, and thus causes the experimental results to rise faster than the model is predicting.

2.8 Conclusions

This study showed that a decrease in the tissue water content level reduced the thermal conductivity of canine spleen, liver and heart tissue. A similar decrease in thermal conductivity was observed in spleen tissue subjected to compression at higher water content levels. The change in thermal conductivity shown during the water content experiment indicated that the water loss during ablation will have little effect on the thermal conductivity. However, when there are significant water content losses in the tissue, the thermal conductivity of the tissue will drop dramatically. In the case of spleen tissue, when the water content level was reduced from 70% to 20% the thermal conductivity fell by 43%. This reduction in tissue thermal conductivity was expected, since the water within the tissue is the primary carrier medium for the thermal energy.

Compression was found to decrease the tissue thermal conductivity. For spleen tissue that had not been subjected to desiccation, the tissue thermal conductivity fell by 9% after 69% compression. Desiccating the tissue to an average water content level of 64% had a similar decrease in the thermal conductivity (12%) as the tissue was compressed by 71%.

The Maxwell-Eucken model predicted a comparable reduction in the thermal conductivity, and was within 12% of the experimental results.

Further investigation into how the air and fluids within the tissue are transported during compression and the resulting change in the thermal conductivity is needed. As the fluids and air within the tissue are lost, the cellular structure will change, but how this structural change impacts the thermal conductivity has not been identified. This effect, along with the thermal conductivity results obtained from this experiment, can then be used to improve the finite element models applied to study thermal transport phenomenon during surgery. This will enhance both the understanding of the overall physical tissue temperature interactions, as well as allow for improvement in the algorithms used to control the energy being delivered during surgical processes.

References

Anderson, G.T., Valvano, J.W., and Santos, R.R. (1992), "Self-heated thermistor measurements of perfusion," *IEEE Transactions on Biomedical Engineering*, Vol. 39, pp. 877-885.

Baish, J.W. (2006), "Thermal conductivity measurements of biomaterials." In: *Encyclopedia of Biomedical Engineering*," John Wiley and Sons, New Jersey.

Balasubramaniam, T.A., and Bowman, H.F. (1977), "Thermal conductivity and thermal diffusivity of biomaterials: A simultaneous measurement technique," *Journal Biomechanical Engineering, Transactions ASME*, Vol. 99, pp. 148-154.

Bhattacharya, A. and Mahajan, R.L. (2003), "Temperature dependence of thermal conductivity of biological tissues," *Physiological Measurement*, Vol. 24, pp. 763-783.

Bowman, H.F., Cravalho, E.G, and Wood, M., (1975), "Theory, measurement, and application of thermal properties of biomaterials," *Annual Review of Biophysics and Bioengineering*, Vol. 4, pp. 43-80.

Chang, I., (2003), "Finite element analysis of hepatic radiofrequency ablation probes using temperature-dependent electrical conductivity," *Biomedical Engineering Online*, Vol. 2(12), pp. 1-18.

Chato, J.C., (1968), "A method for the measurement of thermal properties of biological materials," *Thermal Problems in Biotechnology*, American Society of Mechanical Engineers, New York: pp. 16-25.

Chen, M.M., Holmes, K.R., and Rubinskas, V., (1981), "Pulse-decay method for measuring the thermal conductivity of living tissues," *Journal of Biomechanical Engineering*, Vol. 103, pp. 253-260.

Cooper, T.E., and Trezek, G.J., (1971), "Correlation of thermal properties of some human tissue with water content," *Aerospace Medicine*, Vol. 42, pp. 24-27.

Cooper, T.E., and Trezek, G.J., (1972), "A probe technique for determining the thermal conductivity of tissue," *Journal of Heat Transfer*, Vol. 94, pp. 133-138.

Dodde R.E., Miller, S.F., Geiger, J.D., and Shih, A.J., (2008), "Thermal-electric finite element analysis and experimental validation of bipolar electrosurgical cautery," *Journal of Manufacturing Science and Engineering*, Vol. 130, pp. 021015-1-8.

Eucken, A., (1940), "Allgemeine gesetzmassig keiten für das wärmeleitvermögen verschiedener stoffarten und aggregatzustände," *Forschung Gebeite Ingenieur*, Vol. 11(1), pp. 6-20.

Hamdami, N., Monteau, J.Y., and Le Bail, A., (2003), “Effective thermal conductivity of a high porosity model food at above and sub-freezing temperatures,” *International Journal of Refrigeration*, Vol. 26, pp. 809-816.

Harold, K.L., Pollinger, H., Matthews, B.D., Kercher, Sing, R.F., and Heniford, T., (2003), “Comparison of ultrasonic energy, bipolar thermal energy, and vascular clips for the hemostasis of small-, medium-, and large-sized arteries,” *Surgical Endoscopy*, Vol. 17, pp. 1228-1230.

Kravets, R.R., (1988), “Determination of thermal conductivity of food materials using a bead thermistor,” *Ph.D. Thesis in Food Science and Technology, Virginia Polytechnic Institute and State University.*

Maroulis, Z.B., Drouzas, A.E., and Saravacos, G.D., (1990), “Modeling of thermal conductivity of granular starches,” *Journal of Food Engineering*, Vol. 11(4), pp. 255-271.

Matthews, B.D., Pratt, B.L., Backus, C.L., Kercher, K.W., Mostafa, G., Lentzner, A., Lipford, E.H., Sing, R.F., and Heniford, B.T., (2001), “Effectiveness of the ultrasonic coagulating shears, LigaSure vessel sealer, and surgical clip application in biliary surgery: A comparative analysis,” *The American Surgeon*, Vol. 67, pp. 901-906.

Nieto de Castro, C.A., Li, S.F.Y., Nagashima, A., Trengrove, R.D., and Wakeham, W.A., (1986), “Standard reference data for the thermal conductivity of liquids,” *Journal of Physical Chemistry Reference Data*, Vol. 15, pp. 1073-1086.

Olsrud, J., Friberg, B., Ahlgren, M., and Persson B.R.R., (1998), “Thermal conductivity of uterine tissue *in vitro*,” *Physics in Medicine and Biology*, Vol. 43, pp. 2397-2406.

Ong, A.M., Su, L-M., Varkarakis, I., Inagaki, T., Link, R.E., Bhayani, S.B., Patriciu, A., Crain, B., and Walsh, P.C., (2004), "Nerve sparing radical prostatectomy: Effects of hemostatic energy sources on the recovery of cavernous nerve function in a canine model," *Journal of Urology*, Vol. 172, pp. 1318-1322.

Patel, P.A. Valvano, J.W., Pearce, J.A., Prahl, S.A., and Denham, C.R., (1987), "A self-heated thermistor technique to measure effective thermal properties from the tissue surface," *Journal of Biomechanical Engineering*,” Vol. 109, pp. 330-335.

Perez, M.G.R., and Calvelo, A., (1984), “Modeling the thermal conductivity of cooked meat,” *Journal of Food Science*, Vol. 49(1), pp. 152-156.

Reinoso, R.F., Telfer, B.A., and Rowland, M., (1997), “Tissue water content in rats measured by desiccation,” *Journal of Pharmacological and Toxicological Methods*, Vol. 38, pp. 87-92.

Sweat, V.E., (1986), “Thermal Properties of Foods.” In: Rao, M.A. and. Rizhvi, S.S.H, Editors, *Engineering Properties of Foods*, Marcel Dekker, New York, pp. 49–87, Chapter 2.

Thomsen, S., Pearce, J.A., and Cheong, W.F., (1989), “Changes in birefringence as markers of thermal damage in tissues,” *IEEE Transactions on Biomedical Engineering*, Vol. 36, pp. 1174-1179.

Tisavipat, A., Vibulsreth, S., Sheng, H.P., and Huggins R.A., (1974), “Total body water measured by desiccation and by tritiated water in adult rats,” *Journal of Applied Physiology*, Vol. 37(5), pp. 699-701.

Valvano, J.W., Cochran, J.R., and Diller, K.R., (1985), “Thermal conductivity and diffusivity of biomaterials measured with self-heated thermistors,” *International Journal of Thermophysics*, Vol. 6, pp. 301-311.

Yang, D., Converse, M.C., Mahvi, D.M., and Webster, J.G., (2007), “Expanding the bioheat equation to include tissue internal water evaporation during heating,” *IEEE Transactions on Biomedical Engineering*, Vol. 54, pp. 1382-1388.

Yuan, D.Y., Valvano, J.W., and Anderson, G.T., (1993), “Measurement of thermal conductivity, thermal diffusivity, and perfusion,” *Biomedical Sciences Instrumentation*, Vol. 29, pp. 435-442.

CHAPTER 3

VESSEL TISSUE TEMPERATURE PROFILE DURING BIPOLAR ELECTROSURGICAL SEALING

ABSTRACT

Experimental temperature profile analysis of bipolar electrosurgical vessel sealing in a porcine model was conducted. Electrosurgical sealing utilizes electrical energy to coagulate and denature proteins in the vessel, creating a bond. The femoral artery and mesenteric artery vasculature were sealed and the temperature distributions in the vessel tissue and the electrical voltage and current were measured. The maximum temperature at 1 mm away from the edge of the electrode was measured to be about 83°C for both the femoral artery and mesenteric artery vasculature. The temperature profile and electrical voltage and current delivered in each pulse were analyzed to predict change in the tissue impedance and water content during vessel sealing. Results in both vessel sealing experiments show that, during the first three to four pulses, the tissue impedance remains relatively constant. In subsequent pulses, the tissue water content decreased as the tissue temperature increased from resistive heating. This was indicated by the increasing tissue impedance and the reduction in temperature increase per pulse.

3.1 Introduction

Blood vessel sealing is important to prevent the loss of excessive amounts of blood during surgery. Typically, this sealing is accomplished by ligating the vessel [Siperstein et al., 2002], applying a vessel clip [Spivak et al., 1998] or by using an ultrasonic or electrosurgical device [Underwood et al., 1998]. Electrosurgical devices are widely used for both cutting and sealing of tissue during surgery. During electrosurgery, an electrical current is sent through the tissue, which generates the resistive heating and causes the proteins in the tissue to denature into a colloidal state that forms a permanent seal [Heniford et al., 2001].

There are two types of electrosurgery: bipolar and monopolar. In bipolar electrosurgery, both the active and passive electrodes are contained within a single device. The tissue is clamped between two electrodes and the electrical current passes through the tissue. This is different from monopolar electrosurgery, in which an active electrode is held in the surgeon's hand and a grounding electrode is placed under the patient with the current passing through the body [Lee and Lambert, 2001]. Modern bipolar electrosurgical devices use high current (4 A), low voltage (<200 V) energy to seal vessels [Carbonell et al., 2003]. This electrical current heats the tissue and generates a large thermal spread to the surrounding tissue, which in turn exposes the vessel tissue to high temperatures [Carlander et al., 2005].

High tissue temperature during electrosurgery alters the biological properties of the tissue permanently. As the tissue is heated, melting of the collagen and elastin within the tissue occurs as the tertiary hydrogen bonds between the collagen and the matrix denature and realign [Thomsen et al., 1989]. Once the heat is removed from the tissue, the collagen cools and realigns, which permanently alters the state of the collagen and creates a flexible seal within the tissue [Matthews et al., 2001]. The temperature at which tissue damage begins varies widely in the literature as it is temperature, time, and tissue type dependent [Eman and Cuschieri, 2003; Reidenbach and Buess, 1992]. Eman and Cuschieri [2003] determined that protein denaturing occurred above 60°C, as the tissue turns from a colloidal state into an insoluble gel. Reidenbach and Buess [1992] observed

that protein denaturing was occurring at temperatures as low as 45°C with suitable vessel occlusion.

During electrosurgery, surgeons typically use visual cues, such as tissue drying, shrinkage, whitening, disruption, charring, combustion, and/or ablation [Thomsen et al., 1989], to determine if the tissue has reached an elevated temperature. However, using these visual cues as a confirmation method is imprecise, as they may not be accurately predicting the internal tissue damage.

The level of thermal damage depends on several factors, including the tissue being sealed, power level and sealing time [Washington et al., 2003]. Using a 5 mm bipolar scalpel, Campbell et al. [2003] showed that the average thermal spread was 4.4 mm. However, this thermal spread was coupled with a bipolar jaw temperature of 97°C, which in turn took 14 s for the jaw to equilibrate back to the ambient temperature. These results are similar to the thermal spread obtained by Harold et al. [2003], which indicated that the thermal spread was 3.3 mm when sealing a 6 to 7 mm vessel. However, the past research did not quantify the level and profile of vessel temperature during the sealing process. Thus, this becomes one of the goals of this research.

As the size of the vessel increases, the sealing time must increase in order for a quality seal to be formed. However, this increase in sealing time causes more energy input into the vessel and causes the temperature to rise in the surrounding tissue. A better understanding of the thermal damage to surrounding tissue during electrosurgical vessel sealing is needed, since limiting the thermal spread to nearby nerves is of great importance [Carlander et al., 2005]. The goal of this research is to better understand the temperature profile in the vessel during sealing and to study how the changes in impedance and temperature are related to the tissue water content. The influence of vessel size and type are also investigated.

In this study, using a porcine model, *in vivo* vessel sealing is used to examine the thermal profile of the femoral artery and mesenteric artery vasculature during bipolar electrosurgical vessel sealing. The tissue temperature at specific locations on the vessel, and the voltage and current data from the electrosurgical device is measured. The impedance of the tissue and the tissue temperature change during each electrical pulse are

calculated and related to the changes in tissue water content during the electrosurgery process.

3.2 In Vivo Vessel Sealing Experiment

By using an *in vivo* animal model for sealing the blood vessels, the corresponding thermal profile within the vessel tissue replicates the conditions that would be seen during surgery. The *ex vivo* setting for vessel sealing can lead to inaccurate temperature results as there is no simple way to replicate the flow of blood at body temperature through the vessel as it is being sealed.

3.2.1 Experimental Setup

A porcine (50% Duroc, 25% Yorkshire and 25% Landrace) model weighing approximately 45 kg was used for the *in vivo* vessel sealing experiments at the University of Michigan Medical School under an approved animal protocol. Anesthesia was induced in the animal with an intramuscular injection of Telazol® (6 mg/kg) mixed with Xylazine (2.2 mg/kg). The animal was intubated and placed under general anesthesia using Isoflurane (2 to 2.5%). The animal was then placed on a ventilator (10 ml/kg) at 12 bpm. Oxygen saturation, pulse rate, and respiratory rate were monitored with pulse oximetry at regular intervals.

The 5 mm bipolar cutting forceps (Gyrus ACMI #3005PK), as shown in Fig. 3.1, were used to seal the vessels. The device was attached to a generator (Gyrus ACMI, SuperPulse Generator #744000), which was set to the VP1 setting with a power level of 30 W. The leads of the device were attached to a digital oscilloscope (Agilent #54833A) in peak detect mode with a 100:1 high voltage probe (Agilent 10076A) and a current probe (Agilent 1147A). The voltage and current data were collected at 10 kHz. Using Ohm's law, the impedance of the tissue was determined by dividing the voltage by the current [Pasic et al., 2007].

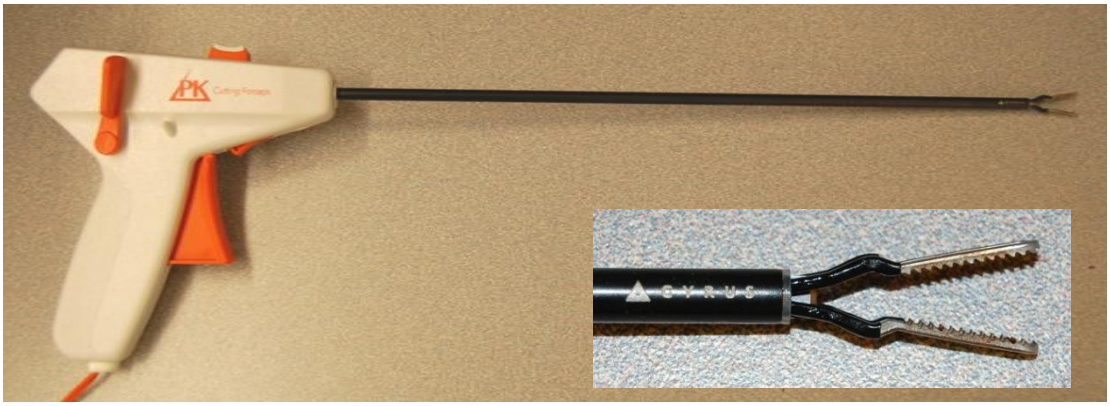

Figure 3.1 The bipolar electrosurgical device used in this study and a close-up view of electrode tip.

The tissue temperature was measured using a series of thermistors set into a polycarbonate fixture, as shown in Fig. 3.2. The polycarbonate fixture, epoxied to the top of the electrodes, held the thermistors in position relative to the edge of the electrode. Three thermistors were epoxied into the fixture with the tip exposed to a depth of 0.75 mm. In the fixture, the distance between the edge of the electrode and the three thermistors were 1, 2 and 3 mm, corresponding to Thermistor #1, #2 and #3, respectively. The micro thermistor (Alpha Technics Model #56A1002-C8) used in this study has an outside diameter of 0.46 mm. The measurement tolerance is ±0.1°C at 25°C with a time constant of 250 ms. A data acquisition system sampling at 40 Hz was utilized to record thermistor data. It should be noted that the thermistors were reading a surface temperature, as no puncturing of the blood vessel was observed. However, since the vessel walls are very thin (less than 0.3 mm), it is expected that the measured external tissue temperature is close to the internal tissue temperature.

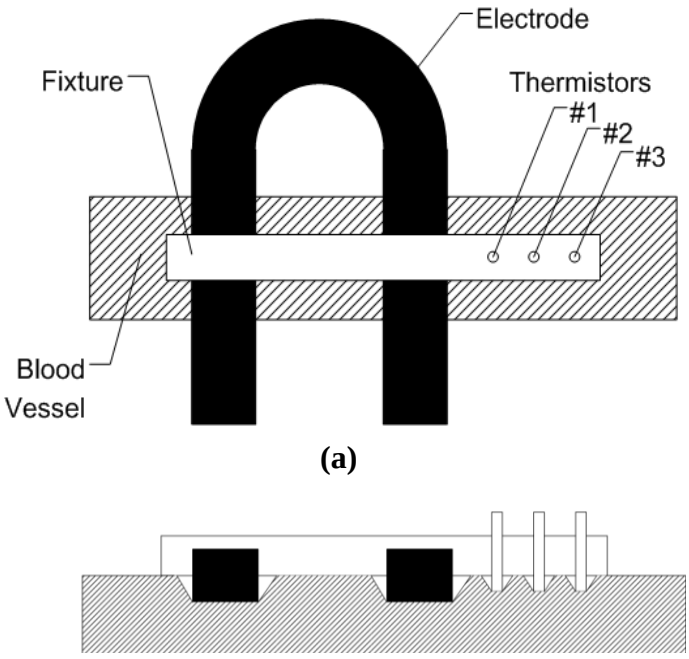

Figure 3.2 Fixture used to hold the thermistors for temperature profile measurement (a) top view and (b) side view schematic showing thermistor location relative to the bipolar forceps.

3.2.2 Experimental Procedure

Fig. 3.3 shows the overall experiment setup for the mesenteric artery vasculature in the porcine model. The tissue around the vessel was cut away using a scalpel and scissors; a spreader was used to hold the incision open. The blood vessel was then pulled slightly away from the tissue using a pair of forceps. This allowed for the electrodes of the device to grasp the vessel tissue to be sealed.

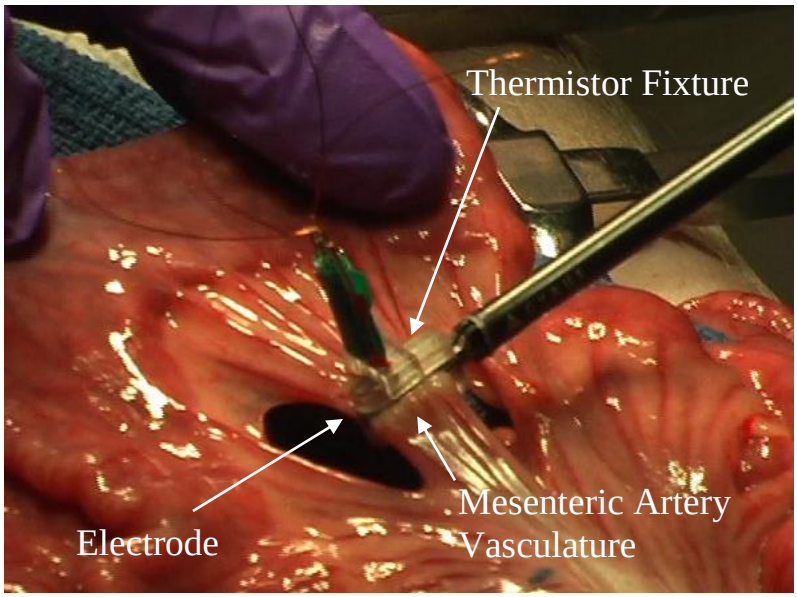

Figure 3.3 (a) Overview of the porcine model used for the bipolar mesenteric artery vasculature vessel sealing experiment.

Once the device was in place, the procedure began by starting the thermistor data acquisition. After confirmation that the thermistors were working correctly, the generator was activated and the electrical current was delivered to the tissue via the electrodes. The Gyrus generator delivers the current to the tissue in a pulsed waveform, in an attempt to mitigate issues with charring and sticking of the electrode to the tissue. The experiment was stopped once the audible tone from the generator was heard. The temperature readings were collected for an additional 10 to 15 s, while the tissue cooled.

Two sets of experiment were conducted to study the thermal profile during bipolar electrosurgery. The sealing of a 3 mm femoral artery is marked as Exp I. Exp. II seals the vasculature of the mesenteric artery by first dividing out the section of interest, and then by clamping down across the vasculature tissue, which contained a series of small arteries running through it. The width of the mesenteric artery vasculature sealed was 7 mm. Experiments were repeated to affirm the results. However, statistical variations were not calculated, since the number of suitable sealing locations in the porcine model was limited.

3.3 Experimental Results

3.3.1 Exp. I (Femoral Artery)

Figure 3.4(a) shows the temperature at the three thermistor locations during the sealing of the 3 mm femoral artery. The starting internal temperature of the porcine model vessel was 29°C, while the addition of the energy caused the vessel temperature to rise to 83°C at Thermistor #1 (1 mm from the electrode). Once the tissue reached the maximum temperature, additional electrical pulses did not cause the tissue temperature to rise, due to the lack of resistive heating. Based on the temperature at Thermistor #1, it is expected that the tissue closer to the electrode reached an even higher temperature, since steam was given off from the sealing site. In a separate *ex vivo* experiment to test the effect of the steam on the temperature readings of the thermistors, the steam was found to increase the thermistor temperatures by less than 8°C. This steam effect and the corresponding water loss will be discussed further in the next section.

At Thermistor #2, the first six pulses caused the tissue temperature to rise beyond 60°C. Subsequent pulses only raised the tissue temperature by another 4°C, as the tissue had already dried out. This is in contrast to Thermistor #3 where the tissue temperature continued to rise throughout the experiment due to conduction and reached a maximum temperature of 53°C at the end of the electrical pulsing.

The temperature change, ΔT, is defined as the rise of temperature in a pulse. For example, the ΔT of first three pulses at Thermistor #1 are marked as ΔT_1 (4°C), ΔT_2 (5°C) and ΔT_3 (18°C) in Fig. 3.4(a). Fig. 3.4(b) presents the ΔT for Exp. I. From the temperature profile results, three distinct phases were identified to represent the physiological changes occurring in the tissue during the sealing process. These are marked as Phases 1, 2 and 3, as shown in Fig. 3.4.

Phase 1 is from the beginning of the sealing process, up until the ΔT at Thermistor #1 reaches a maximum at the end of the fourth pulse, as shown in Fig. 3.4(b).

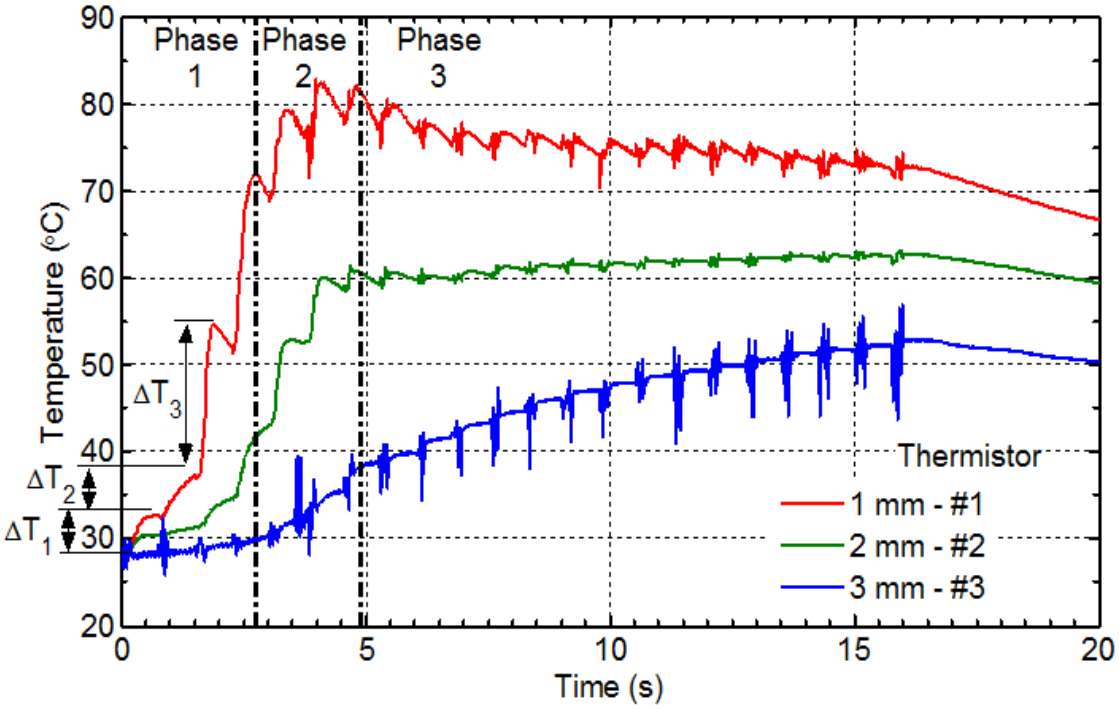

(a)

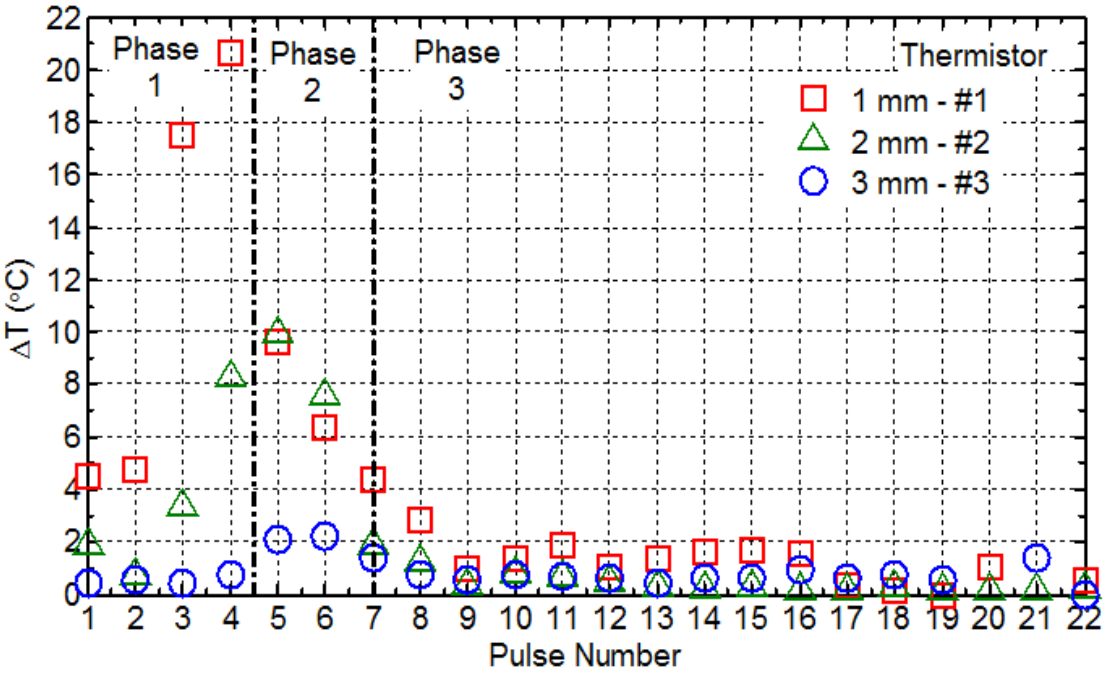

(b)

Figure 3.4 Exp. I - Femoral artery (a) temperature profile at Thermistors #1, #2, and #3 and (b) Δ*T* for each electrical pulse.

Phase 2 is defined when Δ*T* at Thermistor #1 is falling and the Δ*T* at Thermistor #2 is rising.

The final phase, Phase 3, occurs when there is minimal resistive heating at all three temperature measurement locations and the tissue water content level has stabilized. The tissue water content level is stabilized in Phase 3. The tissue water content level stabilized in Phase 3. The boundary between Phases 2 and 3 is vague since each vessel type and size will behave differently during sealing.

Figure 3.4(b) shows that during Phase 1, the ΔT at Thermistor #1 increased very quickly (ΔT_1 = 4°C, ΔT_2 = 5°C, ΔT_3 = 18°C and ΔT_4 = 21°C), due to the resistive heating of the tissue near the electrode. However, at Thermistors #2 and #3 the ΔT value never exceeded 8°C and 1°C. This indicates that most of the heating within the tissue is centered near the electrode in Phase I, because the tissue water content level is still relatively high and the electrical energy is able to easily pass through the tissue.

During Phase 2, the ΔT at Thermistor #1 begins to decrease rapidly. By the end of Phase 2, the ΔT of each additional pulse is less than 4°C, indicating that the tissue water content near the electrodes is likely falling rapidly. It has been shown that as the tissue temperature increases, the tissue water content is reduced [Ramachandran et al., 1996]. This water content reduction occurs because the elevated tissue temperature forces the fluids in the tissue to either be transferred to the nearby tissues by mass diffusion or to be given off as steam vapor. This water movement from the high to low temperature regions in the tissue causes the effective heat transfer rate within the tissue to be higher than if only thermal conduction was considered. A secondary effect of the water movement is that as the water content of the tissue near the electrodes is reduced, more of the electrical energy is directed towards the tissue further away from the electrode. The spread of electrical energy outward is seen at Thermistor #2 as the ΔT reaches a maximum during Phase 2.

In Phase 3, it appears that the tissue water content level begins to stabilize as the ΔT for Thermistors #1, #2 and #3 levels off. Minimal resistive heating is seen at all three thermistor locations, as ΔT does not increase by more than 2°C. This is caused by tissue being unable to carry the electrical current to locations away from the sealing site, due to its lower water content. The final observation from Fig. 3.4(b) is the relatively constant heating of the tissue at Thermistor #3, independent of time. This indicates that the tissue

temperature at this location, further away from the electrode, is more dependent on thermal effects rather than the resistive heating of the tissue.

Figure 3.5(a) shows the measured voltage and current being applied to the tissue during the femoral artery sealing. Each of the electrical pulses was determined to be approximately 0.22 s long and applied about 100 V AC to the tissue, as shown in the first 6.5 s of Exp. I in Fig. 3.4(b). Between each of the pulses, there was a cool down period of 0.5 s in an attempt to reduce the temperature of the surrounding tissue and to reduce the amount of sticking between the sealed tissue and the electrodes. The voltage being applied to the tissue remained relative constant throughout the entire experiment; however, the current being applied to the tissue varied from 5.5 to 0.5 A. The current of each pulse was the highest at the beginning of the pulse as the generator detected the low tissue impedance. As the impedance of the tissue rose from the resistive heating, the current gradually dropped.

The impedance of tissue at every data point in Fig. 3.5(b) is calculated by dividing the voltage by the current. The average impedance of the tissue during the first pulse was 28 Ω and by the ninth pulse, the average impedance had increased to 193 Ω. The calculated tissue impedance results could be related to the ΔT results in Fig. 3.4(b). During Phase 1, the average impedance value increased by 135%, from 28 Ω at the first pulse to 66 Ω at the forth pulse, as the water within the tissue was lost. The water carries the electrical energy. As it is lost, the tissue impedance increases since a greater proportion of the electrical energy must pass through the higher resistance tissue fibers.

In Phase 2, the average impedance of the tissue increased an additional 150%, from 66 Ω in the fourth pulse to 165 Ω in the seventh pulse, as additional water was lost from within the tissue due to the elevated tissue temperature. In Phase 3, the average tissue impedance remained high and did not change significantly, as the tissue water content stabilized.

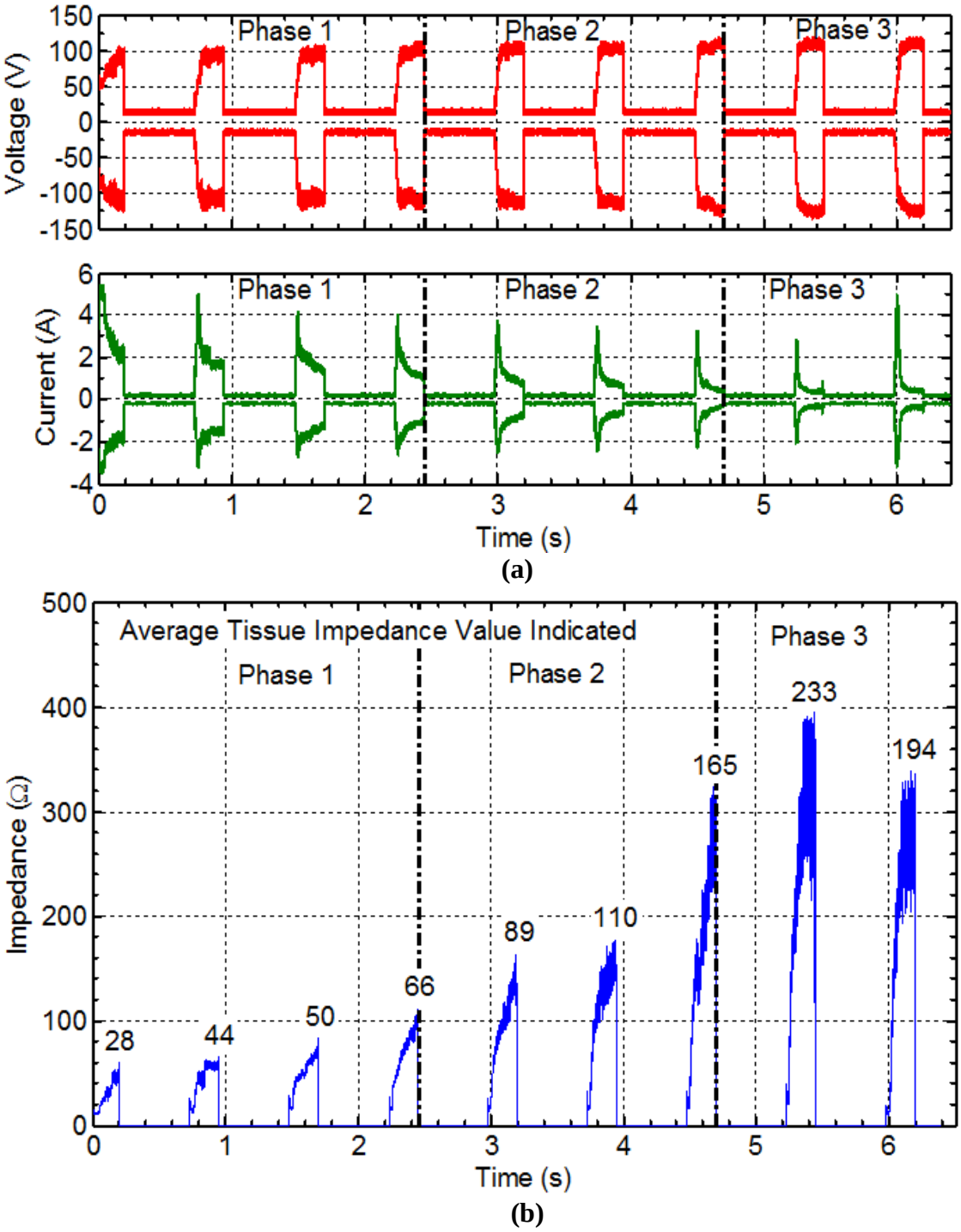

Figure 3.5 Exp. I - Femoral artery (a) measured electrical current and voltage in the first nine pulses and (b) calculated tissue impedance during each pulse.

3.3.2 Exp. II (Mesenteric Artery Vasculature)

Figure 3.6(a) shows the temperature profiles obtained from the three thermistors during sealing of the mesenteric artery vasculature. The starting internal temperature of the mesenteric vasculature was 31°C, while the energy addition caused the temperature at Thermistor #1 to rise to 83°C, which is identical to the femoral artery results. The temperature at Thermistor #1 increased quickly, but then the temperature remained relatively constant once the peak temperature was reached. However, fewer pulses were needed to reach this maximum temperature in the mesenteric artery vasculature since the vasculature was comprised of a series of smaller diameter vessels. Thermistor #2 reached a maximum temperature of 63°C at the end of the pulses in Phase 3. This is also identical to the maximum temperature reached at Thermistor #2 during the femoral artery sealing. However, once the electrical pulses ended, the temperature of both Thermistors #1 and #2 fell quickly. The reduction in temperature was caused by the conduction of the thermal energy towards the surrounding (Thermistor #3) regions of lower temperature tissue. This is confirmed by the slow rising temperature to 43°C after 15 s at Thermistor #3. Overall, similar temperature trends were observed between the two different vessels..

During Phase 1, Fig. 3.6(b) shows that the ΔT at Thermistor #1 increased very quickly (ΔT_1 = 4°C, ΔT_2 = 9°C and ΔT_3 = 19°C), similar to the femoral artery results. At Thermistors #2 and #3, the ΔT value did not exceeded 3 and 0°C, respectively. This indicates that most of the electrical resistive heating within the tissue occurs near the electrodes.

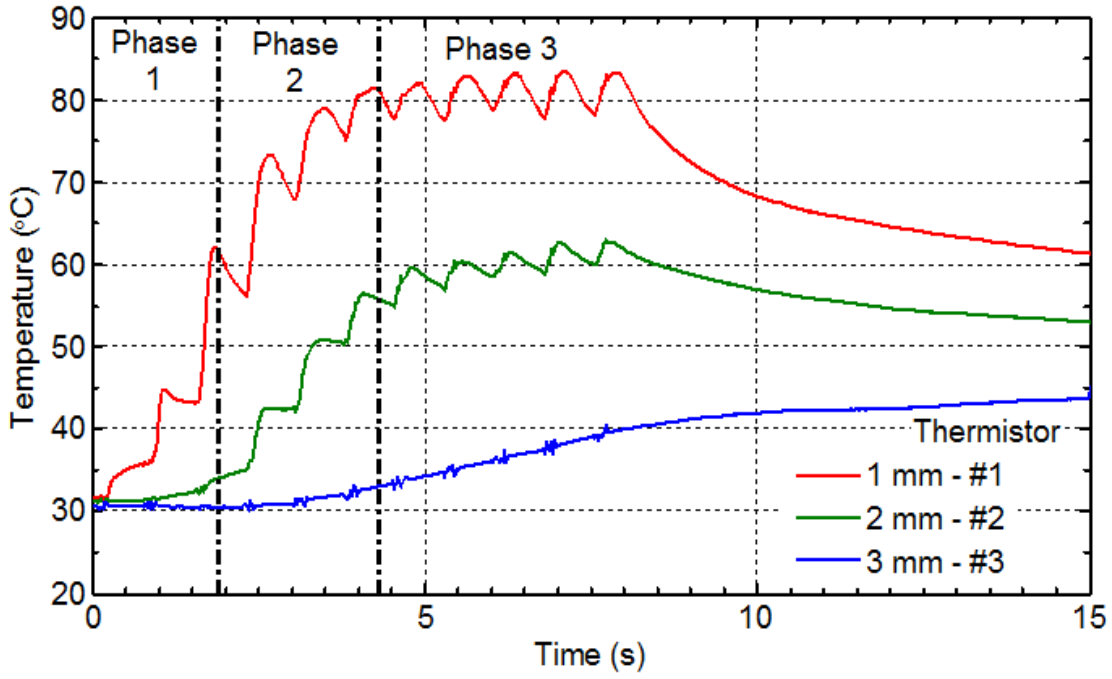

(a)

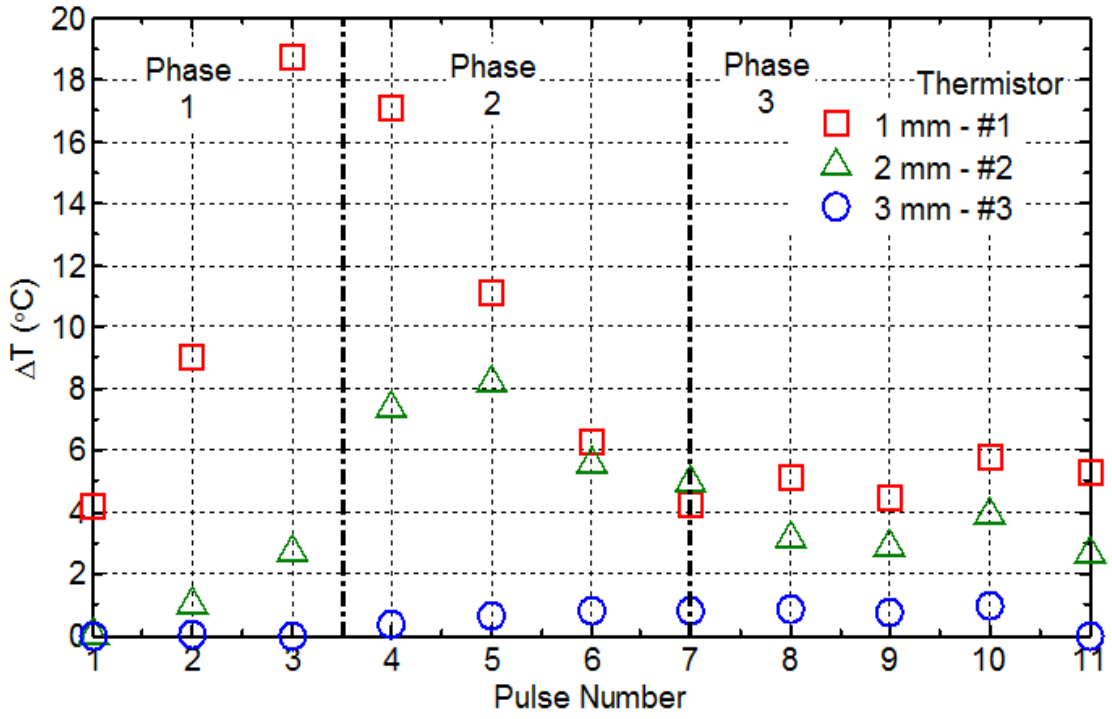

(b)

Figure 3.6 Exp. II - Mesenteric artery vasculature (a) temperature profile at Thermistors #1, #2, and #3 and (b) Δ*T* for each electrical pulse.

As Phase 2 begins, the tissue undergoes a change in water content as the ΔT at Thermistor #1 falls due to the reduced tissue water content near the electrodes. This causes the electrical energy to be diverted out to the tissue near Thermistor #2. The ΔT at Thermistor #2 reaches a maximum value of 8°C in the fifth pulse. As Phase 2 ends, the ΔT of Thermistor #2 falls as the water content is reduced further and Phase 3 begins. During Phase 3, the tissue water content stabilizes and the resistive heating at all three thermistor locations is reduced. The ΔT does not increase by more than 1°C for any of the thermistors during Phase 3. However, throughout the entire experiment, the ΔT for Thermistor #3 never increases above 1°C. This indicates a lack of resistive heating near this location.

Figure 3.7(a) shows the measured voltage and current being applied to the tissue during sealing of the mesenteric vasculature. The voltage for most of the pulses was 100 V AC, while the current at the beginning of each pulse was nearly 6 A, both comparable to the femoral artery results. During the first three pulses, the current dropped off rapidly, which was different from the trend observed in femoral artery. This was caused by the smaller vessel size and the spread out structure of the vasculature

Figure 3.7(b) shows the tissue impedance for the mesenteric vasculature during each electrical pulse. The average impedance of the tissue during the first pulse was 14 Ω and by the ninth pulse, the impedance had steadily increased to 225 Ω. During Phase 1, the average impedance value increased by 88%, from 14 Ω at the first pulse to 26 Ω at the third pulse, as the water in the tissue near the electrode is lost. The impedance is much lower than the femoral artery in Phase 1 due to the smaller vessel sizes of the mesenteric artery vasculature. The tissue impedance increased by more than fivefold (from 26 Ω to 156 Ω) in Phase 2, likely .due to a significant reduction in the tissue water content. In Phase 3, the tissue impedance only increased by 45%, between the seventh pulse (156 Ω) and the ninth pulse (225 Ω), as the tissue water content level stabilized.

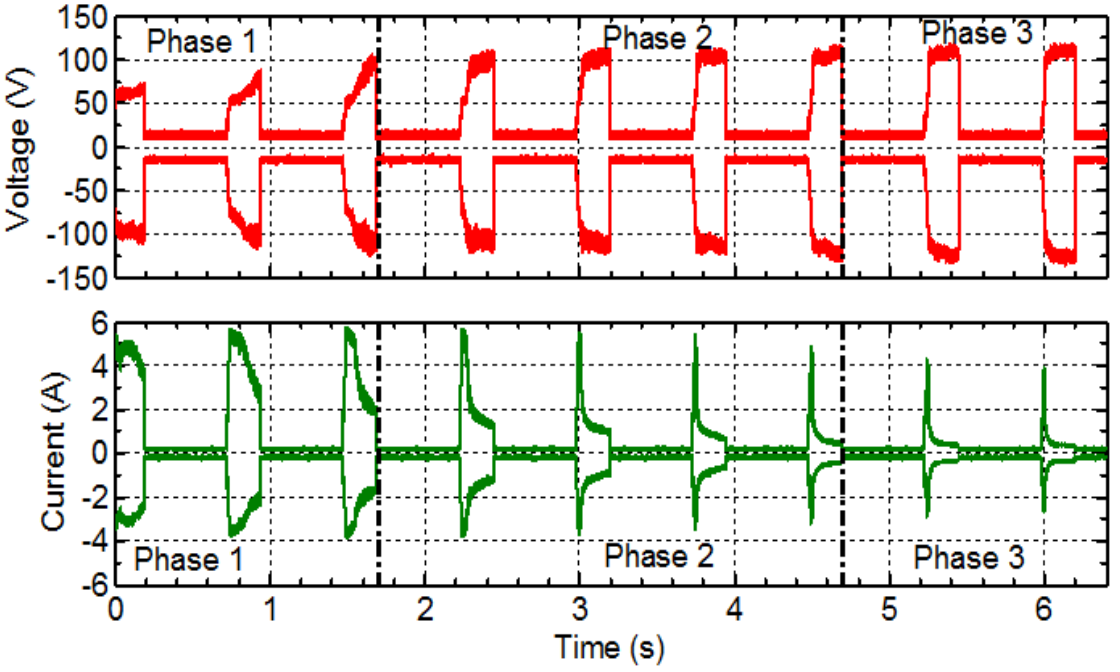

(a)

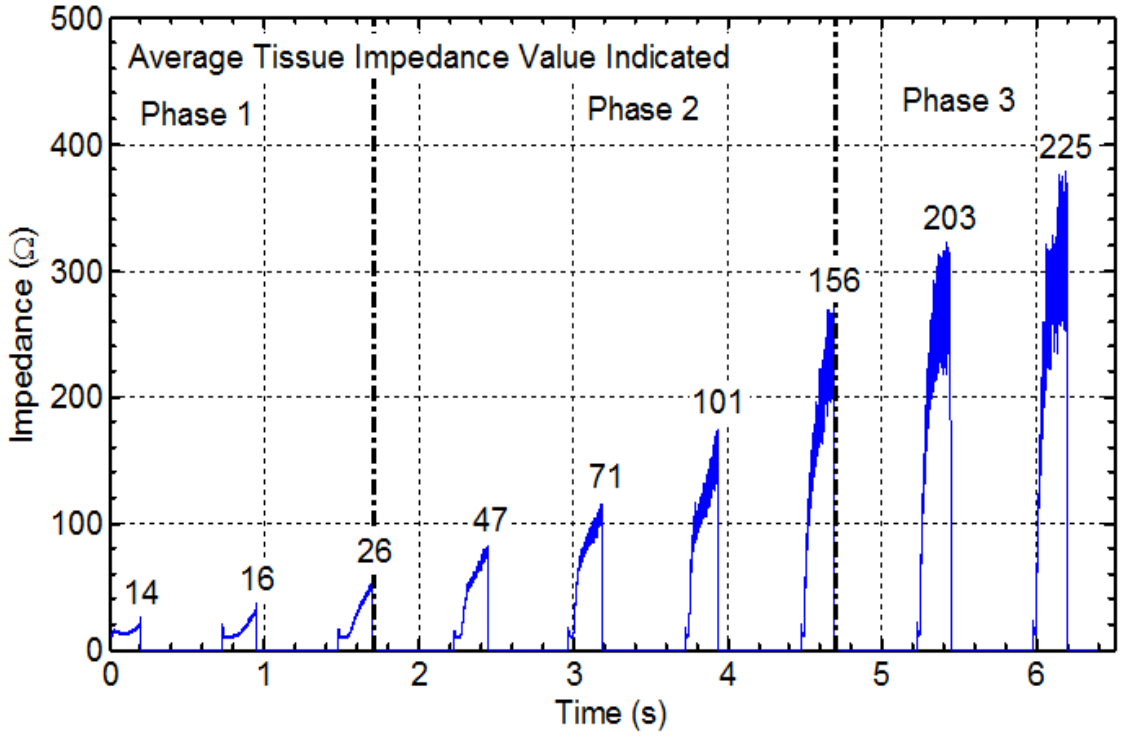

(b)

Figure 3.7 Exp. II - Mesenteric artery vasculature (a) measured electrical current and voltage in the first nine pulses and (b) calculated tissue impedance during each pulse.

3.4 Conclusions

The tissue temperature profile along with the electrical voltage and current for *in vivo* bipolar electrosurgical sealing of the femoral artery and mesenteric artery vasculature were measured with comparable trends and magnitudes for both vessels. For the electrical pulses, the rise in temperature ΔT was the highest during the first few pulses and quickly decayed to an insignificant level. The average impedance increased with each additional pulse due to the reduction in tissue water content as the tissue temperature increased due to resistive heating and steam being given off. This work showed that there was a connection between ΔT and the tissue impedance for both the femoral artery and mesenteric artery vasculature.

Further work is needed to develop a relationship between the tissue temperature profile and the quality of the bipolar vessel seal. Modeling of the measured temperature profile using the finite element method is an on-going research topic aimed at predicting the temporal and spatial distribution of vessel temperature during electrosurgery.

References

Campbell, P.A., Cresswell, A.B., Frank, T.G., and Cuschieri, A., (2003), "Real-rime thermography during energized vessel sealing and dissection," *Surgical Endoscopy*, Vol. 17, pp. 1640-1645.

Carbonell, A.M., Joels, C.S., Kercher, K.W., Matthers, B.D., Sing, R.F., and Heniford, B.T., (2003), "A Comparison of laparoscopic bipolar vessel sealing devices in the hemostasis of small-, medium-, and large-sized arteries," *Journal of Laparoendoscopic and Advanced Surgical Techniques*, Vol. 13, pp. 377-380.

Carlander, J., Johansson, K., Lindstrom, S., Velin, A.K., Jiang, C.H., and Nordborg, C., (2005), "Comparison of experimental nerve injury caused by ultrasonically activated scalpel and electrosurgery," *British Journal of Surgery*, Vol. 92, pp. 772-777.

Eman, T. and Cuschieri, A., (2003), "How safe is high-power ultrasonic dissection?" *Annals of Surgery*, Vol. 237, pp. 186–191.

Harold, K.L., Pollinger, H., Matthews, B.D., Kercher, Sing, R.F., and Heniford, T., (2003), "Comparison of ultrasonic energy, bipolar thermal energy, and vascular clips for the hemostasis of small-, medium-, and large-sized arteries," *Surgical Endoscopy*, Vol. 17, pp. 1228-1230.

Heniford, B.T. Matthews, B.D., Sing, R.F., Backus, C., Pratt, B., and Greene, F.L., (2001), "Initial results with an electrothermal bipolar vessel sealer," *Surgical Endoscopy*, Vol. 15, pp. 799-801.

Lee M. and Lambert, S., (2001), "Thermal modification of connective tissue," *Current Orthopedics*, Vol. 15, pp. 364-375.

Matthews, B.D., Pratt, B.L., Backus, C.L., Kercher, K.W., Mostafa, G., Lentzner, A., Lipford, E.H., Sing, R.F., and Heniford, B.T., (2001), "Effectiveness of the ultrasonic coagulating shears, LigaSure vessel sealer, and surgical clip application in biliary surgery: A comparative analysis," *The American Surgeon*, Vol. 67, pp. 901-906.

Pasic, R.P. and Ronald Leon Levine, R.L. (Eds.), (2007), *Practical manual of laparoscopy and minimally invasive gynecology: A clinical cookbook*, Second Edition, Informa Healthcare, United Kingdom, pp. 480.

Ramachandran, T., Sreenivasan, K., and Sivakumar, R., (1996), "Water vaporization from heated tissue: An *in vitro* study by differential scanning calorimetry," *Lasers in Surgery and Medicine*, Vol. 19, pp. 413–415.

Reidenbach, H.D. and Buess, G., (1992), "Ancillary technology: Electrocautery, thermoregulation and laser," In: Cuschieri, A., Buess, G., Perrisat, L., (Eds.), *Operative Manual of Endoscopic Surgery*, Springer, Berlin, pp. 44-60.

Siperstein, A.E., Berber, E., and Morkoyun, E., (2002), "The use of the harmonic scalpel vs. conventional knot tying for vessel ligation in thyroid surgery," *Archives of Surgery*, Vol. 137, pp. 137-142.

Spivak, H., Richardson, W.S., and Hunter, J.G., (1998), "The use of bipolar cautery, laparoscopic coagulating shears and vascular clips for hemostasis of small and medium-sized vessels," *Surgical Endoscopy*, Vol. 12, pp. 183-185.

Thomsen, S., Pearce, J.A, and Cheong, W.F., (1989), "Changes in birefringence as markers of thermal damage in tissues," *IEEE Transactions on Biomedical Engineering*, Vol. 36, pp. 1174-1179.

Underwood, R.A., Dunnegan, D.L., and Soper, N.J., (1998), "Prospective, randomized trial of bipolar electrosurgery vs ultrasonic coagulation for division of short gastric vessels during laparoscopic nissen fundoplication," *Surgical Endoscopy*, Vol. 13, pp. 763-768.

Washington, E. Zaddem, V. Gordon, and D. Pendekanti, R., (2003), "Offset bipolar electrode technology for minimizing collateral thermal damage," *Engineering in Medicine and Biology Society, Proceedings of the 25th Annual International Conference of the IEEE*, Vol. 1, pp. 142-144.

CHAPTER 4

FINITE ELEMENT MODELING OF THE TEMPERATURE PROFILE IN BIPOLAR ELECTROSURGICAL VESSEL SEALING

ABSTRACT

A finite element model (FEM) is presented to predict the thermal profile of a 3 mm femoral artery sealed using a bipolar electrosurgical device. Large thermal gradients within the tissue are present, since the bipolar device resistively heats the tissue. The development of a thermal FEM can lead to improved bipolar device designs that minimize the spread of this thermal energy to nearby tissues. Differences between the temperature results from FEM and experimental measurements indicate that the thermal energy is being transferred to the measurement locations further from the electrode faster than the model is predicting. A damage function based on the tissue temperature was developed for the electrical conductivity; however, it is unable to account for the movement of the water within the tissue during the vessel sealing process. A comparison of the temperature results between similar 2D and 3D models indicates that the 2D model can be used to predict the tissue temperature during vessel sealing. The effect of blood within the vessel reduced the temperature at the location closest to the electrode, but had minimal effect on the tissue temperature. The modeling results indicate that the development of a FEM that accounts for mass transfer and incorporates tissue thermal damage during the vessel sealing process is needed to accurately predict the temperature profile.

4.1 Introduction

Modeling of surgical operations is important for advancing the design of surgical devices and to enhance the capability of simulation during surgical procedure training. Experimental testing of surgical devices on animal models is expensive, time consuming and requires lengthy approvals. A modeling based approach serves as a means of testing and verifying concepts quickly, while saving time and experimental resources if the process does not behave as expected. This study investigates thermal modeling for electrosurgical devices.

Electrosurgery, the delivering of high frequency electrical energy to tissue was developed in the 1920s. In recent years, a variety of different devices have been developed to ablate tumors [Goldberg, 2001], cauterize tissue [Pearce, 1986], and to seal vessels [Newcomb et al., 2009]. For vessel ligation operations, bipolar electrosurgery has replaced traditional suturing, especially during laparoscopic surgery. These electrosurgical devices work by clamping down on the vessel, while applying an electrical current to the tissue to resistively heat it. This resistive heating causes the tissue temperature to rise and the proteins within the tissue begin to denature [Wright and Humphrey, 2002]. Once the application of the energy stops, the tissue cools and forms a bond.

Since the tissue must be heated to form the vessel seal, often the adjacent tissue around the sealing site is also subjected to the elevated temperature. Most of the current devices attempt to mitigate these issues through the use of generators that implement control algorithms for the energy output [Kennedy et al., 1998]. Devices may also use other means, such as "smart electrodes" that turn on and off depending on the local tissue temperature [Smaldone et al., 2008] or a heat pipe in the electrode for cooling [Vellimana et al., 2009]. However, even with these advanced techniques, the thermal spread from these devices often exceeds 3 mm [Campbell et al., 2003]. This is a major problem with most of the current devices, as they are unable to prevent the spread of heat to the nearby tissues. The tissue thermal damage, often referred to as thermal spread, can lead to major postoperative issues and can be detrimental to a patient's long-term recovery. Understanding the tissue temperature distribution in electrosurgical vessel sealing is

important. The goal of this study is to develop a finite element thermal model to predict the spatial and temporal distributions of tissue temperature during vessel sealing.

Past electrosurgical modeling has focused primarily on tumor ablation within: the liver [Haemmerich et al., 2003], uterus [Angelone and Martin, 2009] and heart [Tungjitkusolmun et al., 2000]. In the ablation process, the amount of energy being delivered is relatively low and the heating times are often on the order of 480 to 720 s. This is different from the electrosurgical process used to seal blood vessels, which utilizes a high voltage (about 100 V) in about 20 s to occlude the vessel. Research into how to accurately model the electrosurgical vessel sealing process is lacking. Dodde et al. [2008] developed a FEM to predict the thermal spread from a bipolar electrosurgical device when used to cauterize porcine spleen. For electrosurgical vessel sealing, modeling the temperature profile is more challenging due to the small volume of tissue being sealed.

A good understanding of the tissue thermal and electrical properties, which vary depending on the level of water content, damage, and compression during vessel sealing, is critical for accurate modeling of electrosurgical tissue joining. During the application of electrical energy to the tissue, the tissue temperature increases quickly from the resistive heating. Even before the tissue reaches these elevated temperatures, major irreversible damage has occurred within the tissue. Incorporation of the damage effect into the modeling process has been attempted by altering the specific heat of the tissue [Yang et al., 2007], changing the electrical conductivity of the tissue [Haemmerich et al., 2003], or by simulating the diffusion of water vapor within the tissue [Ward et al., 2007]. The choice of which method to use is often at the discretion of the researcher, since no single parameter has been identified as being the most important. This study identifies critical parameters that affect the accuracy of the FEM temperature prediction during electrosurgical sealing.

In this study, the thermal spread from a bipolar electrosurgery sealing device is predicted using a 3 mm blood vessel FEM developed using COMSOL Multiphysics. The modeling temperature results are then compared to the temperature results obtained from experimental data [Chastagner, 2010a]. Key parameters within the model are presented

and discussed, since they can be used to guide the direction of future work related to modeling of the bipolar vessel sealing process.

4.2 Vessel Sealing Temperature Modeling

The bio-heat transfer equation for tissue, similar to the heat equation for conduction, but with added terms for heat sources, was developed in the late 1940s by Pennes [1948] and can be expressed as:

$$\rho c \frac{\partial T}{\partial t} = k\nabla^2 T - w_b c_b (T - T_a) + q_m + q_g \tag{4.1}$$

where t is the time, ρ is the tissue density, c is the tissue heat capacity, k is the tissue conductivity, w_b is the effective blood perfusion parameter, c_b is the blood heat capacity, T is the local tissue temperature, T_a is the blood inlet temperature or steady-state temperature of the tissue, q_m is the metabolic heat generation rate of the tissue, and q_g is the heat generation term due to the externally induced electro-surgical heating of the tissue. The heat generation term is defined as:

$$q_g = \boldsymbol{J} \cdot \boldsymbol{E} \tag{4.2}$$

where $\boldsymbol{J}$ is the current density (A/m^2) and $\boldsymbol{E}$ is the electric field intensity (V/m).

The voltage in the tissue and electrode can be calculated by solving the Laplace's equation:

$$\nabla[\sigma(T)\nabla V] = 0 \tag{4.3}$$

where $\sigma(T)$ is the temperature-dependent conductivity and V is the voltage.

In this study, the blood perfusion and metabolic heat sources are assumed to be negligible, and Eq. (4.1) reduces to:

$$\rho c \frac{\partial T}{\partial t} = k\nabla^2 T + q_g \tag{4.4}$$

In the model, Eqs. (4.3) and (4.4) are simultaneously solved, since an iterative computation of both the electrical field and temperature is needed.

4.2.1 Modeling Procedure

The temperature profile of a 3 mm diameter femoral artery sealed with a 5 mm bipolar electrosurgery device (Gyrus ACMI #3005PK) is modeled in this study. A thermal-electric-partial differential equation (PDE) multi-physics model was created in COMSOL 3.5a and solved with the direct COMSOL PARDISO solver, using a stationary time iterative stepping process [Dodde et al., 2008]. The time steps for the energy delivery and cooling stages were 0.025 s and 0.25 s, respectively. Experimentally measured electrical voltage from the *in vivo* bipolar electrosurgical vessel sealing of femoral artery was applied as the input [Chastagner, 2010a].

4.2.2 Material Properties

Properties for the vessel tissue, blood and electrode are presented in Table 4.1, except for the electrical conductivity, which will be discussed in the next section. The thermal conductivity was assumed to be temperature dependent. The temperature-dependent vessel tissue thermal conductivity is [Valvano et al., 1985]:

$$k(T) = k_{ref} + 0.0013 \cdot (T - T_{ref}) \tag{4.5}$$

where k_{ref} (=0.45 W/m·K) is the baseline tissue thermal conductivity [Duck, 1990]. For the vessel tissue between the electrodes, the water content and thermal conductivity of the tissue will decrease as the tissue is compressed. Therefore, a 10% reduction in the thermal conductivity was used for the tissue between the electrodes [Chastagner, 2010b].

Table 4.1 Material properties used in FEM of the vessel.

Material property	Vessel tissue	Blood	Electrode (AISI 301 stainless steel)
Density (ρ) [kg/m^3]	1050**	1060*	8000
Specific heat (C) [J/g·K]	3314**	3890*	500
Thermal conductivity (k) [W/m·K]	Eq. (4.5)	0.53**	16.2
Electrical conductivity (σ) [S/m]	Eq. (4.6)	0.667***	1.39 x 10^6

* Golombeck et al. [1999]
** Duck [1990]
*** Tungjitkusolmun et al. [2002]

4.2.3 Damage Model for Tissue Electrical Conductivity

During bipolar electrosurgery, the thermal and electrical conductivity of the tissue will change based on the tissue water content and the amount of tissue damage. The temperature effect on the electrical conductivity is more than a magnitude of order higher than on the thermal conductivity. Therefore, the effect of tissue damage is only considered for the electrical conductivity.

In this study, when T<100°C, the electrical conductivity $\sigma(T)$ was assumed to increase at a rate of 2%/°C [Schwan and Foster, 1980]: Once the tissue became damaged (T>100°C), the electrical conductivity was set at a low, constant value, designated as σ_d. In this study, σ_d = 0.01 S/m. Haemmerich et al. [2003] used a reduction in the electrical conductivity of 10,000 to define the effect of thermal damage on tissue electrical conductivity. To implement this tissue damage within the model, the following expression was used for the electrical conductivity:

$$\sigma(T) = \sigma_{ref}\left[1 + 0.02\left(T - T_{ref}\right)\right] \cdot (1.01 - u) \tag{4.6}$$

where σ_{ref} is the reference electrical conductivity of the tissue (0.55 S/m [Duck, 1990]). T_{ref} is the reference temperature and u is the dependent variable from the PDE mode.

The PDE mode in the model allows for the irreversible physiological changes in the tissue to be represented. The flux vector within the PDE mode was set to zero, while the source term was defined by an expression to represent the temperature at which the electrical conductivity will change:

$$F = flc1hs\left[T - (T_{change} + dT), dT\right] \tag{4.7}$$

where *flc1hs* is a smoothed heaviside function with continuous first derivative continuity, T_{change} is the temperature at which the transition occurs (100°C for the model) and dT is the range of the temperature transition (0.1°C). Once the temperature exceeds T_{change}, the source term switches state from 0 to 1 and remains at this value. The source term is then coupled, through u, with Eq. (4.6), which causes $\sigma(T)$ to drop to σ_d when the temperature exceeds 100°C.

This reduction in electrical conductivity is caused by the loss of water in the tissue as it is vaporized. Water is the primary carrier medium for the electrical energy in the tissue. Thus, the loss of water causes the electrical conductivity of the tissue to fall. This in turn causes the resistive heating of the tissue to decrease at the location in which this elevated temperature has been reached.

A secondary effect caused by the vaporization of water in the tissue is the mass transfer. The water is vaporized and moves away from the heating region [Ward et al., 2007]. This fluid movement occurs by either mass diffusion in the tissue or by water vapor being given off from tissue surface. It is expected that as the heated water vapor moves from the high tissue temperature regions to low temperature regions, it will condensate in the lower temperature regions [Yang et al., 2007].

4.2.4 Vessel Geometry, FEM Meshing and Techniques

In this study, two 2D and one 3D vessel and electrode geometries, as shown in Fig. 4.1, were developed. Fig. 4.1(a) shows a simplified 2D model with a tissue height (h) equal to 1 mm, which corresponds to the average height of tissue next to the two jagged electrodes. In the simplified 2D model, the vessel is deformed by the thermistors contacting the tissue. This causes the tissue to be deformed throughout the entire 7 mm

length of the vessel. This represents the actual vessel sealing process, where both the electrodes and thermistors compressed the tissue into a flattened elliptical shape.

Fig. 4.1(b) shows another 2D model with h = 1 mm next to the electrodes and a smooth transition to the 3 mm vessel diameter. This model represents a vessel that is not deformed by the thermistors.

A 3D model with h = 1 mm next to the electrodes and a smooth transition to the 3 mm vessel diameter is shown in Fig. 4.1(c). For simplification, the jagged electrodes [Dodde et al., 2008] of the bipolar device were modeled as a flat surface.

For all vessels, a 0.25 mm artery wall was modeled, with blood in between the artery walls. If blood was not considered, the space within the vessel wall was left empty. The automatic meshing generator within COMSOL was used to generate the finite element mesh. The mesh shown in Figs. 4.2(a) to (c), corresponds to three FEM models shown in Figs. 4.1(a) to (c) and consisted of 3,654, 7,770 and 12,335 elements, respectively. The 2D model uses a triangular shape with six nodes, while the 3D model uses a tetrahedral shape with ten nodes. Each node has three degrees of freedom: temperature, voltage and the PDE value for the damage function.

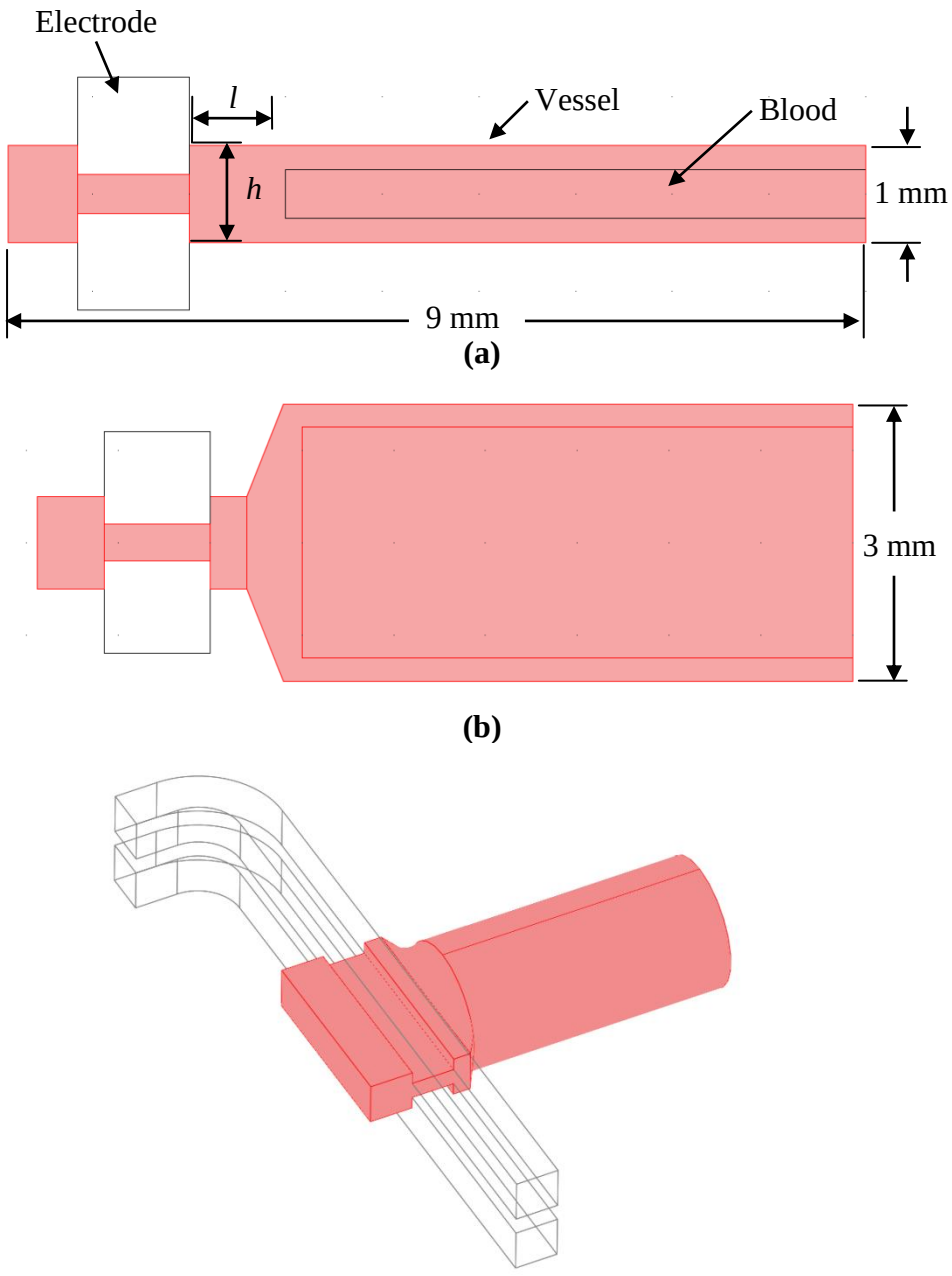

Figure 4.1 Vessel and electrode geometry used to represent the vessel sealing process in the model, showing the length of the vessel, height of the tissue and location of the temperature measurement points (a) 2D with compressed vessel, (b) 2D with gradually expanded vessel and (c) 3D with gradually expanded vessel.

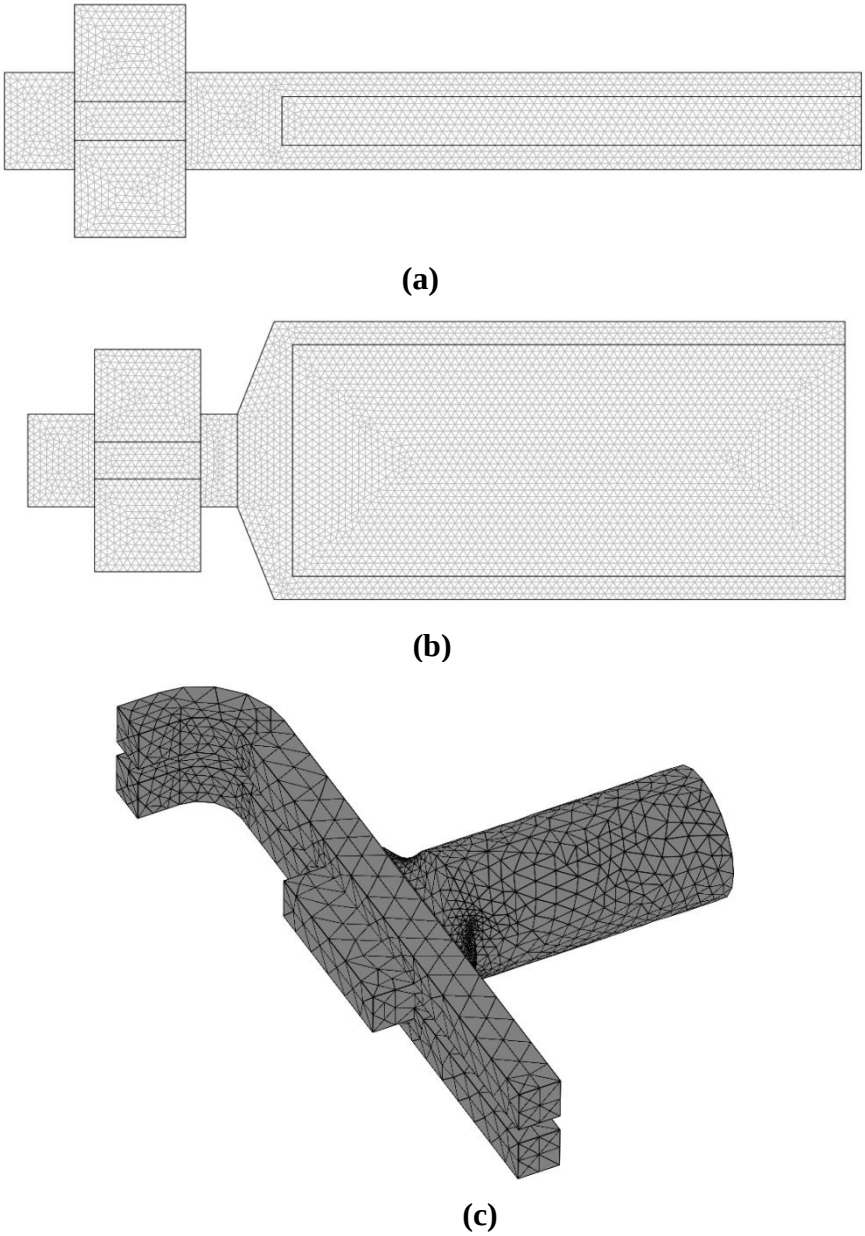

Figure 4.2. The finite element meshes used for (a) 2D with compressed vessel, (b) 2D with gradually expanded vessel and (c) 3D with gradually expanded vessel.

To simulate the physical conditions of the experiment porcine artery sealing, the end of the blood vessel away from the electrodes was constrained to the measured initial vessel temperature of 29°C, throughout the simulation. The end of the vessel near the sealing location was constrained by symmetry, modeled as a zero heat flux condition, since the vessel model is symmetric about this plane. Convective heat transfer was assumed for all of external surfaces, except for the two ends of the vessel. A convective

heat transfer coefficient of 25 W/m^2·K was used for all surfaces and the effect of water turning into vapor was not considered. The effect of desiccation, shrinkage, ablation and coagulation on the tissue was also not considered since the magnitude of their effects on the tissue has not been reported within the literature. It was also assumed that there was no blood perfusion within the vessel tissue.

Thermal and electrical continuity was applied to all of the internal surfaces between the tissue, the blood, and the electrodes. For the electrical boundary conditions, an electrical insulating boundary condition was applied to all outer surfaces of the model. For the surfaces of the active electrode that touch the tissue, the AC voltage of the experiment was converted to a DC source voltage, V_0 (= 70 V) by calculating its root-mean-square value [Berjano, 2006]. Figure 4.3 shows a comparison between the experimentally measured voltage data and the simplified voltage input for the active electrode. For the model it was assumed that the source voltage oscillated between 0 and 70 V DC. For the passive electrode, a ground condition V_g (= 0 V), was applied to all surfaces touching the tissue.

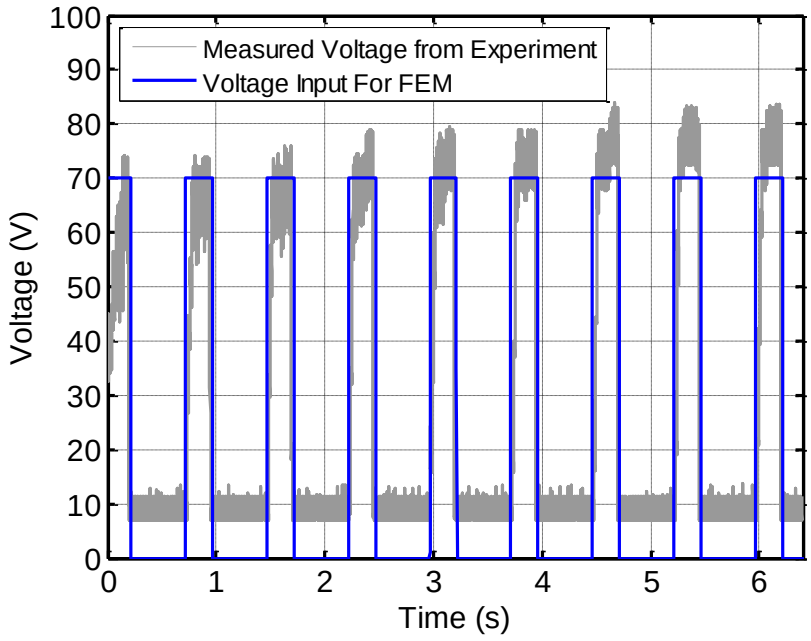

Figure 4.3 Comparison between the measured voltage (converted to DC) from the experiment and the voltage input used in the model.

4.3 Modeling Results and Comparison with Experimental Measurements

Figure 4.4 shows a comparison between the experimentally measured temperature [Chastagner, 2010a] and the predicted results of the 2D model with vessel compression (Figs. 4.1(a) and 4.2(a)). The location of the temperature measurement is at the surface of the tissue and at the specified distances (1, 2, and 3 mm) from the edge of the electrode. In the experiment, the temperature at the 1 mm location increases very rapidly during the initial six pulses, and then reaches a maximum temperature of 83°C before falling slightly. This is in contrast to the modeling results, where there is smaller temperature increase during the first six pulses. In the model, after the first two pulses, the temperature increase per pulse is gradually reduced. This reduction in the model occurs because the thermal damage function begins to reduce the electrical conductivity of the tissue near the electrodes after the second pulse. This reduces the amount of resistive heating and thus the temperature increase per pulse. If the damage function is not included in the electrical conductivity calculation, the tissue temperature near the electrodes will reach temperatures in excess of 500°C.

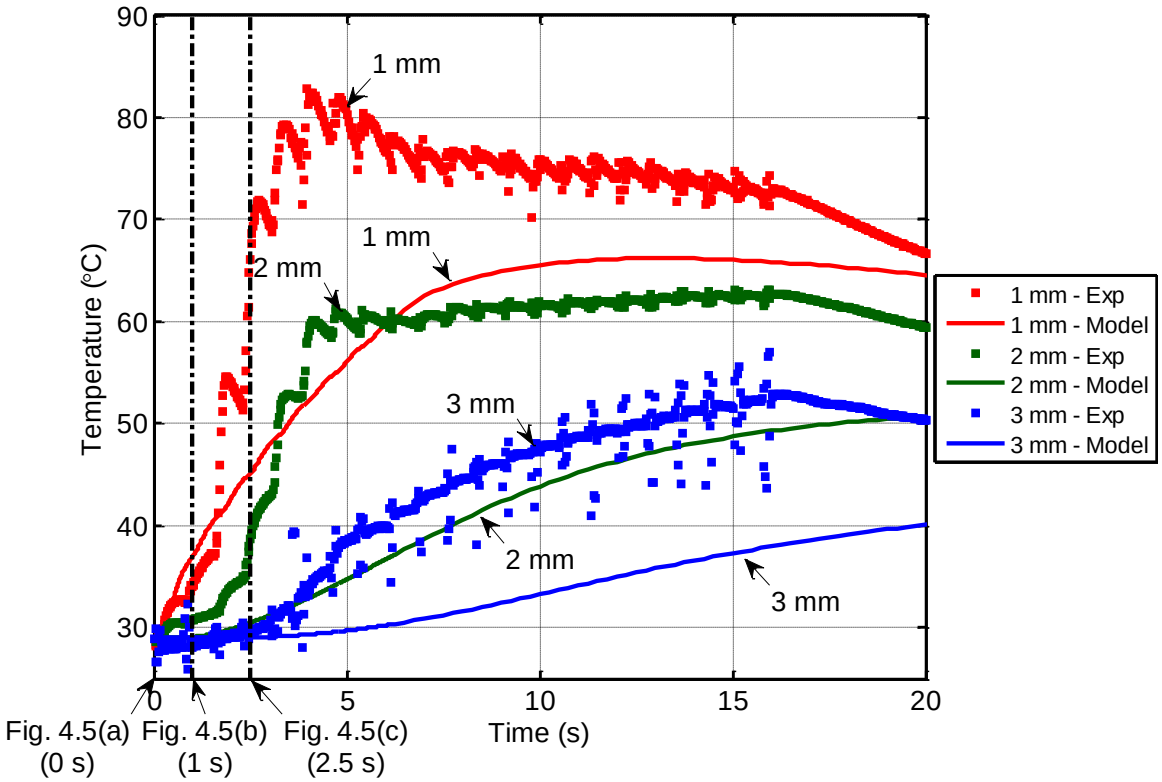

Figure 4.4 Comparison of the tissue temperature at thermistors 1, 2 and 3 mm away from electrode for experimental and modeling results.

The discrepancy between the model and the experiment is likely caused by two factors. First, the model is unable to account for mass transfer in the tissue due to the movement of the water as it is vaporized. This water vaporization will move the water from the high temperature regions in the tissue to the low temperature regions, increasing the effective heat transfer rate. Second, the model is under predicting the electric field in the tissue during the sealing process. At the 1 mm location in the experiment, there is a large increase in the tissue temperature due to the resistive heating. This effect is not seen in the modeling results, where only a slight amount of resistive heating is seen at the 1 mm location.

Figure 4.5 shows the electric field in the model at selected times during the sealing process. At the beginning of the first pulse (0 s), Fig. 4.5(a), the electric field only reaches about 0.9 mm away from the electrodes. Since the first temperature measurement point is at 1 mm, little resistive heating is occurring near this measurement point, thus causing the temperature results of the model to be lower than the experiment.

The majority of the electrical field is concentrated in the tissue between the electrodes. By the end of the second pulse (1 s), Fig. 4.5(b), the electric field only reaches 0.3 mm away from the electrodes and the overall magnitude has dropped. This corresponds to the reduction in the temperature increase per pulse that was observed in Fig. 4.3. Between the end of the second pulse and the end the fourth pulse (2.5 s), Fig. 4.5(c), the electric field remains relatively constant, but the magnitude falls, causing even less resistive heating in the tissue.

In the experiment, the temperature at the 2 mm location also increases quickly and reached a maximum temperature of 63°C by the end of the seventh pulse. This rapid increase was caused by the resistive heating of the tissue near the 2 mm location. However in the model, this increase is not seen. Instead, the model has a gradual increase through the entire experiment, and reaches a maximum temperature of 50°C at 20 s. This gradual temperature increase in the model indicates that almost no resistive heating is occurring in the tissue near the 2 mm location.

At the 3 mm location, the temperature difference between the experimental and modeling results was 20% at 20 s. At the 3 mm location, the temperature increase is dominated by the conduction of thermal energy away from the sealing site rather than resistive heating. The model predicts this conductive increase, but is unable to account for the rapid temperature increase at the 3 mm location during the first 6 s, causing the temperature results to be different.

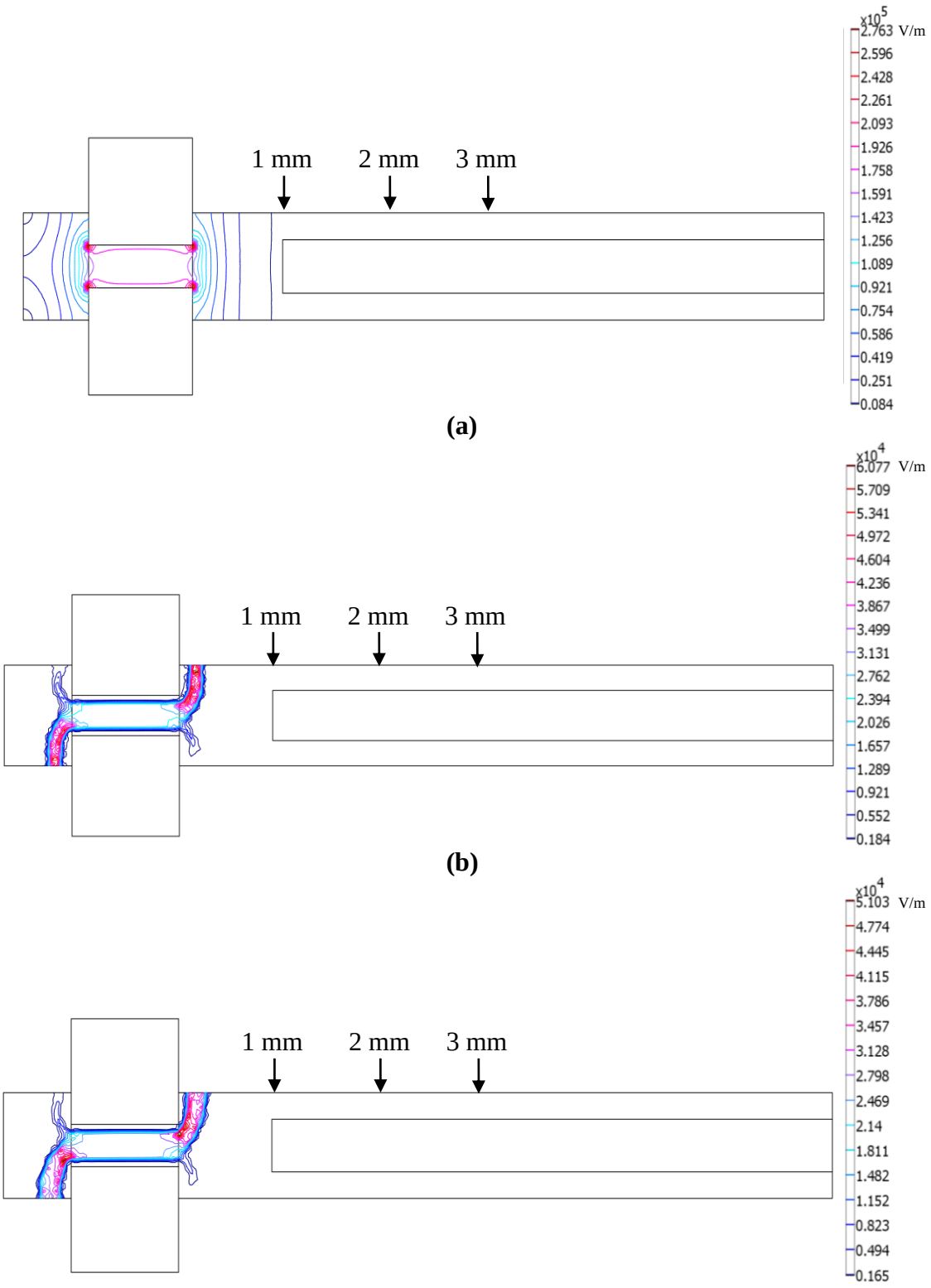

Figure 4.5 Electric field in the 2D compressed vessel model at the: (a) start of the first pulse (0 s), (b) end of the second pulse (1 s) and (c) end of the fourth pulse (2.5 s). The three temperature measurement locations (1, 2 and 3 mm) are also identified.

4.3.1 Comparison of 3D and 2D models

Figure 4.6 shows the tissue temperature modeling results from the 2D (Figs. 4.1(b) and 4.2(b)) and 3D (Figs. 4.1(c) and 4.2(c)) models with the gradually expanded vessel. Since this was a baseline comparison, the thermal conductivity was not varied in either model as a function of temperature or compression level. In order to increase the computational efficiency, no blood was modeled within the vessel either.

By comparing these two geometries, the two closely matched temperature profiles demonstrate the feasibility of using a 2D model to approximate the 3D model, which is time-consuming and prone to stability problems. For the two models, the temperature at three thermistor locations agreed very well during the first 10 s. After 10 s, the temperatures at the 1 mm location started to deviate depending on the model. For the 3D model, the temperature started to decrease, while in the 2D model the temperature continued to increase. This difference occurs because, in the 3D model, the electrodes are much larger than the actual vessel (see Fig. 4.1(c)) and conduct heat away from the sealing site, causing the tissue temperature at the 1 mm location to be reduced. The temperatures at the 2 and 3 mm locations were less affected by this electrode conduction effect and the temperature difference between the two models was less than 5% for most of results.

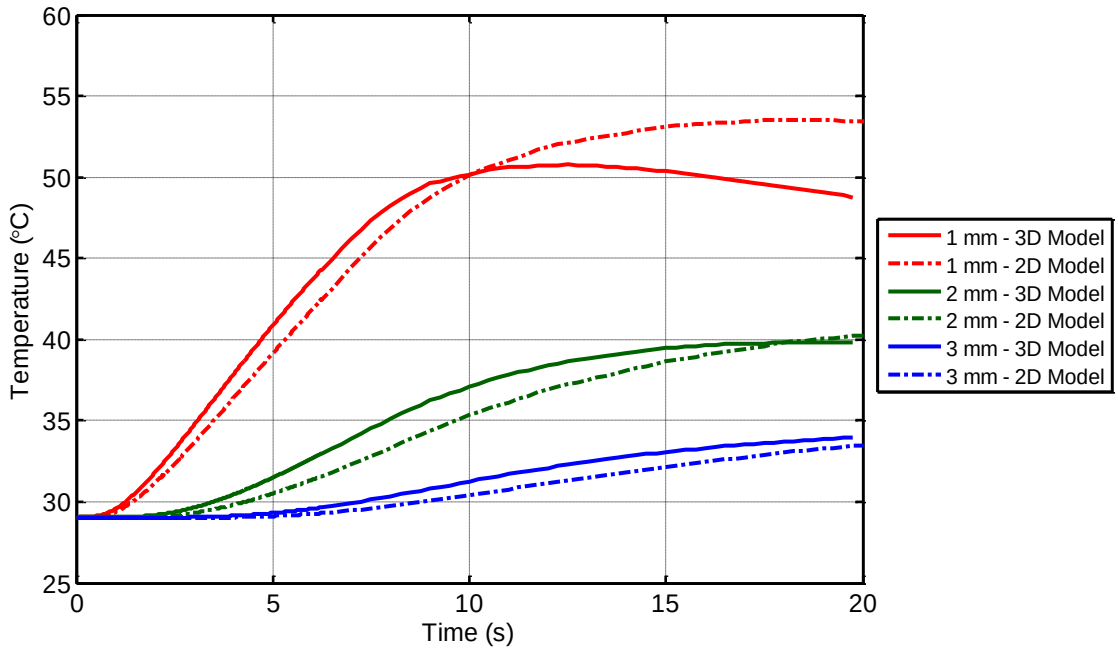

Figure 4.6 Comparison between the 2D and 3D (both without vessel compression) femoral artery sealing model tissue temperatures at the three thermistor locations.

4.3.2 Effect of Blood in the Vessel

Figure 4.7 compares the temperature results with and without blood in the 2D model with compressed vessel thickness (Figs. 4.1(a) and 4.2(a)). With blood in the vessel, the maximum tissue temperature falls by 8°C at the 1 mm location. The additional volume of blood causes the temperature to fall since the thermal energy near the electrodes heats both the tissue as well as blood. The effect of blood is less pronounced at the locations further from the electrodes, since the temperature rise is less dependent on resistive heating and more on thermal conduction. For the 2 mm location, the temperature difference was less than 5%, and the maximum temperature of the two models was nearly identical.

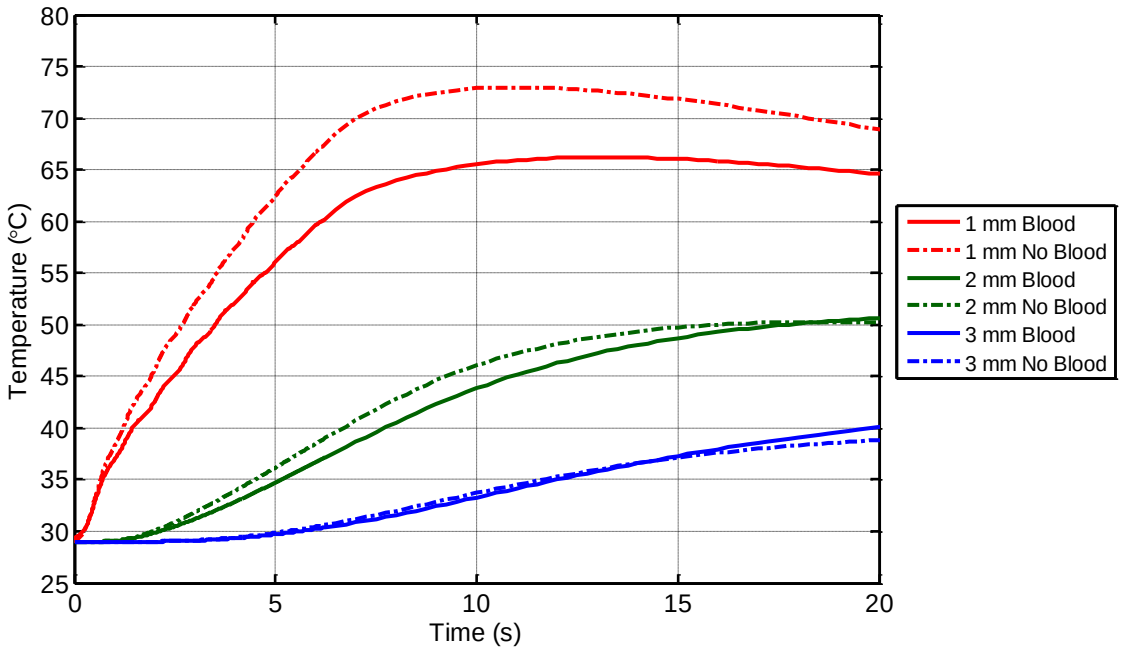

Figure 4.7 Temperature comparison between the 2D model, with and without blood, at the three thermistor locations.

4.4 Conclusions

The differences between the experimental and modeling results show that the thermal energy was being created and transferred to the temperature measurement locations faster than the model predicted. At both the 1 and 2 mm locations, the temperature difference between the model and experiment occurred because the model did not predict the resistive heating in the tissue very well near either location. This effect was less pronounced at the 3 mm location, since the temperature is dominated by conduction within the vessel. When the 2D model was compared to the 3D model, the temperature differences were slight. The effect of blood in the model was found to cause a slight temperature reduction.

To account for physiological changes in the tissue during electrosurgery, the current model used a damage function to vary the electrical conductivity of the tissue. Future work will need to be undertaken to improve the model to account for the changes in the tissue water content and the diffusion of water from the high temperature to the low temperature regions during the sealing process. Incorporation of these effects into the

model is important since they both affect the electrical and thermal properties of the tissue. This should lead to an improved model for predicting the temperature profile of the vessel during sealing.

References

Angelone, L. and Martin, G.L., (2009), "Multiphysics model of the NovaSure endometrial ablation procedure," *Proceedings of the COMSOL Conference*, Boston, MA.

Berjano, E.J., (2006), "Theoretical modeling for radiofrequency ablation: State-of-the-art and challenges for the future," *Biomedical Engineering Online*, Vol. 5, pp. 24-41.

Campbell, P.A., Cresswell, A.B., Frank, T.G., and Cuschieri, A., (2003), "Real-time thermography during energized vessel sealing and dissection," *Surgical Endoscopy*, Vol. 17, pp. 1640-1645.

Chastagner, M.W., (2010a), "Vessel tissue temperature profile during bipolar electrosurgical sealing," *PhD Thesis in Mechanical Engineering, University of Michigan,* Chapter 3.

Chastagner, M.W., (2010b), "Effect of compression and water content on the thermal conductivity of tissue," *PhD Thesis in Mechanical Engineering, University of Michigan,* Chapter 2.

Dodde, R.E., Miller, S.F., Geiger, J.D., and Shih, A.J., (2008) "Thermal-electric finite element analysis of electrosurgical cautery surgical process," *ASME Journal of Manufacturing Science and Engineering*, Vol. 130, pp. 021015-1-8.

Duck, F.A., (1990), *Physical Properties of Tissue: A Comprehensive Reference*, Academic Press, London.

Goldberg, S., (2001), "Radiofrequency tumor ablation: Principles and techniques," *European Journal of Ultrasound*, Vol. 13(2), pp. 129-147.

Golombeck, M.A., Dossel, O., Saubert, A., and Tonnier, V.M., (1999), "Magnetic resonance imaging with implanted neurostimulators: A first numerical approach using finite integration theory," *International Symposium on Electromagnetic Compatibility*, Magdeburg, Germany.

Haemmerich, D., Chachati, L., Wright, A.S., Mahvi, D.M., Lee, F.T. Jr., and Webster, J.G., (2003), "Hepatic radiofrequency ablation with internally cooled probes: Effect of coolant temperature on lesion size," *IEEE Transactions on Biomedical Engineering*, Vol. 50, pp. 493-500.

Kennedy, J.S., Stranahan, P.L., and Taylor, K.D., (1998), "High burst strength, feedback-controlled bipolar vessel sealing," *Surgical Endoscopy*, Vol. 12, pp. 876-878.

Newcomb, W.L., Hope, W.W., Schmelzer, T.M., Heath, J.J., Norton, H.J., Lincourt, A.E., Heniford, B.T., and Iannitti, D.A., (2009), "Comparison of blood vessel

sealing among new electrosurgical and ultrasonic devices," *Surgical Endoscopy*, Vol. 23(1), pp. 90-96.

Pearce, J.A., (1986), *Electrosurgery*. Wiley, New York.

Pennes, H.H., (1948), "Analysis of tissue and arterial blood temperatures in the resting human forearm," *Journal of Applied Physiology*, Vol. 1, pp. 93-122.

Schwan, H.P., and Foster, K.R., (1980), "RF-field interactions with biological systems: Electrical properties and biophysical mechanisms," *Proceedings of the IEEE*, Vol. 68, pp. 104-113.

Smaldone, M.C., Gibbons, E.P., and Jackman, S.V., (2008), "Laparoscopic nephrectomy using the Enseal Tissue Sealing and Hemostasis System: Successful therapeutic application of nanotechnology," *Journal of the Society of Laparoendoscopic Surgeons*, Vol. 12, pp. 213-216.

Tungjitkusolmun, S., Staelin, S.T, Haermmerich, D., Tsai, J-Z., Cao, H., Webster, J.G., Lee, F.T., Mahvi, D.M. and Vorperian, V.R., (2002), "Three-Dimensional Finite Element Analyses for Radio-Frequency Hepatic Tumor Ablation," *Transactions on Biomedical Engineering*, Vol. 49, pp. 3-9.

Tungjitkusolmun, S., Woo E.J., Cao, H., Tsai, J.Z., Vorperian, V.R., and Webster, J.G., (2000), "Thermal - electrical finite element modeling for radio frequency cardiac ablation: Effects of changes in myocardial properties," *Medical and Biology Engineering and Computing*, Vol. 38, pp. 562-568.

Valvano, J.W., Cochran, J.R., and Diller, K.R., (1985), "Thermal conductivity and diffusivity of biomaterials measured with self-heated thermistors," *International Journal of Thermophysics*, Vol. 6, pp. 301-311.

Vellimana, A.K., Sciubba, D.M., Noggle, J.C., and Jallo, G.I., (2009), "Current technological advances of bipolar coagulation," *Neurosurgery*, Vol. 64(3), pp. ons11-ons19.

Ward, A.K., Ladtkow, C.M., and Collins, G.J., (2007), "Material removal mechanisms in monopolar electrosurgery," *Conference Proceedings: Annual International Conference of the IEEE Engineering in Medicine and Biology Society*, pp. 1180-1183.

Wright, N.T. and Humphrey, J.D., (2002), "Denaturation of collagen via heating: An irreversible rate process," *Annual Review of Biomedical Engineering*, Vol. 4, pp. 109-128.

Yang, D., Converse, M.C., Mahvi, D.M., and Webster J.G., (2007), "Measurement and analysis of tissue temperature during microwave liver ablation," *IEEE Transactions on Biomedical Engineering*, Vol. 54(1), pp. 150-155.

CHAPTER 5

BIPOLAR ELECTROSURGICAL VESSEL SEALING WITH COMPRESSIVE FORCE MONITORING

Abstract

Bipolar electrosurgical vessel sealing is commonly used in surgery to perform hemostasis. The electrode compressive force has been demonstrated to be an important factor affecting the vessel seal burst pressure, which is an index of the seal quality. This study utilizes a piezoresistive force sensor at the handle of a laparoscopic surgical device to measure the applied handle force and to estimate the vessel compressive force at the electrode based on the measured handle force. This approach enables the monitoring of vessel compressive force during surgery. The compressive forces during sealing are investigated at four different levels with three different types of porcine vessels: carotid arteries, femoral arteries and jugular veins. The burst pressures of vessel seals done at the lower compressive force are significantly lower than those done at the higher two levels of force. A threshold compressive force value is required to form a quality seal. The need to develop a surgical device with the capability to monitor the clamping force during bipolar vessel sealing is also identified.

5.1 Introduction

Bipolar electrosurgical vessel sealing is widely used in open and laparoscopic surgery for hemostasis. Different approaches have been developed to perform surgical hemostasis, such as ultrasonic energy, bipolar electrosurgical energy, robotic suturing, stapling and vascular clips [Harold et al., 2003]. Bipolar electrosurgical vessel sealing techniques have gained popularity among surgeons as they are considered to be a safe, simple and an inexpensive way to control bleeding [Campagnacci et al, 2007; Ponsky et al., 2008]. Research has been conducted in the past few years on the use of bipolar vessel sealing device in gastrointestinal [Landman et al., 2003; Lee et al., 2003; Matthews et al., 2001], gynecologic [Dubuc-Lissoir, 2003], urological [Franklin et al, 2003; Jayne et al., 2002; Muzi et al., 2002] and thyroidectomical [Shen et al., 2005] operations. In comparison with conventional ligation, bipolar electrosurgical vessel sealing devices can reduce the operating time without increasing the complication rate [Shen et al., 2005; Heniford, 2001].

Electrosurgical vessel sealing applies high-frequency, high-current, and low-voltage electrical energy to generate resistive heating. This heating denatures the collagen of the tissue. However, once the electrical energy is stopped and the vessel tissue begins to cool, the collagen realigns and forms a fused seal [Massarweh et al., 2006]. The vessel seal quality is commonly evaluated using the burst pressure (BP) testing method [Campagnacci et al., 2007; Carbonell et al., 2003; Harold et al, 2003; Shen et al., 2005;]. After electrosurgical vessel sealing, the seal is subjected to a gradual intraluminal pressure increase until the seal fails by bursting. The maximum pressure is recorded as the BP of the vessel seal.

Past research of BP in electrosurgical vessel sealing focuses on three aspects: compressive force effect, performance comparison of commercial electrosurgical devices and vessel size effect. For the compressive force effect, Dilley et al. [1995] suggested that adequate sealing time and compressive forces are necessary to generate a quality seal. Wallwiener et al. [2008] evaluated the effect of compressive pressure, which is the compressive force divided by the electrode-tissue contact area, on vessel sealing and confirmed that adequate compressive pressure is necessary for a good seal to be formed.

They also found that a very high compressive pressure does not always result in a seal with higher BP. In summary, previous studies [Dilley et al., 1995; Wallwiener et al., 2008] concluded that the compressive force during electrosurgical vessel sealing is an important factor for determining BP. Also, for each specific vessel size and type, there likely exists an upper and a lower bound of vessel compressive force for achieving a quality seal.

Two studies [Carbonell et al., 2003; Newcomb et al., 2009] have compared five bipolar laparoscopic electrosurgical devices for vessel sealing:

1. LigaSure™ V with LigaSure™ generator, denoted as LS [Valleylab (Boulder, CO)],
2. PKS™ Cutting Forceps, denoted by PK [Gyrus ACMI (Maple Grove, MN)],
3. EnSeal™ Tissue Sealing System, denoted as RX, [SurgRX (Redwood City, CA)],
4. Plasma Trissector™, denoted as PT, [Gyrus ACMI (Maple Grove, MN)], and
5. LigaSure™ V with Force Triad™ generator, denoted as FT [Valleylab (Boulder, CO)].

Figure 5.1 summarizes the BP results from these five devices (LS, PK, RX, PT, FT) for three vessel size groups [Carbonell et al., 2003; Newcomb et al., 2009]. For the large vessel sizes (6-8 mm), the RX, LS and FT, which utilize a linkage mechanism for the electrodes, have a higher BP and lower failure rate than the PK device, which has a compliant mechanism for the electrode. Fig. 5.2(a) shows the overview of the PK electrosurgical device with its tip shown in Fig. 5.2(b). Components of the compliant mechanism are shown in Fig. 5.2(c). As will be further discussed in the following section, the PK device's compliant mechanism has limited capability to create sufficiently high vessel compressive force for larger vessels. On the contrary, the linkage mechanism used provides a greater compressive force and thus is able to seal larger vessels with higher BP and lower failure rates.

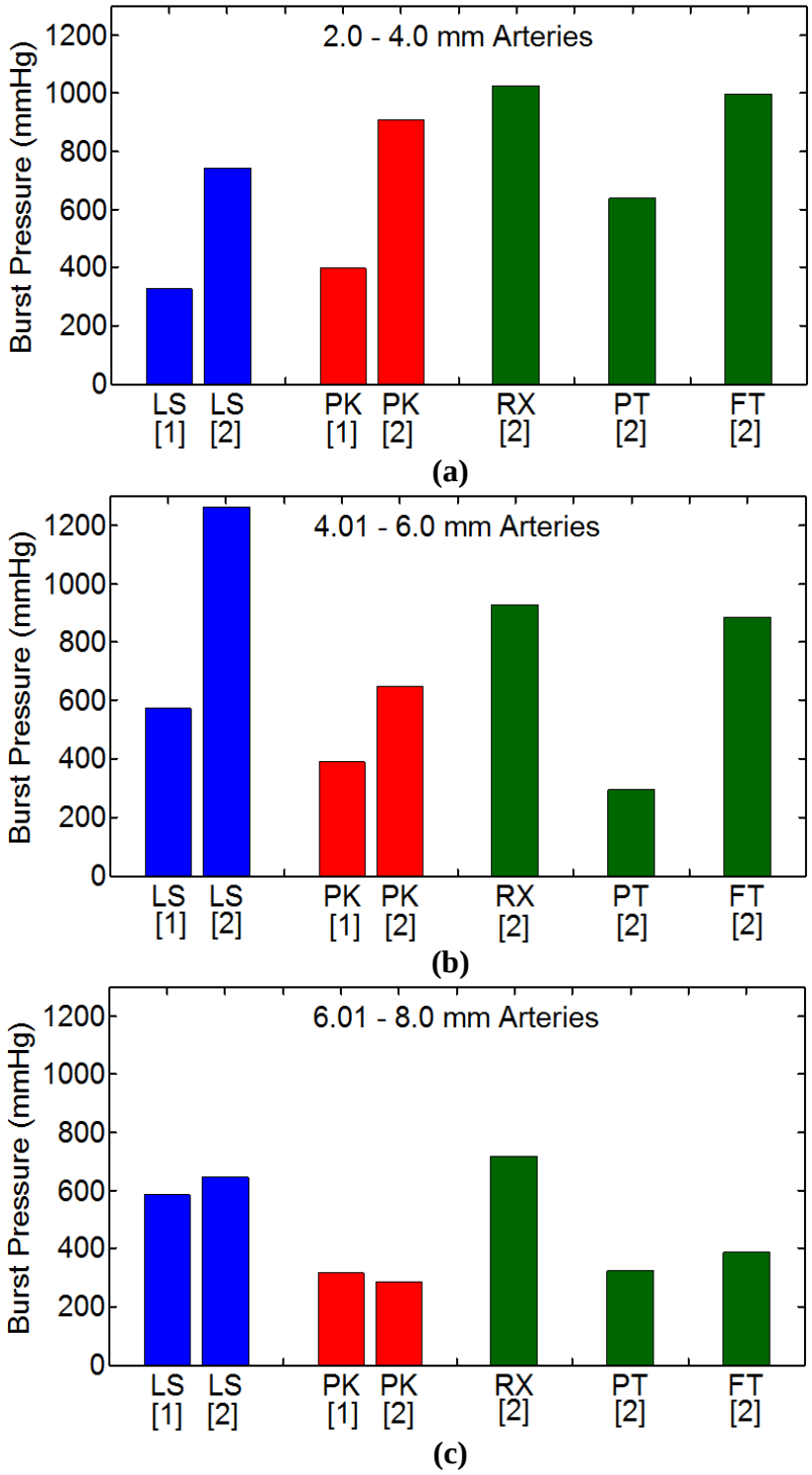

Figure 5.1 Summary of BP sealing results for five different commercial devices (a) arteries ranging from 2-4 mm, (b) arteries ranging from 4-6 mm and (c) arteries ranging from 6-8 mm. (Numbers in brackets indicate reference: (1) Carbonell et al. [2003] and (2) Newcomb et al., [2009])

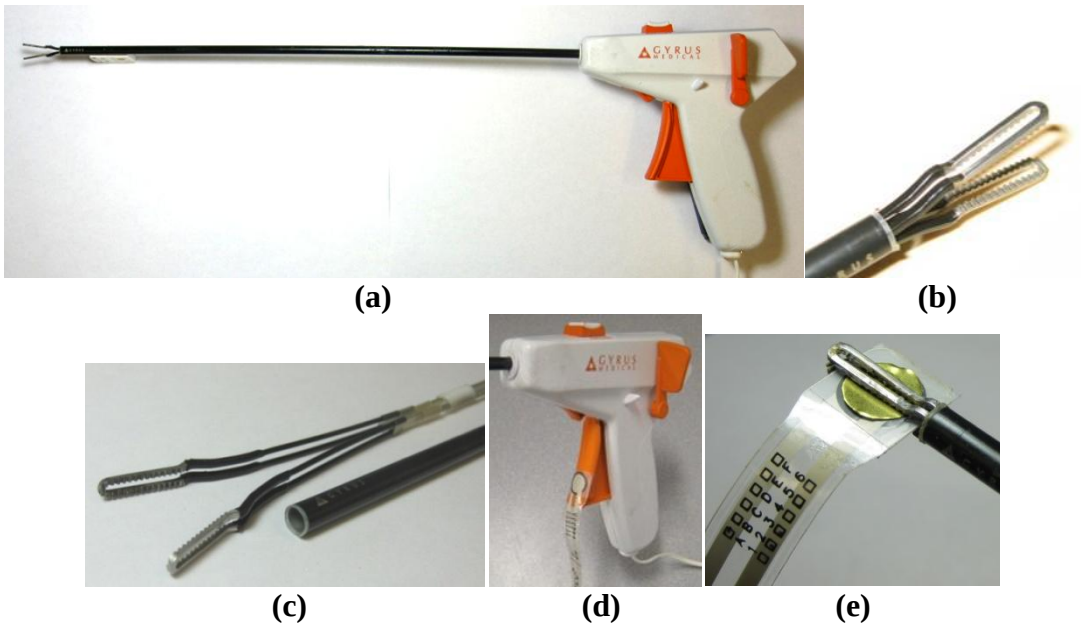

Figure 5.2 Gyrus PKS^{TM} cutting forceps (a) overview of device, (b) bipolar electrodes, (c) compliant mechanism, (d) handle with force sensor attached and (e) electrodes with force sensor clamped between electrodes.

The vessel size effect is also illustrated in Fig. 5.1. In general, larger vessel sizes require a higher compressive force to generate adequate compressive pressure for effective sealing. Without providing sufficient compressive pressure, the seals tend to have a lower BP [Landman et al., 2003; Dilley et al., 1995; Newcomb et al., 2009, Kennedy et al., 1998]. The effect of vessel size is most apparent for the PK device. There are reports showing that the smallest vessel has the lowest BP when using the LS device [Harold et al, 2003; Carbonell et al., 2003; Newcomb et al., 2009]. This is likely due to the linkage-based electrode of the device generating too large of a compressive force on the vessel, thus causing the seal to fail at a lower pressure.

An adequate level of compressive force is important to form a quality seal in electrosurgical vessel sealing. Current electrosurgical vessel sealing devices do not measure and display the compressive force. The goal of this study is to investigate a new electrosurgical device design with a force sensor on the handle for real-time monitoring of the compressive force for clamping the vessel. Surgeons can only estimate the applied force based on experience and visual observation of the sealing process. If a surgeon applies either too high or too low of a compressive force, a low BP seal is expected. A

low BP seal is likely to have leakage, which can result in bleeding complications [Wallwiener et al., 2008]. Both intraoperative prevention and postoperative monitoring were suggested for use in surgery to minimize complications [Wu et al., 2000]. To develop an intraoperative prevention system for vessel sealing, a safe zone of compressive force needs to be defined and a device that can display the compressive force needs to be developed.

In this study, an electrosurgical device with force monitoring capability is introduced. The force applied by a surgeon on the handle of an electrosurgical device for vessel sealing was measured and converted to vessel compressive force. Different levels of vessel compressive force were used to seal a variety of vessels and the BP of the seals was examined. Finally, ANOVA was performed to analyze the significance of the compressive force on the BP.

5.2 Materials and Methods

5.2.1 Electrosurgical Device with Force Monitoring

The Gyrus ACMI 5 mm laparoscopic instrument (PK) was used to seal vessels in this study. Two flexible piezoresistive force sensors, FlexiForce Model A201-100 by Tekscan (South Boston, MA), as shown in Figs. 5.2(d) and 5.2(e), were used. These force sensors are 0.2 mm thick and can measure forces up to 440 N. One of the sensors was attached to the handle, as shown in Fig. 5.2(d), to measure the force applied by the surgeon.

5.2.2 Vessel Compressive Force

The vessel compressive force was measured by clamping the other sensor between the two electrodes, as shown in Fig. 5.2(e). This compressive force for the PK device is generated by the compliant mechanism (Fig. 5.2(c)) and is representative of the force experienced by the vessel during sealing. Six different handle forces were applied to the handle, and the corresponding compressive force was measured. The results are shown

in Fig. 5.3. The compressive force increases linearly with the applied force up until about 30 N. However, the compressive force then plateaus around 16.5 N, as the applied handle force is increased further. This is a limitation of the PK device due to the flexibility of the compliant electrodes. This limited clamping force can explain the low BP results from the large vessels sealed with the PK device (Fig. 5.1(c)) since these vessels require larger compressive forces for sealing.

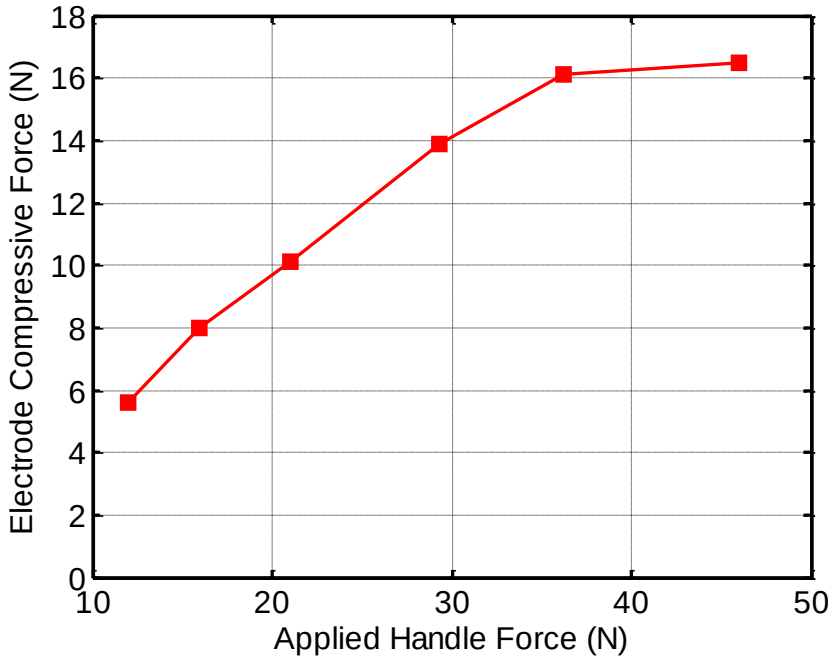

Figure 5.3 Conversion chart for applied handle force to electrode compressive force.

The handle force applied by an experienced surgeon was measured to be from 19 to 22 N when sealing vessels with sizes ranging from 3 to 6 mm. In this study, four levels of applied handle force, 12.0, 15.9, 21.0, and 29.3 N, were applied to the vessels, with corresponding compressive force being estimated to be 5.6, 8.0, 10.1, and 13.9 N. These four force levels include the surgeon's applied force (21 N), and two decremental levels (12.0 and 15.9 N) and one incremental level (29.3 N). All of the forces were within the linear range of Fig. 5.3. Three different vessel types were used including: carotid arteries (4 to 6 mm), femoral arteries (4 to 6 mm), and jugular veins (2 to 4 mm).

5.2.3 Materials

An *ex vivo* porcine vessel sealing experiment was done using four compressive force levels. The vessels were harvested from porcine models with weights ranging from 50 to 55 kg. Table 5.1 summarizes the vessel sizes and number of samples. A total of 82 porcine vessels were used in this study. The adipose tissue was removed from the adventitia before the vessel sealing operation. All of the sealing experiments and BP testing were conducted within 12 hours of the vessels being harvested. The vessels were kept in saline solution before testing.

Table 5.1 Summary of vessels used for electrosurgical vessel sealing using the PK device under controlled compressive force. (Failure is defined as a BP less than 100 mm Hg.)

Compressive force (N)	Parameter	Jugular veins	Carotid arteries	Femoral arteries	Overall
5.6	No. of samples	8	9	8	25
	Avg. size (mm)	3.0	4.6	4.8	4.1
	Failure rate	12.5%	22.2%	62.5%	32%
8.0	No. of samples	6	7	4	17
	Avg. size (mm)	2.8	5.1	4.5	4.1
	Failure rate	0%	14.3%	50%	17.6%
10.1	No. of samples	7	6	6	19
	Avg. size (mm)	3.3	4.7	4.1	4.0
	Failure rate	0%	0%	0%	0%
13.9	No. of samples	8	6	7	21
	Avg. size (mm)	2.4	4.4	4.0	3.5
	Failure rate	0%	0%	0%	0%

5.2.4 Experimental Procedure

The vessel sealing experiment was conducted with the PK device attached to a Gyrus ACMI generator (Model G400). The generator was set to the coagulation mode setting of VP2 35W for all of the vessels in this experiment. The four compressive force levels were randomly applied to the vessels.

The sealing times used in this study were obtained from an experienced surgeon. For each vessel type, the surgeon sealed three vessels and the average sealing time was calculated. This sealing time was then used for the rest of the vessel seals. The average

vessel sealing time for the jugular veins femoral arteries and carotid arteries were 15, 17 and 25 seconds, respectively.

To test the BP, the open lumen of the vessel was connected to a catheter attached to a Transpac IV pressure transducer by Hospira (Lake Forest, IL) and a pump. Saline solution was then gradually pumped into the vessel, and the intraluminal pressure was monitored continuously by the pressure transducer. The seal failed when the pressure exceeded its sealing strength. The intraluminal pressure released right after the seal failed, indicting the BP of the seal. A data acquisition system, PXI 6221 by National Instruments (Austin, TX), was used to record the values of pressure and the maximum recorded pressure was defined as the BP of the seal.

5.2.5 Statistical Analysis

Due to the non-normal distribution of the BPs, a non-parametric Kruskal-Wallis one-way analysis of variance (ANOVA) was performed using statistical analysis software SPSS 17.0 (Chicago, IL) to determine the significance of the differences of BP among the force levels for each type of vessel types. Statistical significance was defined as $p < 0.05$.

5.3 Results

No statistically significant differences existed in vessel size between each force group. The BP results for the jugular veins, femoral arteries, and carotid arteries are shown in Figs. 5.4(a), 5.4(b), and 5.4(c), respectively. The bottom and the top of the box are the first and the third quartile, and the band is the median. The ends of the whiskers mark the minimum and maximum of the data.

For the jugular veins (Fig. 5.4(a)), the lowest mean BP, 251 mm Hg, occurred at the 8.0 N compressive force. The mean BP of the lowest compressive force level was 329 mm Hg. As the compressive force increased to 10.1 and 13.9 N, the mean BPs were 510 and 660 mm Hg, which were more than two times the lowest BP. The differences among the four force groups were statistically significant (p=0.022).

Fig. 5.4(b) shows the results for the femoral arteries. The mean BP for the lower two compressive force groups, 5.6 and 8.0 N, was 142 and 120 mm Hg, respectively. When the compressive force was further increased, the mean BP increased to 198 (10.1 N) and 289 mm Hg (13.9 N). For the femoral arteries, the differences in BP between the four compressive force levels were statistically significant (p=0.047).

For the carotid arteries, results shown in Fig. 5.4(c), the mean BP for the lower two compressive force levels, 5.6 and 8.0 N, was 274 and 302 mm Hg, respectively. As the compressive force increased to 10.1 N, the mean BP increased to 541 mm Hg. When the compressive force was further increased to 13.9 N, the mean BP decreased back to 380 mm Hg. However, these differences were not statistically different (p=0.066) likely due to the limited number of vessel samples.

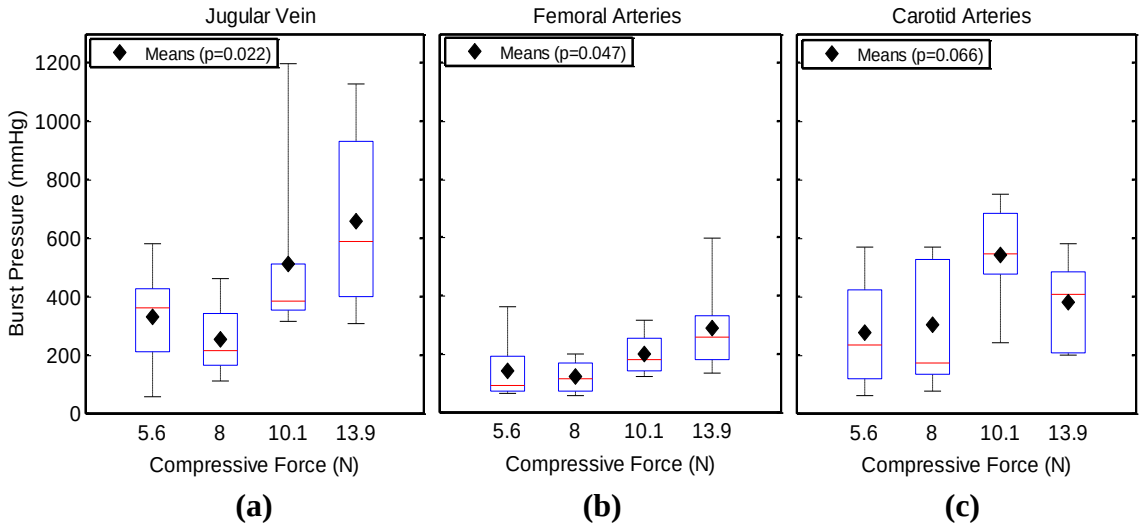

Figure 5.4 BP results of at four compressive force levels (a) jugular veins, (b) femoral arteries and (c) carotid arteries.

5.4 Discussion

In general, within the applied compressive force range studied, as the BP increases the compressive force also increases. There are some exceptions to this relationship. First, when the compressive force increases from 10.1 N to 13.9 N in carotid arteries, the mean BP decreased by 160 mm Hg, approximately 50%. This result implies that a higher

compressive force does not always lead to a better seal. Wallweiner et al. has reported the same phenomenon before [2008]. An optimum compressive force which varies by vessel type and size could exist for achieving the best quality seal. With the force monitoring capability presented in Fig. 5.2, it is possible to create a guideline for surgeons on the required handle force and sealing time based on the type of vessel being sealed. Second, the BP decreases as the force increased from 5.6 to 8.0 N in all three vessel types. However, the differences are only 27, 22 and 77 mmHg, which are relatively small and may be attributed to slight variations within the experiments.

The non-parametric ANOVA analysis of the BP results shows that the compressive force is a significant factor. Statistically significant differences among the four force levels for jugular veins and femoral arteries (p=0.022 and 0.047, respectively) were observed. Although the p-value of the carotid arteries (p=0.066) is not statistically significant, the result is very close to the significance level.

The seal failure rate is summarized in Table 5.1. BPs below 100 mm Hg are considered as a seal failure [Wallwiener et al., 2008]. The failure rate for the lower two force levels is 18.8% (3 out of 16) for carotid arteries and 75% (8 out of 12) for femoral arteries, while the failure rates for the higher two force levels are zero for all the three vessel types. It is clear that if there is insufficient compressive force during sealing, the seal quality will be low and failure may be a problem. A device with the capacity to warn surgeons if they fail to apply sufficient compressive force will be helpful to ensure a high quality vessel seal.

An accurate correlation between handle force and vessel compressive force depends on the size of the opening between the electrodes, which is positively related to the thickness of a vessel. For a given handle force, the thicker the vessel being clamped, the larger the induced compressive force. When compressing the Flexiforce sensor, the electrode opening was 0.2 mm (as shown in Fig. 5.2(e)). This 0.2 mm value is close to the size of the opening when compressing a 5 mm artery, indicating that similar compressive forces should be present on the vessel. In general, arteries have a thicker vessel wall than veins, which will change the compressive force level. This effect can be considered in future studies by adding a tip position sensor to allow for the detection of

the electrode position for more accurate prediction of vessel clamping force [Odom, 2006].

5.5 Conclusions

This study demonstrates the need to accurately measure the electrode clamping force during bipolar electrosurgery. The clamping force plays a vital role in the development of a high quality seal. The capability of a surgical device that is able to measure the handle force, while maintaining an adequate electrode clamping force will improve the vessel seal quality and reduce the seal failure rate. This force monitoring concept can be used as the foundation for an intelligent surgical device that can provide feedback to the surgeon during vessel sealing operations. A device with an electrode position sensor can also be developed to further improve the accuracy of the vessel clamping force prediction.

References

Campagnacci, R., de Sanctis, A., Baldarelli, M., Rimini, M., Lezoche, G., and Guerrieri, M., (2007), "Electrothermal bipolar vessel sealing device vs. ultrasonic coagulating shears in laparoscopic colectomies: A comparative study," *Surgical Endoscopy*, Vol. 21, pp. 1526-1531.

Carbonell, A.M., Joels, C.S., Kercher, K.W., Matthers, B.D., Sing, R.F., and Heniford, B.T., (2003), "A Comparison of laparoscopic bipolar vessel sealing devices in the hemostasis of small-, medium-, and large-sized arteries," *Journal of Laparoendoscopic and Advanced Surgical Techniques*, Vol. 13, pp. 377-380.

Dilley, A.V., Friend, M-A.G., and Morris, D.L., (1995), "An experimental study of optimal parameters for bipolar electrocoagulation," *Gastrointestinal Endoscopy* Vol. 42(1), pp 27-30.

Dubuc-Lissoir, J., (2003), "Use of new energy-based vessel ligation device during laparoscopic gynecologic oncologic surgery," *Surgical Endoscopy*, Vol. 17(3), pp. 466-468.

Franklin, E., Seetharam, S., Lowney, J., Horgan, P., (2003), "Randomized, clinical trial of Ligasure™ vs. conventional diathermy in hemorrhoidectomy," *Diseases of the Colon and Rectum*, Vol. 46(10), pp. 1380-1383.

Harold, K.L., Pollinger, H., Matthews, B.D., Kercher, Sing, R.F., and Heniford, T., (2003), "Comparison of ultrasonic energy, bipolar thermal energy, and vascular clips for the hemostasis of small-, medium-, and large-sized arteries," *Surgical Endoscopy*, Vol. 17, pp. 1228-1230.

Heniford, B.T. Matthews, B.D., Sing, R.F., Backus, C., Pratt, B., and Greene, F.L., (2001), "Initial results with an electrothermal bipolar vessel sealer," *Surgical Endoscopy*, Vol.15, pp. 799-801.

Jayne, D.C., Botterill, I., Ambrose, N.S., Brennan, T.G., Guillou, P.J., and O'Riordain, D.S., (2002), "Randomized clinical trial of Ligasure™ versus conventional diathermy for day-case haemorrhoidectomy," *British Journal of Surgery*, Vol. 89(4), pp. 428-432.

Kennedy, J.S., Stranahan, P.L., Taylor, K.D, and Chandler, J.G., (1998), "High-burst strength, feedback-controlled bipolar vessel sealing," *Surgical Endoscopy*, Vol. 12(6), pp. 876-878.

Landman, J., Kerbl, K., Rehman, J., Andreoni, C., Humphrey, P.A., Collyer, W., Olweny, E., Sundaram, C., Clayman, R.V., (2003), "Evaluation of vessel sealing system, bipolar electrosurgery, harmonic scalpel, titanium clips, endoscopic gastrointestinal

anastomosis vascular staples and sutures for arterial and venous ligation in a porcine model," *The Journal of Urology*, Vol. 169, pp. 697-700.

Lee, W.J., Chen, T.C., Lai, I.R., Wang, W., and Huang, M.T., (2003), "Randomized clinical trial of Ligasure versus conventional surgery for extended gastric cancer resection," *British Journal of Surgery*, Vol. 90, pp. 1493-1496.

Massarweh, N.N., Cosgriff, N., and Slakey, D.P., (2006), "Electrosurgery: History, principles, and current and future uses," *Journal of the American College of Surgeons*, Vol. 202, pp. 520-530.

Matthews, B.D., Pratt, B.L., Backus, C.L., Kercher, K.W., Mostafa, G., Lentzner, A., Lipford, E.H., Sing, R.F., and Heniford, B.T., (2001), "Effectiveness of the ultrasonic coagulating shears, LigaSure vessel sealer, and surgical clip application in biliary surgery: A comparative analysis," *The American Surgeon*, Vol. 67, pp. 901-906.

Muzi, M.G., Milito, G., Nigro, C., Cadeddu, F., Andreoli, F., Amabile, D., and Farinon, A.M. (2007), "Randomized clinical trial of Ligasure™ and conventional diathermy haimorrhoidectomy," *British Journal of Surgery*, Vol. 94(8), pp. 937-942.

Newcomb, W.L., Hope, W.W., Schmelzer, T.M., Heath, J.J, Norton, H.J., Lincourt, A.E., Heniford, B.T., and Iannitti, D.A., (2009), "Comparison of blood vessel sealing among new electrosurgical and ultrasonic devices," *Surgical Endoscopy*, Vol. 23, pp. 90-96.

Odom, D., (2006) "System and method for controlling electrode gap during tissue sealing," U.S. Patent Application Publication US 2006/0224158 A1 October 5, 2006.

Ponksey, T.A., Khosla, A., Rothenberg, S.S., (2008), "Experience with a new energy source for tissue fusion in pediatric patients," *Journal of Laparoendoscopic and Advanced Surgical Techniques*, pp. S207-209.

Shen, W.T., Baumbusch, M.A., Kebebew, E., Duh, Q.-Y., (2005), "Use of electrothermal vessel sealing system versus standard vessel ligation in thyroidectomy," *Asian Journal of Surgery*, Vol. 28(2), pp. 86-89.

Wallwiener, C.W., Rajab, T.K., Zubke, W., Isaacson, K.B., Enderle, M., Schaller, D., and Wallwiener, M. (2008), "Thermal conduction, compression, and electrical current-an evaluation of major parameters of electrosurgical vessel sealing in a porcine *in vitro* model," *Journal of Minimally Invasive Gynecology*, Vol 15(5), pp. 605-610.

Wu, M.P., Ou, C.S., Chen, S.L., Yen, E.Y., Rowbotham, R.. (2000), "Complications and recommended practices for electrosurgery in laparoscopy," American Journal of Surgery, Vol. 179(1), pp, 67-73.

CHAPTER 6

CONCLUSIONS AND FUTURE WORK

6.1 Conclusions

The need to minimize thermal spread during bipolar vessel sealing has been identified as one of the major problems with using bipolar devices during surgery. To date, most bipolar devices attempt to mitigate this thermal spread by altering the electrical energy being delivered to the tissue. However, in order to actually minimize the thermal spread from these devices, an improved understanding of how the key physiological tissue parameters factor into the vessel sealing process is needed. It is important since these parameters directly affect both the temperature profile of the tissue during sealing and the quality of the vessel seal. This thesis aims to fulfill a portion of this gap by addressing how the tissue water content level, thermal conductivity, resistive heating and applied compressive force affect the sealing process. The results from this thesis enhance the understanding of these parameters and their effect on both the thermal profile developed during the sealing process and the quality of the seal. The results from this thesis can be used to develop bipolar devices that are capable of minimizing the thermal spread in the tissue during sealing.

The major achievements of this dissertation are:

- *Effect of water content and compression on the thermal conductivity of tissue:* During electrosurgery, the tissue is subjected to both compression and water loss due

to the surgical process. Using a thermistor-based measurement technique, experimental results show that the tissue thermal conductivity is directly tied to the water content of the tissue. Reducing the tissue water content, compressing the tissue and the combination of the two were all found to reduce the tissue thermal conductivity. The results show that thermal conductivity of the tissue decreases during the electrosurgical process. A three-phase Maxwell-Eucken model was applied to each set of experimental data to predict the thermal conductivity of the tissue with reasonably good agreement. These results can help the development of improved finite element models for predicting temperatures in energy-based surgery.

- *Tissue temperature profile during bipolar vessel sealing:* Experimentally measured temperature profile analysis of bipolar electrosurgical sealing of *in vivo* femoral artery and mesenteric artery vasculature was conducted. The temperature profile, electrical voltage and current delivered during the electrical pulses were analyzed to predict changes in tissue impedance and water content during vessel sealing. Initially, the temperature increase per pulse was substantial. However, as water was lost from the tissue, the tissue impedance increased and the change in tissue temperature per pulse was reduced. This shows that there is a relationship between these three parameters. A finite element model was developed to predict the thermal profile in the vessel during sealing. The discrepancies between experimental and modeling results are discussed and the need to include mass transfer in the model is identified.
- *Effect of compressive load on the vessel seal quality:* The compressive force acting on the vessel during sealing was measured and related to the applied handle force. Experimental tests were conducted to examine the effect of the compressive force on

the burst pressure, a measure of the vessel seal quality, at four different force levels. The results showed that there is likely an optimal compressive force range for each vessel type and size. In general, the two higher compressive forces significantly increased the burst pressure.

The original contributions of this research are as follows:

(1) A process to determine the thermal conductivity of tissue subjected to varying water content and compression levels. Both compression and a reduction in the tissue water content were found to reduce the thermal conductivity of tissue.

(2) A three-phase Maxwell-Eucken model was used to predict the thermal conductivity of the tissue subjected to both compression and varying water content.

(3) An experimental method to determine the thermal profile in the vessel during electrosurgery.

(4) Relationships between the increasing tissue temperature and impedance, and the reduction in the resistive heating of the tissue were identified. The changing tissue water content during the electrosurgical process was identified as the affecting all of these parameters.

(5) A finite element model incorporating a damage function for the electrical conductivity was developed to predict the tissue temperature profile during vessel sealing. The discrepancies between the modeling and experimental results indentified the need to account for mass transfer within the tissue during modeling of the process.

(6) A process to estimate the applied compressive force acting on the vessel tissue during electrosurgical sealing.

(7) A relationship between the vessel compressive force and the burst pressure was identified.

(8) Identification of the need for real-time display of the compressive force being applied to the vessel during electrosurgical sealing.

6.2 Future work

Both the experimental and modeling results presented in this dissertation can be improved and expanded through the following research:

(1) Development of a method that allows for the direct measurement of the amount of water lost during the tissue compression process. Combining such a method with the thermal conductivity measurements will eliminate the need to assume the amount of water lost and will improve the accuracy of the thermal conductivity results.

(2) Investigation into how the fluids within the tissue are transported during electrosurgery is needed to improve the understanding the diffusion of water from the high temperature to the low temperature regions during the vessel sealing process.

(3) Expansion of the finite element model to account for changes in the tissue water content, mass transfer within the tissue and the effect of tissue damage during vessel sealing.

(4) Improvement of the connection between the tissue temperature profile and the quality of the bipolar vessel seal.

(5) Development of an electrosurgical device that allows for the direct measurement and display of the compressive force being applied to the vessel tissue during vessel sealing.

APPENDICES

APPENDIX A

THERMISTOR AND THERMAL DIFFUSION PROBE CALIBRATION

The process to calibrate the thermistors and thermal diffusion probes used in the thermal conductivity study are presented in this Appendix.

A.1. Background

Calibration of the thermal diffusion probe is a two-step process. First, the thermistor used in the thermal diffusion probe must be calibrated to determine its temperature-resistance relationship. Secondly, the thermal diffusion probe needs to be calibrated to allow for the determination of the thermal conductivity.

A.1.1 Thermistor

In order to obtain accurate thermal conductivity measurements with the thermal diffusion probe, calibration of the specific thermistor that is used to build the probe is needed. Thermistors are temperature dependent resistors, which, depending on the materials of construction, are either positive temperature coefficient (PTC) or negative temperature coefficient (NTC). For the PTC thermistors, the resistance rises as the temperature rises. However, for NTC thermistors, the resistance falls as the temperature increases [Sachse, 1974]. For measuring the thermal conductivity, NTC thermistors are employed due to their better stability [Valvano, 1992]. The non-linear relationship

between the temperature and the resistance is defined by the Steinhart-Hart equation [Steinhart and Hart, 1968]:

$$\frac{1}{T} = c_0 + c_1 \ln(R) + c_2[\ln(R)]^3 - 273.15 \tag{A.1}$$

where T is the temperature (°C), R is the resistance (Ω), and c_0, c_1, and c_2 are curve fitting constants.

A.1.2. Thermal Diffusion Probe

The thermal diffusion probe delivers an excess amount of power to the thermistor, causing it to self-heat. This self-heating effect causes the nearby tissue temperature to rise. By measuring this temperature rise with the thermistor, the thermal conductivity of the tissue can be determined. The use of self-heated thermistors to measure thermal conductivity has been demonstrated by Chato [1968], Jain [1979], Valvano et al. [1984] and Patel et al. [1987].

The thermal diffusion probe method uses the following equations to determine the thermal conductivity. The power (P) applied to the thermistor during the heating process is:

$$P = \frac{V_2(V_1 - V_2)}{R_{set}} \tag{A.2}$$

where V_i is the voltage at the i location and R_{set} is the resistance of the resistor.

The instantaneous resistance (R_h) of the thermistor can be determined from the voltage passing through the resistor and the resistance calculated in Eq. (A.2):

$$R_h = \frac{R_{set}V_2}{(V_1 - V_2)} \tag{A.3}$$

Since excess power is being applied to the thermistor, the thermistor will self-heat. This self-heating effect causes the temperature of the thermistor to increase. This temperature change (ΔT) is defined as:

$$\Delta T = T_{current} - T_{initial} \tag{A.4}$$

where $T_{current}$ is the current and $T_{initial}$ is the initial temperature.

A linear regression relating the applied power to the change in temperature is then used to separate the steady-state and transient terms [Valvano et al., 1984]:

$$\frac{P}{\Delta T} = A - Bt^{-0.5} \tag{A.5}$$

where A is the steady-state coefficient and B is the transient coefficient. The thermal conductivity of the tissue, k_t, is then determined from the steady-state coefficient [Valvano et al., 1984]:

$$k_t = \frac{1}{\frac{a_1}{A} + a_2} \tag{A.6}$$

where a_1 and a_2 are unknown calibration coefficients, which are determined by placing the thermistor in two substances with known thermal conductivity values at the same temperature as the experiment.

A.2 Thermistor Calibration

Two glass encapsulated bead thermistors were used for measuring the thermal conductivity. The thermistors were both model #P60DA102M (Fig. A.1) manufactured by GE Sensing (Billerica, MA) and had a bead diameter of 1.524 mm. This size of thermistor is recommended by Yuan et al. [1993] and has been previously been used by Patel et al. [1987].

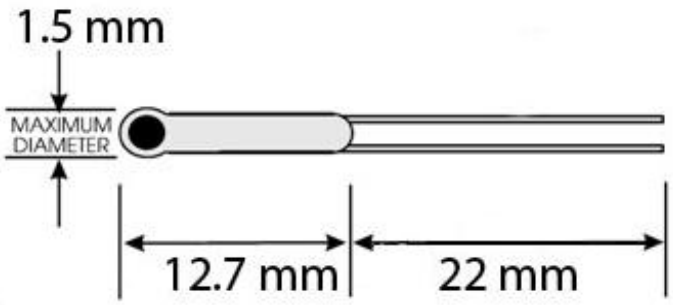

Figure A.1 Specifications of the P60DA102M thermistor used for the thermal diffusion probe (GE Sensing).

Each thermistor was calibrated by placing it inside of a Thermoworks 3001 Dry-Well calibrator (Thermoworks, Orem, UT), shown in Fig. A.2(a). In order to hold the thermistor, a custom machined sleeve was built, allowing the thermistor to have conductive contact with the heating element in the end of the calibrator. The sleeve, shown in Fig. A.2(b), was comprised of a milled brass end for the thermistor to sit in and a fiberglass shaft allowing the wires to travel out of the calibrator. The thermistor was then mounted into the sleeve and placed inside of the calibrator. The leads of the thermistor were attached to a 7.5 digit digital multimeter (DMM) (National Instruments [NI] PXI-4071). A custom program was developed in LabVIEW 8.5 (NI) to collect the resistance data at the desired times.

(a) **(b)**

Figure A.2 (a) Thermoworks 3001 Dry-Well calibrator used to calibrate the thermistor and (b) custom sleeve for thermistor calibration.

In order to collect the temperature-resistance data for the thermistors, the calibrator was set to the desired temperature and was allowed to equilibrate. The resistance of the thermistor was recorded for 30 s at 4 Hz. The lowest temperature that the calibrator could reach was 30°C.

A 0°C temperature calibration was also performed using an ice bath reference. A 1000 ml beaker was filled with a combination of water and crushed ice. Then the thermistor placed into the beaker. The water temperature was recorded using a calibrated thermometer (ERTCO #1003-3S), while the resistance of the thermistor was determined using the DMM.

Figure A.3(a) shows the Steinhart-Hart resistance-temperature plot for the thermistor (T1) used during the tissue water content experiments, while Fig. A.5(b) shows the same plot for the thermistor (T2) used during the compression and the compression combined with the varying water content experiments from Chapter 2.

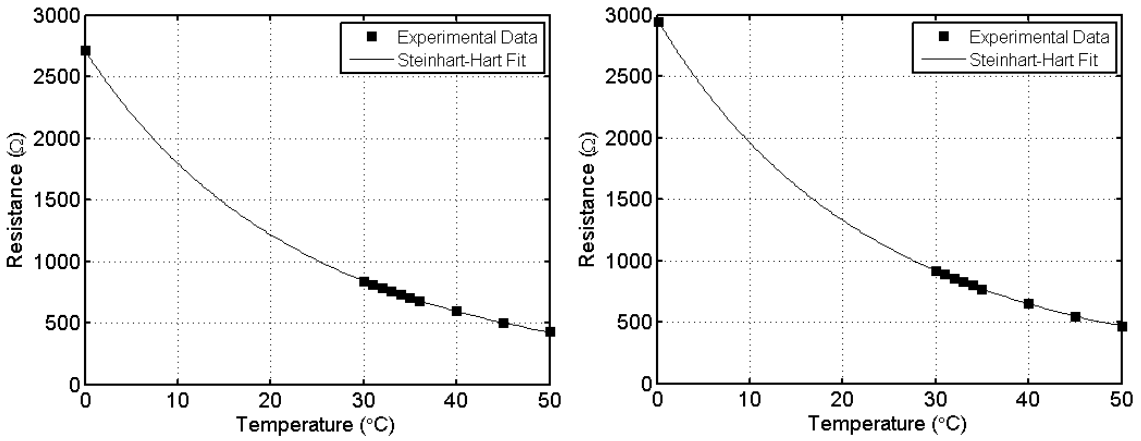

Figure A.3 Temperature-resistances plot for (a) the thermistor (T1) used for the varying water content experiments and (b) the thermistor (T2) used for the compression and the compression combined with the varying water content experiments.

At 25°C, the resistance of the two thermistors was 1007.6 Ω for T1 and 1100.2 Ω for T2. The Steinhart-Hart coefficients, Table A.1, were also determined for the two thermistors.

Table A.1 Steinhart-Hart coefficients for the two thermistors used in the Chapter 2 experiments.

Steinhart-Hart Coefficient	T1	T2
c_0 (K^{-0})	1.3636×10^{-3}	1.3382×10^{-3}
c_1 (K^{-1})	2.7941×10^{-4}	2.7894×10^{-4}
c_2 (K^{-2})	1.8295×10^{-7}	1.8131×10^{-7}

A.3 Thermal Diffusion Probe Calibration

The two calibrated thermistors were then used to build two thermal diffusion probes. In order to calibrate the thermal diffusion probes, two fluids with known thermal conductivities were required. The two fluids used in this study were glycerol (McMaster Carr #3190K236) and agar-gelled water. The agar-gelled water was made by mixing an agar gelling agent, Kelset (ISP Corporation, San Diego, CA) in 0.9% concentration (*w*/*w*) with de-ionized water [van Gelder, 1997]. The addition of the agar to the water limits the amount of thermal convection during the calibration and does not alter the overall thermal conductivity of the solution [Valvano et al., 1985]. Table A.2 lists the thermal conductivities of the two fluids as a function of temperature.

Table A.2 Thermal Conductivity of Calibration Fluids [Ramires et al., 1995; CINDAS, 1988]

Temperature (°C)	Water (W/m-K)	Glycerol (W/m-K)
18	0.5938	0.284
20	0.5975	0.2841
22	0.6011	0.2844
24	0.6046	0.2847
26	0.6080	0.285

In order to replicate the baseline tissue temperature observed during the experimental thermal conductivity measurements, a temperature controlled water bath, Fig. A.4(a), with an immersion circulator (Model #MS, LAUDA-Brinkmann, Delran, NJ) was constructed. A flow through chiller (VWR #1108, West Chester, PA) was attached to the cooling coil of the immersion circulator to cool the bath to temperatures below the ambient temperature.

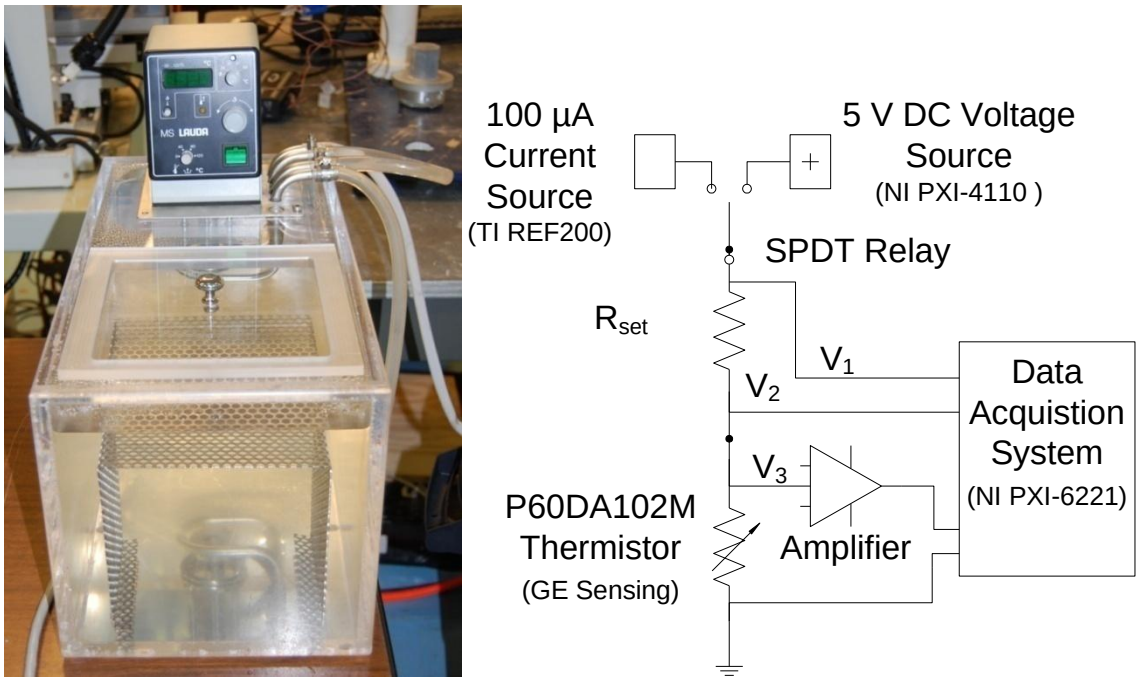

Figure A.4 (a) Water bath used to calibrate the thermal diffusion probe sensor and (b) circuit used to self-heat the thermistor within the thermal diffusion probe.

To provide the desired self-heating effect to the thermal diffusion probe, a circuit (see Figure A.4(b)) was constructed. The circuit uses a relay to control the level of current and voltage being applied to the thermistor depending on the time. The relay switches between a constant voltage source set at 5 V DC (NI PXI-4110 DC) and a constant current source (Texas Instruments REF200) set at 0.1 mA. The voltage drop across both the resistor and the thermistor was measured using a 16-bit data acquisition board (NI PXI-6221). The circuit was attached to the PXI-6221 through a feedthrough module (NI SCC-FT01) contained within a signal conditioning box (NI SC-2345). The data was collected at a rate of 500 Hz with a program written in LabVIEW 8.5 (NI).

During the temperature sensing portion of the experiment (the first 5 s) the relay passed the electrical current to the thermistor to determine the initial temperature of the tissue. During the self-heating portion (the next 30 s of the experiment), the relay was closed to allow for the 5 V to be applied to the thermistor circuit. Based on the initial recorded temperature, the resistance of R_{set}, was changed to provide the desired ΔT during the self-heating portion of the test. For the thermal diffusion probe technique, this ΔT

needs to be above 2.5°C [Valvano et al., 1985]. The R_{set} value used for the calibration procedure matched the same resistance used during the experimental test.

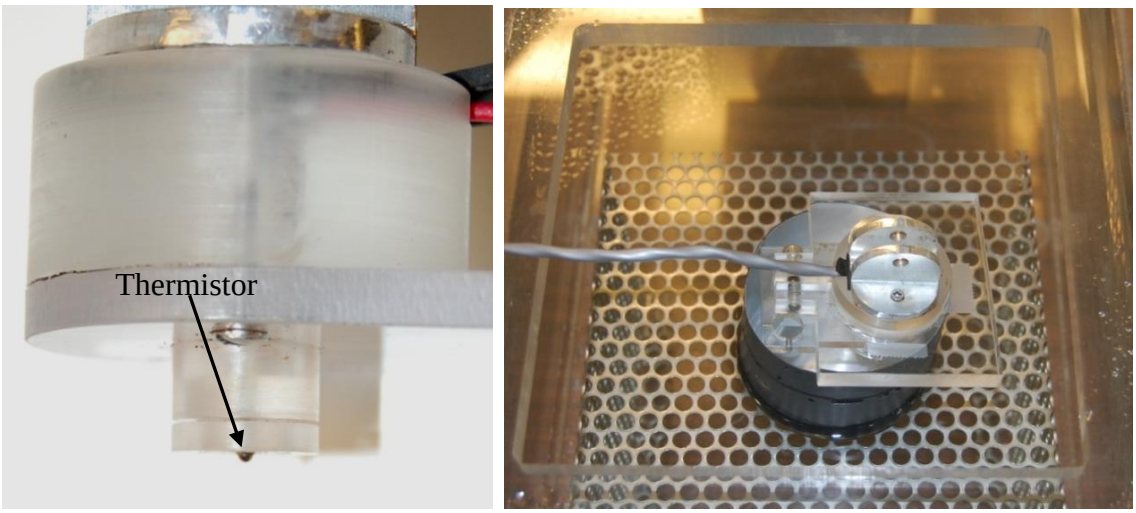

(a) **(b)**

Figure A.5 (a) The thermistor contained within the thermal diffusion probe and (b) the thermal diffusion probe sensor during the water bath during calibration.

To begin the calibration procedure, the thermal diffusion probe, shown in Fig. A.5(a), was placed into a container of calibration fluid. Both the probe and fluid were then placed into the water bath attached to the immersion circulator, Fig. A.5(b). The desired temperature was set on the water bath and the temperature of the fluid was allowed to equilibrate. This process took approximately 45-80 minutes depending on the calibration fluid being used.

Since the temperature of the experimental tests varied slightly, a range of temperatures was used for the calibration process. Regular temperature intervals within this range were selected for the calibration process. For each temperature interval and fluid type, the process was repeated five times. The data obtained from each calibration fluid was then fit to the linear regression, Eq. (A.5), to determine A and B.

For each experiment, the known thermal conductivity of the fluid, along with the A and B results were interpolated to the baseline temperature of the tissue in the experiment. These interpolated values were then used to solve Eq. (A.6), allowing for the two unknown calibration coefficients, a_1 and a_2 to be determined. Then by using the $P/\Delta T$

results of Eq. (A.5) and Eq. (A.6) along with the two calibration coefficients a_1 and a_2, the thermal conductivity of the tissue could be determined.

References

Chato, J.C., (1968), "A method for the measurement of thermal properties of biological materials," *Thermal Problems in Biotechnology,* American Society of Mechanical Engineers, New York, pp. 16-25.

CINDAS, (1998), "Properties of Inorganic and Organic Fluids," In: C.Y. Ho (ed.), *CINDAS Data Series on Material Properties, Vol. V-1.,* Hemisphere Publishing Corporation, New York, pp. 129-132.

Jain, R.K., (1979), "Transient temperature distributions in an infinite, perfused medium due to a time-dependent spherical heat source," *ASME Journal of Biomechanical Engineering*, Vol. 101, pp 82-86.

Ramires, M.L.V., Nieto de Castro, C.A., Nagasaka, Y., Nagashima, A., Assael, M.J., and Wakeham, W.A., (1995), "Standard reference data for the thermal conductivity of water," *Journal of Physical and Chemical Reference Data*, Vol. 24(3), pp.1377-1381.

NTC Termistors: Type P60/65/85/100 Datasheet. GE Sensing, Boston, MA. Accessed: Dec. 14, 2009, http://www.gesensing.com/products/resources/datasheets/p606585.pdf.

Patel, P.A., Valvano, J.W., Pearce, J.A., Prahl, S.A., and Denham, C.R., (1987), "A self-heated thermistor technique to measure effective thermal properties from the tissue surface," *Journal of Biomechanical Engineering*, Vol. 109(4), pp. 330-335.

Steinhart, J.S. and Hart, S.R., (1968), "Calibration curves for thermistors," *Deep Sea Research,* Vol. 15, pp. 497-503.

Sachse, H.B., (1975), *Semiconducting Temperature Sensors and their Applications*, John Wiley & Sons, New York, p. 391.

Valvano, J.W., Allen, J.T., and Bowman, H.F., (1984), "The simultaneous measurement of thermal conductivity, thermal diffusivity, and perfusion in small volumes of tissue," *Journal Biomechanical Engineering,* Vol. 106(3), pp. 192-197.

Valvano, J.W., Cochran, J.R., and Diller, K.R., (1985), "Thermal conductivity and diffusivity of biomaterials measured with self-heated thermistors," *International Journal of Thermophysics*, Vol. 6, pp. 301-311.

Valvano, J.W., (1992), "Temperature measurements," In: Cho, Y.I. (ed) *Advances in Heat Transfer,* Vol. 22, pp. 359-436.

van Gelder, M.F., (1997), "A thermistor based method for measurement of thermal conductivity and thermal diffusivity of moist food materials at high temperatures," *PhD Thesis in Biological Systems Engineering, Virginia Polytechnic Institute and State University.*

Yuan, D.Y., Valvano, J.W., and Anderson, G.T., (1993), "Measurement of thermal conductivity, thermal diffusivity, and perfusion," *Biomedical Sciences Instrumentation,* Vol. 29, pp. 435-442.

APPENDIX B

FINITE ELEMENT MODELING OF COMPRESSION ON TISSUE THERMAL CONDUCTIVITY

In order to measure the tissue thermal conductivity under compression, a thermal diffusion probe was constructed. The probe contained an upper and lower plate to provide compression to the tissue while allowing for the thermal conductivity to be measured. The fundamentals behind the thermal diffusion probe are well developed, however, the use of a second lower plate to provide compression to the tissue has not been studied. In this Appendix, a finite element model is constructed to examine the effect of the lower plate on the thermal conductivity measurements.

B.1. Introduction

In order to better understand the fundamentals behind heat transfer in an electrosurgical setting, the effect of the electrosurgical process on the tissue properties must be explored. During electrosurgery, the tissue is subjected to water loss, permanent damage and compression. All of these effects will alter the thermal conductivity of the tissue. However, measuring the effect of compression on the thermal conductivity during vessel sealing is a challenge due to small vessel size. Therefore, tests were conducted to replicate the surgical setting by using a set of plastic plates to compress spleen tissue. Within one of the plates, a small thermistor was embedded. By self heating a thermistor, the thermal conductivity of the tissue can be measured [Valvano et al., 1985; Valvano and Chitsabesan 1987; Patel et. al, 1987]. This technique uses a small thermistor bead with a radius, a, placed in contact with the tissue. The governing heat conduction

equations for the thermistor and the tissue are [Balasubramaniam and Bowman, 1977]:

$$\frac{1}{r^2}\frac{\partial}{\partial r}\left(r^2\frac{\partial}{\partial r}\theta_{therm}\right)+\frac{\dot{Q}_{therm}}{k_{therm}}=\frac{1}{\alpha_{therm}}\frac{\partial}{\partial t}\theta_{therm} \text{ when } 0\le r\le a \tag{B.1a}$$

$$\frac{1}{r^2}\frac{\partial}{\partial r}\left(r^2\frac{\partial}{\partial r}\theta_{tissue}\right)=\frac{1}{\alpha_{tissue}}\frac{\partial}{\partial t}\theta_{tissue} \text{ when } r > a \tag{B.1a}$$

where

$\dot{Q}_{therm}$ is the heat generation in the thermistor,

θ_{therm} is the temperature rise of the thermistor,

θ_{tissue} is the temperature rise of the tissue,

k_{therm} is the thermal conductivity of the thermistor,

k_{tissue} is the tissue thermal conductivity, and

r is the radial coordinate measured from the thermistor center.

Due to the use of *ex vivo* tissue and the clamping effect, the blood perfusion and metabolic heat sources normally found in the heat conduction equation can be ignored. Initially, the thermal diffusion probe technique is defined by two initial conditions and four boundary conditions [Valvano, 1984a, 1984b; Valvano and Nho, 1991, Zhang et al., 2002]. The two initial conditions are:

$$\nabla^2\theta_{therm}+\frac{P}{V_{therm}}\cdot\frac{1}{k_{therm}}=0 \text{ when } r\le a \tag{B.2a}$$

$$\nabla^2\theta_{tissue}=0 \text{ when } r > a \tag{B.2b}$$

where

V_{therm} is the volume of the thermistor, and

P is the applied power.

The four boundary conditions are defined by the following equations. The change in temperature and thermal flux at the interface is continuous:

$$\theta_{tissue} = \theta_{therm} \text{ when } r = a \tag{B.3a}$$

$$k_{therm} \frac{\partial \theta_{therm}}{\partial r} = k_{tissue} \cdot \frac{\partial \theta_{tissue}}{\partial r} \quad \text{when } r = a \tag{B.3b}$$

There is no heat loss at the center of the thermistor bead:

$$\frac{\partial \theta_{therm}}{\partial r} = 0 \text{ when } r = 0 \tag{B.3c}$$

When the thermistor power is finite and the tissue is infinite, the temperature rise at infinity is zero:

$$\theta_{tissue} = 0 \text{ when } r \to \infty \tag{B.3d}$$

The steady state solution of these six equations can be used to determine the thermal conductivity. The solution to these equations was determined by Balasubramaniam and Bowman [1974, 1977]:

$$\theta_{therm} = \frac{P}{4\pi k_{tissue}} \left[\frac{1}{2a^3} \frac{k_{tissue}}{k_{therm}} \left(a^2 - r^2 \right) + \frac{1}{a} \right] \tag{B.4a}$$

$$\theta_{tissue} = \frac{P}{4\pi k_{tissue}} \frac{1}{r} \tag{B.4b}$$

However, since the temperature rise occurs over the entire thermistor bead, the volume average temperature increase ΔT is calculated by integrating r from 0 to a:

$$\Delta T = \frac{1}{V_{therm}} \int_0^a 4\pi r^2 \theta_{therm} dr = \frac{P}{4\pi a} \left(\frac{1}{k_{tissue}} + \frac{1}{5k_{therm}} \right) \tag{B.5}$$

or reordered as:

$$\frac{1}{k_{tissue}} = 4\pi a \frac{\Delta T}{P} - \frac{1}{5k_{therm}} \tag{B.6}$$

The device used to test the thermal conductivity of the tissue in Chapter 2 incorporates a lower and upper plastic plate to compress the tissue with the thermistor bead embedded within the top plate. The thermistor is placed within the upper plastic plate, so half of the bead is exposed, thus allowing the same governing equations to be used as if the entire bead had been exposed to the tissue [Patel et al., 1987]. The effect of the upper plate is accounted for during the calibration process, in which the thermistor is calibrated in two known fluids. However, the effect of the lower plate on the thermal conductivity is unknown, especially at higher compression levels. Patel et al. [1987] has shown that for a partially exposed thermistor bead, the depth of measurement is approximately 2 thermistor radii. However, they did not speculate as to what effect a second plastic plate would have on the thermal conductivity. Therefore, a finite element model (FEM) is presented in order to study the effect of the lower plastic plate on the thermal conductivity results. The FEM replicates the thermal diffusion probe method used to measure the thermal conductivity of the tissue.

B.2. Thermal Conductivity Formulas

The thermal diffusion probe method determines the instantaneous temperature increase of the thermistor bead during the self-heating process, along with the power being sent through the thermistor to calculate the thermal conductivity of tissue. The formulas used to calculate the thermal conductivity are presented in Appendix A.

B.3. Thermal Conductivity Modeling

B.3.1. Model Setup

A set of thermal FEM were developed in COMSOL 3.5a to test the effect of the two 12.5 mm acrylic plates on the thermal conductivity results obtain in Chapter 2. Figure

B.1 shows a representative 2D axis symmetric model of the experimental setup. Within the center of the top acrylic plate, a glass encapsulated bead thermistor (GE Sensing P60DA102M) was modeled using the dimensions found in Kharalkar and Valvano [2006]. Between the two acrylic plates, a volume of medium was modeled. Depending on the model use, the medium type and height varied, as shown in Table B.1.

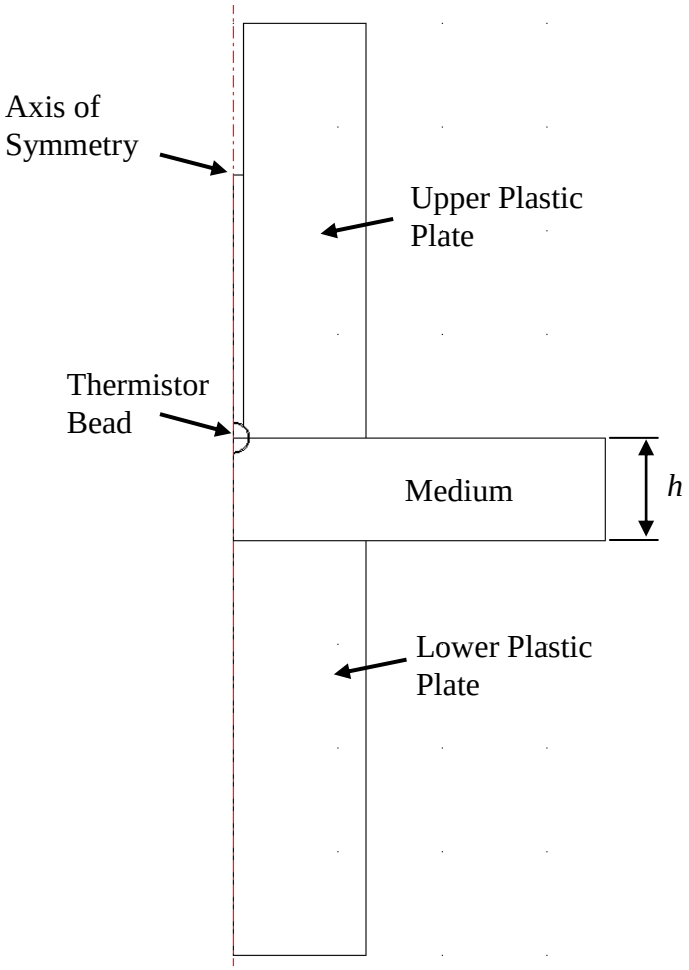

Figure B.1 Schematic of FEM used to simulate the calibration process and to test the effect of the second plate on the thermal conductivity results.

Table B.1 Models used in this study

Model	Height of Medium (mm)	Medium Type Used	Lower Plate	Model Use
#1	30	Water, Glycerol, Tissue	No	Calibration and infinite tissue simulation
#2	1	Tissue	Yes	Compression simulation
#3	1.25	Tissue	Yes	Compression simulation
#4	1.5	Tissue	Yes	Compression simulation
#5	2	Tissue	Yes	Compression simulation
#6	3	Tissue	Yes	Compression simulation
#7	4	Tissue	Yes	Compression simulation
#8	5	Tissue	Yes	Compression simulation

For Model #1, no lower plastic plate was modeled, since it was used to represent both the calibration process and the situation of an infinite tissue medium. In the other models, the lower plate was added and the medium properties were set to represent the compressed tissue. The height of the tissue, *h*, in the models varied between 1 and 5 mm. Using the power determined from the experimental results, 5.535 mW, the volumetric heat generation term of the thermistor bead was calculated to be 3.819×10^6 W/m^3. Material properties for the materials used in the model are presented in Table B.2. It is important to note that the effect of the compression on the specific heat and density of the tissue is unknown. Therefore, these two properties were fixed during the entire modeling process.

Table B.2 Constants used in tissue compression FEM.

Material property	Density, ρ [kg/m^3]	Specific heat, C [J/(g·K)]	Thermal conductivity, k [W/(m·K)]
Acrylic	1190[4]	1420[4]	0.19[4]
Bead (Thermistor)	6300[1]	159[1]	0.10[1]
Glass	2203[4]	703[4]	1.38[4]
Glycerol	1262[2]	2354[3]	0.284[3]
Tissue	1050[1]	3700[1]	0.49[5]
Water (Agar-gelled)	1000[4]	4188[4]	0.592[4]

[1]Kharalkar [2006], [2]van Gelder [1998], [3]CINDAS [1998], [4]COMSOL [2008], [5]Chastagner [2010]

The edge along the axis of symmetry was constrained by thermal symmetry ($r = 0$). A continuity boundary condition was applied to all internal edges of the model. The outer edges of the plastic plate were set to insulation, modeled as a zero heat flux

condition. The outer tissue edges were constrained to the average temperature of the spleen tissue from the tissue compression experiments, 18.4°C. The initial temperature of all the model components was also set to this value. Depending on the tissue thickness, the number of triangular elements used to mesh the model varied from 4,961 to 7,615.

B.3.2. Modeling Procedure

In order to determine the thermal conductivity of the tissue, the calibration procedure was simulated by running Model #1 twice. First, the model was run with glycerol as the medium and the second time with water as the medium. For each model, the change in the averaged volumetric thermistor temperature was calculated as a function of time. Then by using change in ΔT, along with the known power from the experiment, the process outlined in Appendix A could be used to determine the two unknown calibration coefficients, a_1 and a_2, for the model geometry.

Once the calibration coefficients were known, Models #2-8 were run. The averaged volumetric thermistor temperature as a function of time for each model was determined. Then, by using the calculated a_1 and a_2 values for the probe, the predicted thermal conductivity of the tissue for each model was calculated.

B.4. Results

The FEM results indicate that the tissue temperature and thermal conductivity are dependent on the location of the plastic plates. Figure 2(a) shows that the heat was generated in the center of the thermistor bead and was transmitted outward into the tissue and the plastic plates. Fig. 2(b) shows that varying the tissue thickness caused the volume averaged temperature of the bead to vary by less than 0.15°C. The lowest temperature was observed in the infinite tissue medium model. As the plates become closer, the insulating effect of the plastic plates limited the ability of the bead to dissipate the heat into the tissue, thereby increasing the bead temperature.

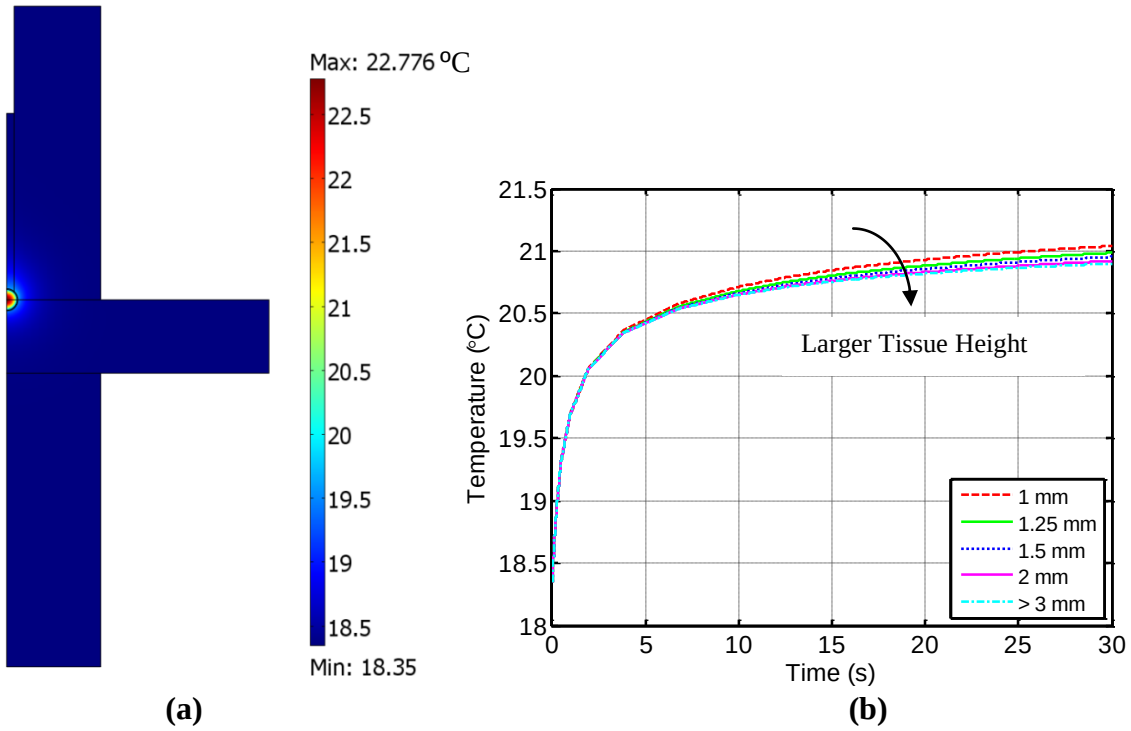

Figure B.2 (a) Representative temperature profile in the model when *h* = 5 mm and *t* = 30 s and (b) the average volumetric temperature of the thermistor bead.

A curve fit can be applied to $P/\Delta T$ response of the thermistor to determine the steady state and transient response of the tissue to the self heating effect of the thermistor, as shown in Fig. B.3(a-b). The steady state response of the fit corresponds to the thermal conductivity of the tissue and is affected by the different tissue heights. There was very little change in the $P/\Delta T$ response when the tissue height, *h*, was greater than 3 mm. Since the applied power was the same for all of the models, this difference is attributed to the higher average temperature in the bead (Fig. B2(b)) when the tissue thickness is smaller.

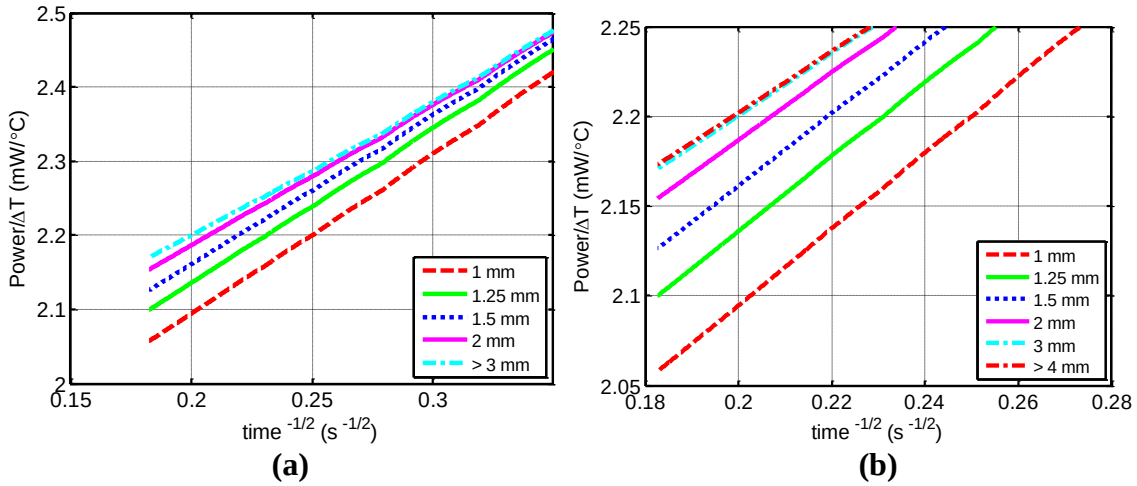

Figure B.3 (a) Plot of *P/ΔT* for the different tissue thickness models used and (b) close-up of the plot.

Figure B.4 shows the radial temperature distribution (at t = 30 s) along the upper plate-tissue interface (location shown in figure inset), when the tissue thickness is at the infinite level (no bottom plate) and at h = 1 mm. The highest temperature gain in both models is at the center of the bead, where the temperature increased by nearly 4.5°C. This is in contrast to the tissue, where the maximum temperature increase was 1.6° C at the thermistor-tissue interface. Similar temperature increases in the tissue-thermistor interface have been reported within the literature [Kharalkar and Valvano, 2006].

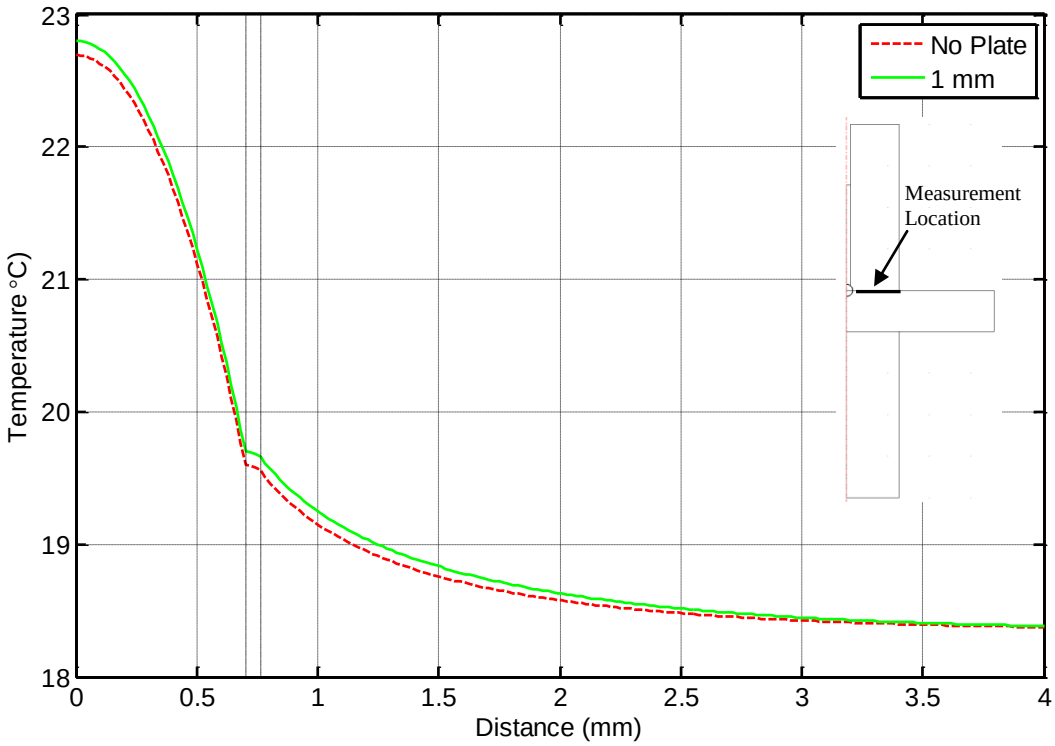

Figure B.4 Radial temperature profile of the thermistor and the tissue at *t* = 30 s. The left dotted line represents the edge of the thermistor bead and the right dotted line represents the thermistor-tissue interface.

Figure B.5 shows the thermal conductivity for the different tissue heights. The predicted thermal conductivity of the infinite model (no bottom plate) was found to be 0.484 W/(m·K). The difference between this predicted thermal conductivity result and the tissue thermal conductivity values used for the input (Table B.2) was caused by the representative geometry of the thermistor bead used in the model. Figure B.5 indicates that as the tissue height is reduced, the thermal conductivity remains relatively constant until a tissue height of 3 mm. Once the tissue height is reduced below this level, the predicted thermal conductivity starts to fall rapidly. Once the tissue height reached 1 mm, the predicted thermal conductivity of the tissue fell to 0.394 W/(m·K), an 18% reduction in the thermal conductivity when compared to the 3 mm tissue height.

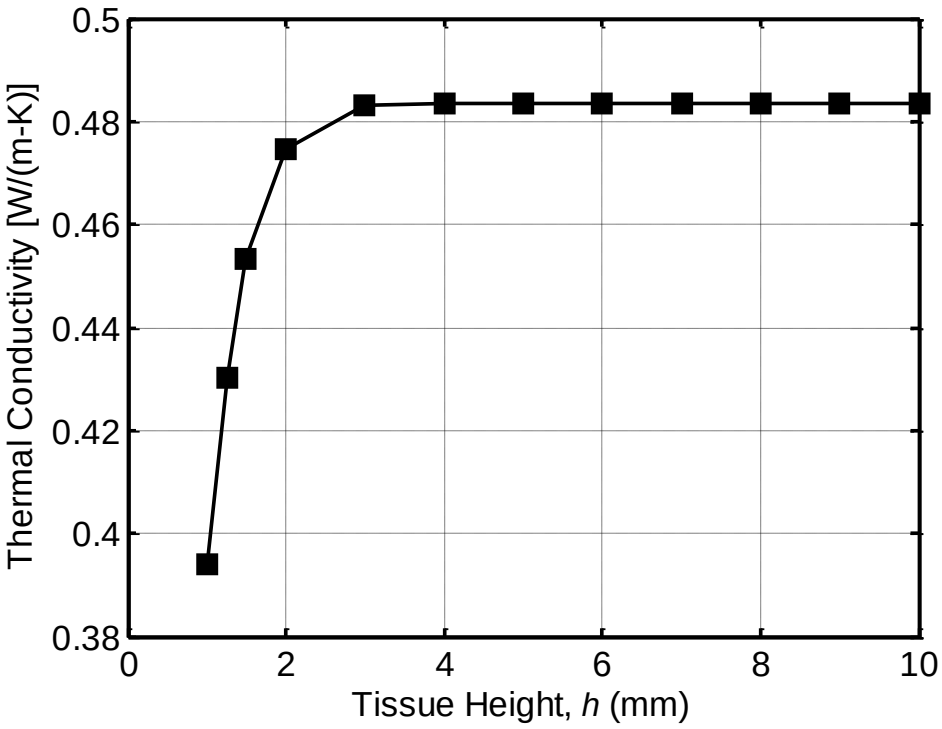

Figure B.5 The effect of compression level on the predicted thermal conductivity of the tissue.

This change in the predicted thermal conductivity is caused by the lower plate invalidating Eq. (B.3.d), which stipulates that at an infinite location, the temperature will remain constant. Figure B.6 shows the effect of the varying tissue thickness on the temperature at the center of the tissue-lower plate interface. As the tissue thickness was reduced, the temperature on the top of the lower plate increased. When h = 1 mm, the plate temperature increased by 1.1°C. The rise in the plate temperature correlates with the increase in the ΔT of the thermistor bead as the tissue thickness is decreased.

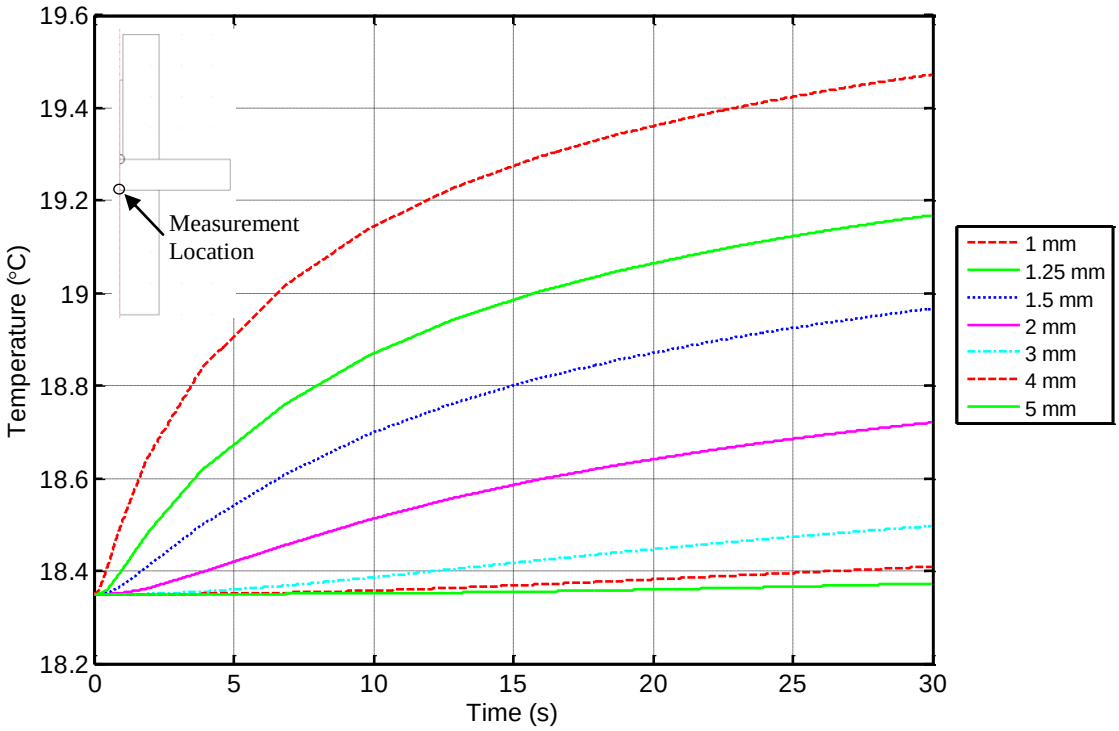

Figure B.6 Temperature at the tissue-lower plate interface along the axis of symmetry.

B.5. Conclusions

For tissue thicknesses greater than h = 3 mm, there was no change in either the average bead temperature or the thermal conductivity of the tissue. However, if the tissue thickness was less than 3 mm, the predicted thermal conductivity of the tissue started to drop off rapidly. The lower plastic plate influenced the results and caused the volumetric bead temperature to increase. This occurred because the lower plate was violating the boundary condition assumptions of Eq. (B.3d).

This simplified model estimates the potential effects of the lower plastic plate on the thermal conductivity results. However, the model does not take into account the effect of compression on either the density or specific heat of the tissue. It is expected that both of these values may change as the compression level is increased. Incorporating these compression induced changes into the thermal conductivity model will need to be undertaken to develop a full understanding of the effect of the plastic plate on the thermal conductivity.

References

Balasubramaniam, T.A. and Bowman, H.F., (1974), "Temperature field due to a time dependent heat source of spherical geometry in an infinite medium," *ASME Journal of Heat Transfer*, Vol. 93, pp. 296-299.

Balasubramaniam, T.A. and Bowman, H.F., (1977), "Thermal conductivity and thermal diffusivity of biomaterials: A simultaneous measurement technique," *ASME Journal of Biomechanicl Engineering*, Vol. 99, pp. 148-154.

Chastagner, M.W., (2010), "Effect of compression and water content on the thermal conductivity of tissue," *PhD Thesis in Mechanical Engineering, University of Michigan,* Chapter 2.

CINDAS, (1998). *Properties of Inorganic and Organic Fluids. CINDAS Data Series on Material Properties Volume V-1,* C.Y. Ho (ed.), Hemisphere Publishing Corporation, New York.

COMSOL, (2008), *Multiphysics* Version 3.5a User's guide, COMSOL, Inc., Burlington, MA.

Kharalkar, N.M. and Valvano, J.W., (2006), "Finite element analysis and experimental verification of multilayered tissue characterization using the thermal technique," *IEEE-Engineering in Medicine and Biology Society Conference Proceedings*, pp. 3182-3185.

Patel, P.A., Valvano, J.W., Pearce, J.A., Prahl, S.A., and Denham, C.R., (1987), "A self-heated thermistor technique to measure effective thermal properties from the tissue surface," Journal of Biomechanical Engineering, Vol. 109, pp. 330-335.

Pennes, H.H., (1948), "Analysis of tissue and arterial blood temperature in the resting human forearm," *Journal of Applied Physiology*, Vol. 1, pp. 93–122.

Valvano, J.W. and Nho, S., (1991), "Tissue thermal diffusivity measured with sinusoidal heated thermistors," *ASME Winter Annual Meeting. Atlanta, HTD*, Vol. 179, pp. 9-14.

Valvano, J.W., (1984a), "The use of thermal diffusivity to quantify tissue perfusion," *Harvard University-MIT Division of Health Sciences and Technology, PhD Thesis.*

Valvano, J.W., Allen, J.T., and Bowman, H.F., (1984b), "The simultaneous measurement of thermal conductivity, thermal diffusivity, and perfusion in small volumes of tissue," *Journal Biomechanical Engineering*, Vol. 106(3), pp. 192-197.

Valvano, J.W., and Chitsabesan, B., (1987), "Thermal conductivity and diffusivity of arterial wall and atherosclerotic plaque," *Lasers in Life Science*, Vol. 1, pp. 3219–3229.

Valvano, J.W., Cochran, J.R., and Diller, K.R., (1985), "Thermal conductivity and diffusivity of biomaterials measured with self-heated thermistors," *International Journal of Thermophysics*, Vol. 6, pp. 301-311.

van Gelder, M.F., (1998), "A thermistor based method for measurement of thermal conductivity and thermal diffusivity of moist food material at high temperatures," *PhD Thesis in Biological Systems Engineering, Virginia Polytechnic Institute and State University*.

Zhang, H., Cheng, S., He, L., Zhang, A., Zheng, Y., and Gao, D., (2002), "Determination of thermal conductivity of biomaterials in the temperature range 233–313K using a tiny detector made of a self-heated thermistor," *Cell Preservation Technology*, Vol. 1(2), pp. 141-147.